12-2011

Designing Predictive Mathematical Models for the Metabolic Pathways Associated with Polyhydroxybutyrate Synthesis in Escherichia coli

Angela Dixon
Utah State University

DESIGNING PREDICTIVE MATHEMATICAL MODELS FOR THE METABOLIC PATHWAYS ASSOCIATED WITH POLYHYDROXYBUTYRATE SYNTHESIS IN *ESCHERICHIA COLI*

by

Angela Dixon

A thesis submitted in partial fulfillment
of the requirements for the degree

of

MASTER OF SCIENCE

in

Biological Engineering

Approved:

_____	_____
Dean H. Scott Hinton Major Professor	Dr. Ronald C. Sims Committee Member
_____	_____
Dr. Charles D. Miller Committee Member	Dr. Mark R. McLellan Vice President for Research and Dean of the School of Graduate Studies

UTAH STATE UNIVERSITY
Logan, Utah

2011

ABSTRACT

Designing Predictive Mathematical Models for the Metabolic Pathways Associated with Polyhydroxybutyrate Synthesis in *Escherichia coli*

by

Angela Dixon, Master of Science

Utah State University, 2011

Major Professor: Dean H. Scott Hinton
Department: Biological Engineering

Polyhydroxybutyrate (PHB) is a polyhydroxyalkanoate that has been extensively studied as a potential biodegradable replacement for petrochemically derived plastics. The synthesis pathway of PHB is native to *Ralstonia eutropha*, but the genes for the PHB pathway have successfully been introduced into *Escherichia coli* through plasmids such as the pBHR68 plasmid. However, the production of PHB needs to be more cost-effective before it can be commercially produced.

A mathematical model for PHB synthesis was developed to identify target genes that could be genetically engineered to increase PHB production. The major metabolic pathways included in the model were glycolysis, acetyl coenzyme A (acetyl-CoA) synthesis, tricarboxylic acid (TCA) cycle, glyoxylate bypass, and PHB synthesis. Each reaction in the selected metabolic pathways was modeled using the kinetic mechanism identified for the associated enzyme. The promoters and transcription factors for each enzyme were incorporated into the model. The model was validated through comparison with other published models and experimental PHB production data.

The predictive model identified 16 enzymes as having no effect on PHB production, 5 enzymes with a slight effect on PHB production, and 9 enzymes with large effects on PHB production. Decreasing the substrate affinity of the enzyme citrate synthase resulted in the largest increase in PHB synthesis. The second largest increase was observed from lowering the substrate affinity of glyceraldehyde-3-phosphate dehydrogenase. The predictive model also indicated that increasing the activity of the *lac* promoter in the pBHR68 plasmid resulted in the largest increase in the rate of PHB production.

The predictive model successfully identified two genes and one promoter as targets for genetic engineering to create an optimized strain of *E. coli* for PHB production. The substrate-binding sites for the genes *gltA* (citrate synthase) and *gapA* (glyceraldehyde-3-phosphate dehydrogenase) should be genetically engineered to be less effective at binding the substrates. The *lac* promoter in the pBHR68 plasmid should be genetically engineered to more closely match the consensus sequence for binding to RNA polymerase. The model predicts that an optimized strain of *E. coli* for PHB production could be achieved by genetically altering *gltA, gapA,* and the *lac* promoter.

(198 pages)

PUBLIC ABSTRACT

Designing Predictive Mathematical Models for the Metabolic Pathways Associated with Polyhydroxybutyrate Synthesis in *Escherichia coli*

by

Angela Dixon

Plastics are a versatile and widely used material. However, traditional plastics are derived from petrochemicals and are not biodegradable. Polymers synthesized from microorganisms that have similar properties to plastic are potential biodegradable replacements. The objective of this project is to use mathematical modeling as a tool to engineer a strain of bacteria optimized for the production of bio-plastics.

Production costs can be reduced by using a bacterial strain specifically optimized for bio-plastic production. By reducing production costs, bio-plastics will be able to commercially compete with traditional plastics. Society will benefit as bio-plastics replace traditional plastics. Fossil fuels will not be depleted by the production of traditional plastics, and the bio-plastics will biodegrade in landfills.

The costs of this research are nominal. Developing a model takes only time and minimal laboratory work. An effective predictive model will reduce laboratory time and cost because it will indicate how to efficiently engineer a microorganism strain optimized for the production of bio-plastics. This design process can also be used to develop predictive models for the production of other bioproducts such as biofuels, biomaterials, and biopharmaceuticals.

ACKNOWLEDGMENTS

I am most grateful for the support of my husband, James. I could not have completed this project without his constant encouragement. I would like to thank Dean H. Scott Hinton and Dr. Ronald C. Sims for providing the opportunity to work on this research. I am grateful for their guidance and involvement in this project. I would like to thank Jia Zeng for the many hours he spent on the LC-MS for me. I am also grateful to Dr. Charles Miller and Dr. Jixun Zhan for allowing me to use their laboratories and equipment. Lastly, I would like to thank the USTAR Synthetic Bio-Manufacturing Center for funding this project.

Angela Dixon

CONTENTS

LIST OF TABLES

LIST OF FIGURES

LIST OF EQUATIONS

INTRODUCTION

Need for Study

Plastic is one of the most heavily used compounds in the United States. Traditional plastics are versatile in use and have low production costs. However, they are produced from non-renewable petrochemicals that are not biodegradable (Reddy *et al*, 2003). A sustainable alternative is needed in order to decrease both the use of non-renewable fossil fuels and the buildup of plastic in landfills (Reddy *et al*, 2003).

Polyhydroxybutyrate (PHB) is a polyhydroxyalkanoate that has been extensively studied as a potential biodegradable replacement for petrochemical plastics (Byrom, 1987). Polyhydroxyalkanoates are storage material for many gram-positive and gram-negative bacteria (Choi & Lee, 1999). The bio-plastic is created and stored intracellularly as a reserve of carbon, energy, and reducing power during periods of stress or nutrient limitation (Doi, 1990; Lee, 1996; Madison & Huisman, 1999). The polymerization of the soluble nutrients into insoluble compounds prevents leakage out of the cell. This process allows the bacteria to have continued access to nutrients at a low maintenance cost.

Many bacteria, such as *Zoogloea ramigera* (Madison & Huisman, 1999; Ploux *et al*, 1988) and *Ralstonia eutropha* (Haywood *et al*, 1988; Haywood *et al*, 1989; Madison & Huisman, 1999; Slater *et al*, 1998; Steinbüchel & Schlegel, 1991), are capable of producing and degrading PHB and other polyhydroxyalkanoates. Genes for PHB synthesis can be cloned into other bacteria such as *Escherichia coli*. One of the advantages of using *E. coli* for the production of PHB is because *E. coli* is unable to degrade PHB into soluble compounds (Madison & Huisman, 1999).

The production of PHB, or any polyhydroxyalkanoate, is costly due to its carbon source and downstream processing costs (Gurieff & Lant, 2007). The high cost of $2.65-5/kg is the main reason for the limited application of these bio-plastics (Choi & Lee, 1997; Choi & Lee, 1999). Further studies are needed to help make PHB production more cost-effective before it can be commercially produced.

Metabolic modeling is a tool that has been used to determine rate-limiting steps and conditions of PHB production. However, metabolic models have focused solely on the three enzymes in the PHB synthesis pathway and have neglected to account for other key pathways in the cell (Leaf & Srienc, 1998; Van Wegen *et al*, 1998; Van Wegen *et al*, 2001). Models have also failed to account for the transcriptional network that is essential in understanding how enzymes of interest are regulated. Most models focus on optimizing the culturing methods to improve PHB production, but seldom address the possibility of optimizing the prokaryotic strain (Choi & Lee, 1997; Choi & Lee, 1999; Jurasek & Marchessault, 2004; Leaf & Srienc, 1998; Mantzaris *et al*, 2002; Shang *et al*, 2007; Van Wegen *et al*, 1998; Van Wegen *et al*, 2001).

A predictive model of the metabolic pathways of the cell should be able to quantitatively predict how changes in one pathway can affect the synthesis rate of a product of interest. This approach would require the predictive model to account for the complex metabolic pathways present in a cell. A model that focuses on one metabolic pathway lacks valuable information on what is happening elsewhere in the cell. A more complex model that accounts for many metabolic pathways and their transcriptional networks could be used as a guide in the laboratory for engineering optimized prokaryotic factories. Utilizing the synthetic biology toolbox, a strain of *E. coli* with its

metabolic pathways optimized for the synthesis of a single product could be engineered. The predictive model will allow one to target specific enzymes, promoters, or transcription factors out of many metabolic pathways for genetic engineering.

A model encompassing the major metabolic pathways associated with PHB synthesis will help determine the amount of energy and reducing power that can be diverted into the PHB synthesis pathway for the optimal PHB production. The major pathways involved in PHB synthesis that are included in the model are glycolysis, acetyl coenzyme A (acetyl-CoA) synthesis, tricarboxylic acid cycle (TCA), glyoxylate shunt, and PHB synthesis (Madison & Huisman, 1999). The model must effectively simulate the individual reactions in the previously mentioned pathways. Kinetic mechanisms, kinetic parameters, genes, and transcription factors must be determined for each reaction. Events and rules can simulate conditions that trigger the regulation of each enzyme to simulate *in vivo* conditions.

Flux balance analysis (FBA) is a tool currently used to model genome-scale metabolic networks. FBA is a constraint approach that focuses on stoichiometric information rather than kinetic data. Stoichiometric data is more widely available than kinetic data for different reactions and organisms. However, the kinetic data needed to build a genome-scale mechanistic model will become available as technology advances the collection of high throughput metabolomic data (Jamshidi & Palsson, 2008). Models based on FBA can be used to predict outcomes of gene deletion or addition, but not gene modification (Feist *et al*, 2009; Oberhardt *et al*, 2009; Orth *et al*, 2010; Price *et al*, 2003; Raman & Chandra, 2009; Schellenberger *et al*, 2011). A mechanistic model based on

kinetics could be used to predict how to genetically modify an existing enzyme to increase production of a specific bioproduct.

A constraint based approach such as FBA results in a static model whereas a kinetic based approach produces a dynamic model. As a static model, FBA also does not account for the transcriptional network that regulates enzyme expression. Attempts have been made to incorporate a regulatory network into FBA through the use of Boolean logic operators (Orth *et al*, 2010; Price *et al*, 2003; Raman & Chandra, 2009). However, a binary system based on Boolean logic operators fails to account for the entire dynamic range of the regulatory system.

Metabolic profiling is a tool capable of providing the details needed for a predictive mechanistic model. Metabolic profiling is a quantitative analysis of specific metabolites over time. The general protocol for metabolic profiling is to take samples from a culture and quench the metabolic activity. The two most common quenching methods are freezing the samples with liquid nitrogen, or shocking with a cold-buffered aqueous methanol mixture (Bajad *et al*, 2006; Buchholz *et al*, 2001; Dettmer *et al*, 2006; Lu *et al*, 2008; Mashego *et al*, 2007; Ohashi *et al*, 2007).

Once samples have been prepared, specific metabolites can be analyzed through combinations of liquid chromatography (LC), gas chromatography (GC), mass spectrometry (MS), capillary electrophoresis (CE), and nuclear magnetic resonance (NMR) (Bajad *et al*, 2006; Buchholz *et al*, 2001; Dettmer *et al*, 2006; Lu *et al*, 2008; Mashego *et al*, 2007; Ohashi *et al*, 2007). Liquid chromatography coupled with mass spectrometry (LC-MS) is a powerful tool because it is capable of analyzing many

metabolites simultaneously using a small sample volume. One study successfully analyzed as many as 69 metabolites simultaneously (Bajad *et al*, 2006).

LC-MS analysis can provide concentrations of metabolites at specific times in the culture when compared to standard curves. These values can then be incorporated into the predictive model so that the model more accurately represents the specific prokaryotic strain under analysis. The predictive model can then be optimized for PHB production and can identify the target genes for genetic engineering. After the prokaryotic strain has been genetically engineered, another round of metabolic profiling can be conducted to determine how the new strain performs compared to the optimized model.

Objectives

The objective of this project was to develop a mathematical model for PHB synthesis in *E. coli* for the identification of key regulators and optimal conditions for PHB synthesis. To achieve this objective, the model included pathways for glycolysis, acetyl-CoA synthesis, TCA cycle, the glyoxylate pathway, and PHB synthesis. The model incorporated enzymes, cofactors, and transcription factors for each reaction in the pathways. The model was fitted to published models and to real-time data in order to increase its accuracy. Metabolic profiling was employed to collect real-time data utilizing LC-MS for metabolite identification and quantification. Sensitivity analysis was used on the model to identify the key regulators and optimal conditions for the best PHB production. The goal of this project was to provide direction for how to genetically engineer *E. coli* to achieve higher production rates of PHB.

PATHWAYS AND REACTIONS

Metabolic pathways are composed of biochemical reactions that allow organisms to both degrade and construct compounds like PHB. Five metabolic pathways were selected to be incorporated into this mathematical model based on criteria that include energy, reducing power, and common substrates with the PHB synthesis pathway. The five metabolic pathways were PHB synthesis, TCA cycle, glyoxylate pathway, glycolysis, and acetyl-CoA synthesis.

Each pathway is a set of reactions that was modeled based on each reaction's kinetic mechanism. The kinetic mechanism and parameters are dependent upon the enzyme that catalyzes each reaction. Studies on these enzymes have revealed many of their kinetic mechanisms and parameters. This chapter explains the justifications behind every equation and parameter used to model each reaction.

PHB Synthesis

The PHB synthesis pathway is composed of three biochemical reactions that convert acetyl-CoA into PHB. This pathway contains two intermediates: acetoacetyl-CoA and 3-hydroxybutyryl-CoA. The cofactors CoA and NADPH/$NADP^+$ contribute to these reactions. The enzymes β-ketothiolase (PhaA), acetoacetyl-CoA reductase (PhaB), and poly-β-hydroxybutyrate polymerase (PhaC) each catalyze one of the three reactions shown in Figure 1.

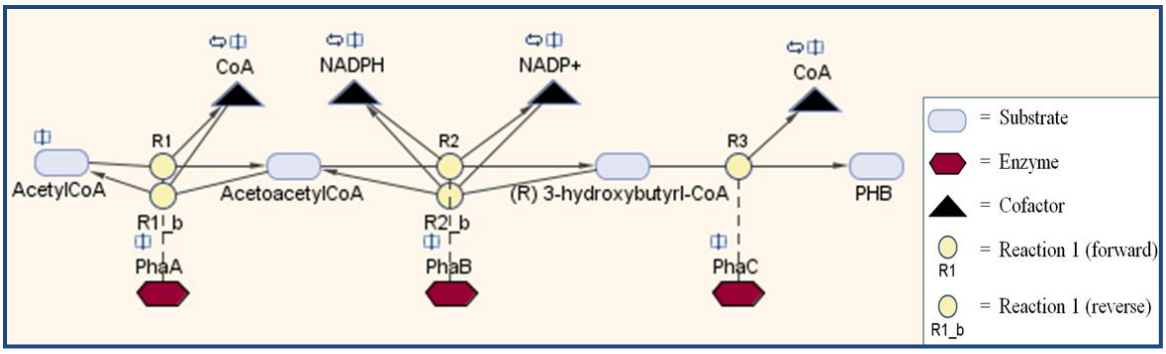

Figure 1. The metabolic pathway for the synthesis of PHB.

Reaction 1:

$$2\ \text{Acetyl-CoA} \xleftrightarrow{\beta\text{-ketothiolase}} \text{Acetoacetyl-CoA} + \text{CoA}$$

Enzyme: β-ketothiolase

The first step in PHB synthesis is catalyzed by the enzyme β-ketothiolase, also known as acetyl-CoA acetyltransferase. The enzyme β-ketothiolase condenses two acetyl-CoA molecules into one acetoacetyl-CoA in the forward reaction. The reversible reaction is known as the thiolysis reaction. In many organisms, such as *Ralstonia eutropha* (also previously known as *Alcaligenes eutrophus* and *Cupriavidus necator*), there are two β-ketothiolases able to synthesize PHB. Enzyme A can utilize the substrates acetoacetyl-CoA and 3-ketopentanoyl-CoA. Enzyme B can cleave a wider variety of substrates that include: acetoacetyl-CoA, 3-ketoheptanoyl-CoA, 3-ketopentanoyl-CoA, 3-ketohexanoyl-CoA, 3-ketooctanoyl-CoA, and 3-ketodecanoyl-CoA. Studies have shown that enzyme B is the primary β-ketothiolase utilized in PHB synthesis (Madison & Huisman, 1999; Slater *et al*, 1998).

Forward Reaction:

The enzyme β-ketothiolase exhibits normal Michaelis-Menten kinetics in the absence of CoA (Oeding & Schlegel, 1973; Senior & Dawes, 1973). In multiple organisms, the enzyme displayed competitive-inhibition in the presence of CoA (Haywood *et al*, 1988; Mothes *et al*, 1997; Oeding & Schlegel, 1973; Steinbüchel & Schlegel, 1991). Based on the non-linear Lineweaver-Burk plots in the presence of CoA, Oeding and Schlegel proposed a ping-pong mechanism with CoA as the binary term. Hill kinetics were observed with coefficients of n = 1 in the absence of CoA and n = 2 in the presence of CoA (Oeding & Schlegel, 1973).

Based on the findings described above, it was decided to use Equation (1) for the condensation reaction. Equation (1) combines the kinetics of competitive-inhibition with Hill cooperativity. Acetyl-CoA was used as the substrate, S, and CoA was used as the inhibitor, I. The kinetic parameters utilized in simulations of this model are shown in Table I. No kinetic data were available on *E. coli* for β-ketothiolase. Because the genes for β-ketothiolase in *E. coli* come from *R. eutropha*, when available, it was preferable to use kinetic data from *R. eutropha* (or *A. eutrophus, C. necator*) rather than from other organisms. Because the enzyme B of β-ketothiolase is preferred over the enzyme A in PHB synthesis (Madison & Huisman, 1999; Slater *et al*, 1998), K_m values for enzyme B were chosen over enzyme A in this model. No value in the literature was found for V_m in *R. eutropha.* All values found for V_m are shown in Table I.

Reverse Reaction:

In the direction of thiolysis, β-ketothiolase does not obey Michaelis-Menten kinetics. Studies indicate that there is a positive cooperativity between acetoacetyl-CoA

and CoA (Haywood *et al*, 1988; Steinbüchel & Schlegel, 1991). Lineweaver-Burk plots yield a family of parallel lines at varied concentrations of acetoacetyl-CoA or CoA. Parallel lines indicate that this reaction follows a ping-pong bi-bi mechanism (Molina *et al*, 1994; Oeding & Schlegel, 1973).

For this model, it was decided to use Equation (2), the ping-pong bi-bi mechanism, for the thiolysis reaction. Acetoacetyl-CoA was used as substrate A, and CoA was used as substrate B. Kinetic parameters utilized in simulations of this model are shown in Table I. No kinetic data were available on *E. coli* for β-ketothiolase.

$$\nu = \frac{V_{MAX}[S]^n}{K_M\left(1+ I/K_i\right)+[S]^n} = \frac{k_{cat}*[E]*[S]^n}{K_M\left(1+ I/K_i\right)+[S]^n} \quad (1)$$

V_{MAX} = k_{cat}*[E] = [μM/s]
K_M = Substrate concentration resulting in $0.5V_{MAX}$ = [μM]
K_i = Inhibitor concentration in $0.5V_{MAX}$ = [μM]
k_{cat} = Maximum number of rxns catalyzed per second = [s^-]
[S] = Concentration of substrate = [μM]
[E] = Concentration of enzyme = [μM]
[I] = Concentration of inhibitor = [μM]
n = Hill cooperativity coefficient

$$\nu = \frac{V_{MAX}}{\frac{K_A}{[A]}+\frac{K_B}{[B]}+1} = \frac{k_{cat}*[E]}{\frac{K_A}{[A]}+\frac{K_B}{[B]}+1} \quad (2)$$

V_{MAX} = k_{cat}*[E] = [μM/s]
K_A = Dissociation constant for substrate A = [μM]
K_B = Dissociation constant for substrate B = [μM]
k_{cat} = Maximum number of rxns catalyzed per second = [s^-]
[A] = Concentration of substrate A = [μM]
[B] = Concentration of substrate B = [μM]
[E] = Concentration of enzyme = [μM]

Table I. Kinetic parameters utilized for Reaction 1 in the model.

	Parameter	Value	Units	Organism	Reference
Fwd Rxn	K_m	230[b]	µM	*A. eutrophus*	Steinbüchel & Schlegel, 1991
		390	µM	*C. necator*	Oeding & Schlegel, 1973
		1100[a]	µM	*A. eutrophus*	Steinbüchel & Schlegel, 1991
	V_m	0.0078	µM/s	*A. beijerinckii*	Senior & Dawes, 1973
		0.0088	µM/s	*M. sedula*	Berg *et al*, 2007
		0.0177	µM/s	*M. sedula*	Berg *et al*, 2007
		0.115	µM/s	*R. sphaeroides*	Alber *et al*, 2006
		0.32	µM/s	*M. rhodesianum*	Mothes *et al*, 1997
		1.92	µM/s	*C. kluyveri*	Sliwkowski & Hartmanis, 1984
	K_i	16	µM	*A. eutrophus*	Steinbüchel & Schlegel, 1991
	n	2	-	*C. necator*	Oeding & Schlegel, 1973
Rev Rxn	K_A	44[a]	µM	*A. eutrophus*	Steinbüchel & Schlegel, 1991
	K_B	394[b]	µM	*A. eutrophus*	Steinbüchel & Schlegel, 1991
		16[a]	µM	*A. eutrophus*	Steinbüchel & Schlegel, 1991
		93[b]	µM	*A. eutrophus*	Steinbüchel & Schlegel, 1991
	V_m	1.24	µM/s	*M. rhodesianum*	Mothes *et al*, 1997

a. Enzyme A of β-ketothiolase
b. Enzyme B of β-ketothiolase

Reaction 2:

$$\text{Acetoacetyl-CoA} + \text{NADPH} + \text{H}^+ \xleftrightarrow{\text{Acetoacetyl-CoA reductase}} \text{3-hydroxybutyryl-CoA} + \text{NADP}^+$$

Enzyme: Acetoacetyl-CoA reductase

Acetoacetyl-CoA reductase catalyzes the second step in PHB synthesis by converting acetoacetyl-CoA into 3-hydroxybutyryl-CoA. It has been classified as a NADPH-dependent reductase. The availability of reducing power is one of the main driving forces for PHB synthesis. Thiolysis is the thermodynamically favored direction; however, under favorable PHB accumulating conditions, acetoacetyl-CoA reductase can pull the reaction in the condensation direction (Madison & Huisman, 1999).

Forward Reaction:

The kinetics of acetoacetyl-CoA reductase vary by organism. The enzyme has been shown to have cooperativity factors in *M. extorquens* for acetoacetyl-CoA and NADPH (Belova *et al*, 2006). However, it has been shown that there are no cooperativity factors in *M. rhodesianum* (Mothes & Babel, 1994). Kinetic behavior indicates inhibition with the substrate acetoacetyl-CoA at high concentrations in multiple organisms (Belova *et al*, 2006; Mothes & Babel, 1994; Ploux *et al*, 1988). Normal Michaelis-Menten kinetics have been observed in *A. beijerinckii* (Ritchie *et al*, 1971). Also, a sequential kinetic mechanism has been observed in *Z. ramigera* (Ploux *et al*, 1988).

The literature contained K_m values for acetoacetyl-CoA and NADPH/NADH (Steinbüchel & Schlegel, 1991) in *A. eutrophus*, but no mechanism was proposed. Due to the dependence on NADPH/NADH and the sequential kinetic mechanism observed in *Z. ramigera*, it was decided to use an ordered bi-bi mechanism, Equation (3), to model this reaction. Substrate A was acetoacetyl-CoA, and substrate B was NADPH/NADH. The NADPH dependent enzyme is the one used in PHB synthesis (Madison & Huisman, 1999); therefore, kinetic parameters for the NADPH dependent enzyme shown in Table II were used in the model.

$$\nu = \frac{V_{MAX}}{\frac{K_A K_B}{[A][B]} + \frac{K_A}{[A]} + \frac{K_B}{[B]} + 1} = \frac{k_{cat} * [E]}{\frac{K_A K_B}{[A][B]} + \frac{K_A}{[A]} + \frac{K_B}{[B]} + 1} \quad (3)$$

V_{MAX} = k_{cat}*[E] = [µM/s]
K_A = Dissociation constant for substrate A = [µM]
K_B = Dissociation constant for substrate B = [µM]
k_{cat} = Maximum number of rxns catalyzed per second = [s^-]
[A] = Concentration of substrate A = [µM]
[B] = Concentration of substrate B = [µM]
[E] = Concentration of enzyme = [µM]

Reverse Reaction:

The literature contained no proposed kinetic mechanism for the thiolysis reaction catalyzed by acetoacetyl-CoA reductase. However, K_m values for β-hydroxybutyryl-CoA and $NADP^+/NAD^+$ were found in *A. eutrophus* (Steinbüchel & Schlegel, 1991). It was decided to model this reaction with the same mechanism utilized in the condensation reaction. An ordered bi-bi mechanism, Equation (3), was employed with substrate A as β-hydroxybutyryl-CoA and substrate B as $NADP^+/NAD^+$.

Although both NADPH and NADH dependent acetoacetyl-CoA reductase exist in *A. eutrophus*, only the NADPH dependent enzyme is used in PHB synthesis (Madison & Huisman, 1999). Therefore, kinetic parameters for the NADPH dependent enzyme were used in the model as shown in Table II. The parameter V_m was not found for the thiolysis reaction. The same value used in the condensation reaction was used in the thiolysis reaction model.

Table II. Kinetic parameters utilized for Reaction 2 in the model.

	Parameter	Value	Units	Organism	Reference
Fwd Rxn	K_A	5[a]	μM	*A. eutrophus*	Steinbüchel & Schlegel, 1991
		22[b]	μM	*A. eutrophus*	Steinbüchel & Schlegel, 1991
	K_B	19[a]	μM	*A. eutrophus*	Steinbüchel & Schlegel, 1991
		13[b]	μM	*A. eutrophus*	Steinbüchel & Schlegel, 1991
	V_m	0.023	μM/s	*R. sphaeroides*	Alber *et al*, 2006
Rev Rxn	K_A	33[a]	μM	*A. eutrophus*	Steinbüchel & Schlegel, 1991
		26[b]	μM	*A. eutrophus*	Steinbüchel & Schlegel, 1991
	K_B	31[a]	μM	*A. eutrophus*	Steinbüchel & Schlegel, 1991
		16[b]	μM	*A. eutrophus*	Steinbüchel & Schlegel, 1991
	V_m	0.023	μM/s	*R. sphaeroides*	Alber *et al*, 2006

a. NADPH dependent
b. NADH dependent

Reaction 3:

$$\text{(n)3-hydroxybutyryl-CoA} \xrightarrow{\text{PHB polymerase}} \text{poly-3-hydroxybutyrate} + \text{(n)CoA}$$

Enzyme: Poly-β-hydroxybutyrate polymerase (PHB synthase)

The enzyme poly-β-hydroxybutyrate polymerase, also known as PHB synthase, catalyzes the third step in the PHB synthesis pathway. This enzyme exists in both soluble and granule-associated forms (Haywood *et al*, 1989; Madison & Huisman, 1999). In carbon-limited environments, most PHB synthase is soluble. In nitrogen-limited environments, the majority of PHB synthase is granule-associated (Haywood *et al*, 1989). PHB synthase can polymerize 3-hydroxybutyrate units to form poly-3-hydroxybutyrate (PHB) and 3-hydroxyvalerate units to form polyhydroxyalkanoate (PHA) (Haywood *et al*, 1989).

Forward Reaction:

Poly-β-hydroxybutyrate polymerase demonstrated normal Michaelis-Menten kinetics in *A. eutrophus* (Haywood *et al*, 1989). Equation (4) was used to model the forward reaction using kinetic parameters from Table III. The molecular weight of PHB assumed for this model was 160,000 Daltons because of its association with the kinetic parameters in Table III (Haywood *et al*, 1989). Using the molecular weight of 160 kDa results in a PHB polymer composed of 1,860 units of 3-hydroxybutyrate. The stoichiometric coefficient *n* in Reaction 3 was set as 1,860 in the model. Kinetic parameters for the granule-associated PHB synthase were used in the model due to the unstable nature of the soluble PHB synthase (Haywood *et al*, 1989).

Reverse Reaction:

The reverse reaction was ignored in this model because *E. coli* do not naturally code for PHB depolymerase (Saito *et al*, 1989). The PHB depolymerase gene will not be cloned into *E. coli* because it is desired to accumulate, not degrade, PHB.

$$\nu = \frac{V_{MAX}[S]}{K_M + [S]} = \frac{k_{cat} * [E] * [S]}{K_M + [S]} \quad (4)$$

V_{MAX} = k_{cat}*[E] = [µM/s]
K_M = Substrate concentration resulting in $0.5V_{MAX}$ = [µM]
k_{cat} = Maximum number of rxns catalyzed per second = [s^-]
[S] = Concentration of substrate = [µM]
[E] = Concentration of enzyme = [µM]

Table III. Kinetic parameters utilized for Reaction 3 in the model.

	Parameter	Value	Units	Organism	Reference
	K_m	680[a,c]	µM	*A. eutrophus*	Haywood *et al*, 1989
Fwd		720[a,d]	µM	*A. eutrophus*	Haywood *et al*, 1989
Rxn		1630[b,c]	µM	*A. eutrophus*	Haywood *et al*, 1989
	V_m	0.0047	µM/s	*A. eutrophus*	Haywood *et al*, 1989

a. (R)-3-hydroxybutyryl-CoA as substrate
b. (R)-3-hydroxyvaleryl-CoA as substrate
c. Granule associated synthase
d. Soluble synthase

TCA Cycle

The tricarboxylic acid (TCA) cycle is composed of nine reactions that utilize acetyl-CoA to generate energy and reducing power. Nine enzymes catalyze the reactions in the TCA cycle as shown in Figure 2. The TCA cycle uses the cofactors CoA, ADP/ATP, NAD^+/NADH, and $NADP^+$/NADPH. The TCA cycle takes a portion of acetyl-CoA away from PHB synthesis. Cells need energy, reducing power, and acetyl-CoA to produce PHB, so the TCA cycle is an important pathway to include in the model.

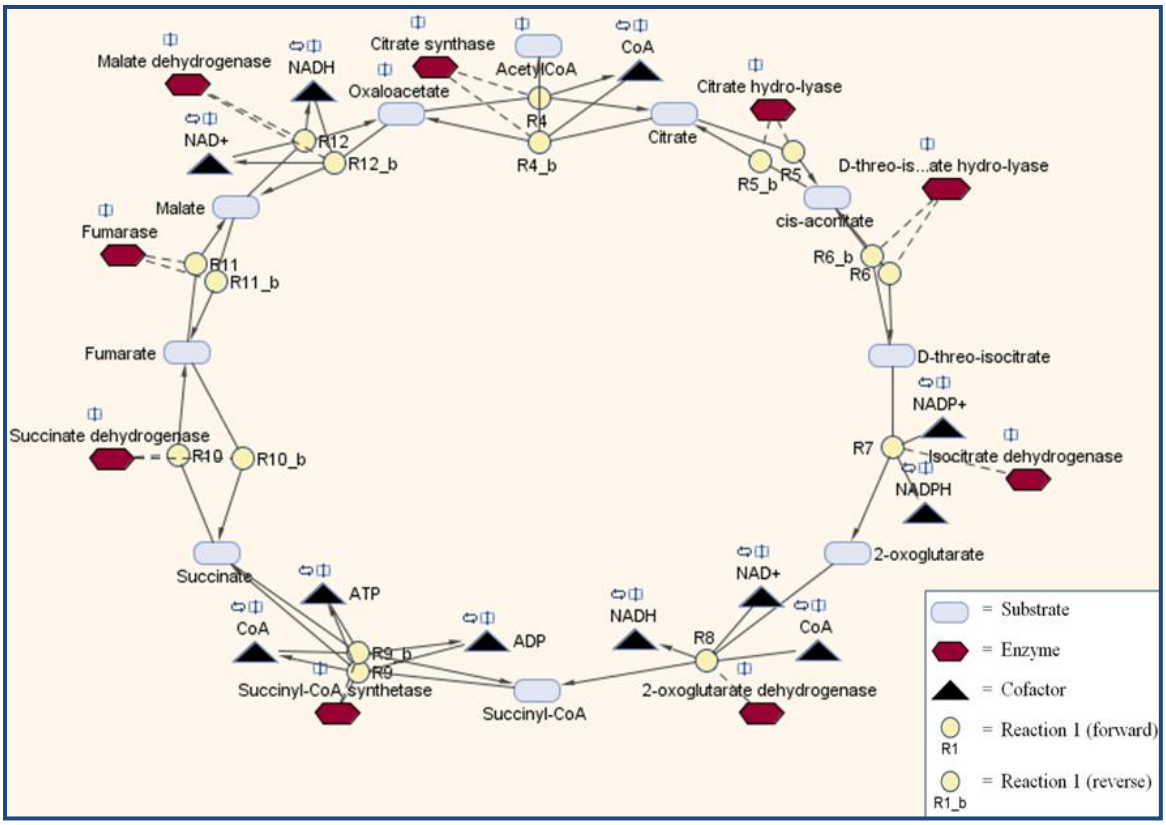

Figure 2. The metabolic pathway for the TCA cycle.

Reaction 4:

$$\text{Oxaloacetate} + \text{Acetyl-CoA} + \text{H}_2\text{O} \xleftrightarrow{\text{Citrate synthase}} \text{Citrate} + \text{CoA} + \text{H}^+$$

Enzyme: Citrate synthase

Citrate synthase catalyzes the Claisen condensation reaction that forms citrate from oxaloacetate and acetyl-CoA. Citrate synthase is controlled through activators and inhibitors. Acetyl-CoA acts as an allosteric activator and K^+ acts as a non-allosteric inhibitor. Allosteric inhibitors include NADH, NAD^+, and oxaloacetate. ATP and 2-oxoglutarate act as competitive inhibitors. Other inhibitors include citrate, isocitrate, and cis-aconitate (Anderson & Duckworth, 1988; Duckworth *et al*, 1987; Man *et al*, 1995; Senior & Dawes, 1973; Walsh & Koshland, 1985).

Forward Reaction:

Studies have demonstrated sequential ordered bi-bi kinetics, with oxaloacetate binding first, in *E. coli* for this reaction (Anderson & Duckworth, 1988). Studies have also demonstrated that citrate synthase exhibits competitive inhibition with 2-oxoglutarate (Anderson & Duckworth, 1988; Pereira *et al*, 1994).

An ordered bi-bi kinetic mechanism, Equation (3), was used to model the forward reaction catalyzed by citrate synthase. Substrate A was oxaloacetate and substrate B was acetyl-CoA. Kinetic parameters utilized in the model are shown in Table IV. The values chosen were from various strains of *E. coli*.

Table IV. Kinetic parameters utilized for Reaction 4 in the model.

	Parameter	Value	Units	Organism	Reference
Fwd Rxn	K_A	460	µM	*E. coli* H229Q	Anderson & Duckworth, 1988
		17	µM	*E. coli* H226Q	Anderson & Duckworth, 1988
		26	µM	*E. coli* wild	Anderson & Duckworth, 1988
	K_B	190	µM	*E. coli* H229Q	Anderson & Duckworth, 1988
		260	µM	*E. coli* H226Q	Anderson & Duckworth, 1988
		120	µM	*E. coli* wild	Anderson & Duckworth, 1988
	k_{cat}	9.3	s^-	*E. coli* H229Q	Anderson & Duckworth, 1988
		98	s^-	*E. coli* H226Q	Anderson & Duckworth, 1988
		81	s^-	*E. coli* wild	Anderson & Duckworth, 1988
Rev Rxn	K_A	159	µM	Rat kidney	Matsuoka & Srere, 1973
		420	µM	Human heart	Mukherjee *et al*, 1980
	K_B	32	µM	Rat kidney	Matsuoka & Srere, 1973
		70	µM	Human heart	Mukherjee *et al*, 1980
	V_m	1.67E-4	µM/s	Rat kidney	Matsuoka & Srere, 1973

Reverse Reaction:

No kinetic data were found for the reverse of Reaction 4 in *E. coli*. Studies of the citrate synthase in rat kidneys and the human heart provided kinetic parameters for the reverse reaction catalyzed by citrate synthase (Matsuoka & Srere, 1973; Mukherjee *et al*,

1980). Studies suggest that a random bi-bi mechanism is employed by this reaction (Matsuoka & Srere, 1973). Equation (5) represents a random bi-bi kinetic mechanism. Therefore, Equation (5) and the kinetic parameters in Table IV were used to model the reverse reaction in SimBiology with substrate A as citrate and substrate B as CoA.

$$\nu = \frac{V_{MAX}}{\frac{\alpha K_A K_B}{[A][B]} + \frac{\alpha K_A}{[A]} + \frac{\alpha K_B}{[B]} + 1} = \frac{k_{cat} * [E]}{\frac{\alpha K_A K_B}{[A][B]} + \frac{\alpha K_A}{[A]} + \frac{\alpha K_B}{[B]} + 1} \quad (5)$$

V_{MAX} = k_{cat}*[E] = [µM/s]
K_A = Dissociation constant for substrate A = [µM]
K_B = Dissociation constant for substrate B = [µM]
k_{cat} = Maximum number of rxns catalyzed per second = [s^-]
[A] = Concentration of substrate A = [µM]
[B] = Concentration of substrate B = [µM]
[E] = Concentration of enzyme = [µM]
α = Binding interaction factor
If α = 1, substrate binding is independent
If α > 1, binding of substrate decreases affinity of other
If α < 1, binding of substrate increases affinity of other

Reaction 5:

$$\text{Citrate} \xleftrightarrow{\text{Citrate hydro-lyase}} \text{Aconitate} + H_2O$$

Enzyme: Citrate hydro-lyase

Citrate hydro-lyase is an aconitase that catalyzes the reversible isomerization of citrate. *E. coli* has two major aconitases, AcnA and AcnB. AcnA is the aerobic-stationary phase enzyme, and AcnB is the major TCA cycle enzyme during exponential growth. AcnA is more stable than AcnB, and has a higher affinity for citrate. AcnB is the main catabolic enzyme because its sensitivity to oxidative or pH stress allows it to regulate the TCA cycle (Jordan *et al*, 1999).

Forward Reaction:

Studies indicate that this reaction exhibits normal Michaelis-Menten kinetics. Equation (4) was used to model the forward reaction. Kinetic parameters were found for both AcnA and AcnB as seen in Table V. It was decided to use AcnB values for this model because AcnB is the major TCA cycle enzyme (Jordan *et al*, 1999).

Reverse Reaction:

Studies indicate that this reaction exhibits Michaelis-Menten kinetics with a Hill cooperativity factor of 2.1 (Tsuchiya *et al*, 2009). Equation (6) represents Hill kinetics and was used to model the reverse reaction with the kinetic parameters found in Table V.

$$\nu = \frac{V_{MAX}[S]^n}{K_M + [S]^n} = \frac{k_{cat} * [E] * [S]^n}{K_M + [S]^n} \quad (6)$$

V_{MAX} = k_{cat}*[E] = [µM/s]
K_M = Substrate concentration resulting in $0.5V_{MAX}$ = [µM]
k_{cat} = Maximum number of rxns catalyzed per second = [s^-]
[S] = Concentration of substrate = [µM]
[E] = Concentration of enzyme = [µM]
n = Hill cooperativity coefficient

Table V. Kinetic parameters utilized for Reaction 5 in the model.

	Parameter	Value	Units	Organism	Reference
Fwd Rxn	K_m	1160[a]	µM	*E. coli* K-12 MG1655	Jordan *et al*, 1999
		11000[b]	µM	*E. coli* K-12 MG1655	Jordan *et al*, 1999
	V_m	0.102[a]	µM/s	*E. coli* K-12 MG1655	Jordan *et al*, 1999
		0.397[b]	µM/s	*E. coli* K-12 MG1655	Jordan *et al*, 1999
Rev Rxn	K_m	58[a]	µM	*E. coli* K-12 MG1655	Jordan *et al*, 1999
		16[b]	µM	*E. coli* K-12 MG1655	Jordan *et al*, 1999
	V_m	0.242[a]	µM/s	*E. coli* K-12 MG1655	Jordan *et al*, 1999
		0.652[b]	µM/s	*E. coli* K-12 MG1655	Jordan *et al*, 1999
	n	2.1	-	*E. coli* K-12 MG1655	Tsuchiya *et al*, 2009

a. *acnA*
b. *acnB*

Reaction 6:

$$\text{Aconitate} + H_2O \xleftrightarrow{\text{Isocitrate hydro-lyase}} \text{Isocitrate}$$

Enzyme: Isocitrate hydro-lyase

Isocitrate hydro-lyase is an aconitase that catalyzes the reversible isomerization of aconitate. As mentioned previously, *E. coli* has two major aconitases, AcnA and AcnB.

Forward Reaction:

Studies show that this reaction exhibits normal Michaelis-Menten kinetics with negative cooperativity (Jordan *et al*, 1999; Tsuchiya *et al*, 2009). Equation (6) was used to model the forward reaction. Kinetic parameters were found for both AcnA and AcnB as seen in Table VI. AcnB values were used for this model because AcnB is the major TCA cycle enzyme (Jordan *et al*, 1999).

Table VI. Kinetic parameters utilized for Reaction 6 in the model.

	Parameter	Value	Units	Organism	Reference
Fwd Rxn	K_m	58[a]	µM	*E. coli* K-12 MG1655	Jordan *et al*, 1999
		16[b]	µM	*E. coli* K-12 MG1655	Jordan *et al*, 1999
	V_m	0.242[a]	µM/s	*E. coli* K-12 MG1655	Jordan *et al*, 1999
		0.652[b]	µM/s	*E. coli* K-12 MG1655	Jordan *et al*, 1999
	n	0.727	-	*E. coli* K-12 MG1655	Tsuchiya *et al*, 2009
Rev Rxn	K_m	14[a]	µM	*E. coli* K-12 MG1655	Jordan *et al*, 1999
		51[b]	µM	*E. coli* K-12 MG1655	Jordan *et al*, 1999
	V_m	0.0595[a]	µM/s	*E. coli* K-12 MG1655	Jordan *et al*, 1999
		0.0987[b]	µM/s	*E. coli* K-12 MG1655	Jordan *et al*, 1999

a. acnA
b. acnB

Reverse Reaction:

Studies indicate that this reaction exhibits Michaelis-Menten kinetics (Jordan *et al*, 1999). Equation (4) was used to model the reverse reaction. Kinetic parameters were found for both AcnA and AcnB as seen in Table VI. AcnB values were used for this model because AcnB is the major TCA cycle enzyme (Jordan *et al*, 1999).

Reaction 7:

$$\text{Isocitrate} + \text{NADP}^+ \xrightarrow{\text{Isocitrate dehydrogenase}} \text{2-oxoglutarate} + \text{NADPH} + \text{CO}_2$$

Enzyme: Isocitrate dehydrogenase

Isocitrate dehydrogenase catalyzes the irreversible oxidative decarboxylation of isocitrate to 2-oxoglutarate. The enzyme is regulated by phosphorylation and dephosphorylation. Isocitrate is important because it allows *E. coli* to switch between the TCA cycle and the glyoxylate bypass pathway.

Forward Reaction:

Studies indicate that the reaction catalyzed by isocitrate dehydrogenase displays normal Michaelis-Menten kinetics (Lee *et al*, 1995). Therefore, Equation (4) was used to model the reaction utilizing the kinetic parameters from Table VII.

Table VII. Kinetic parameters utilized for Reaction 7 in the model.

	Parameter	Value	Units	Organism	Reference
	K_m	11.4	μM	*E. coli*	Lee *et al*, 1995
		6030	μM	*E. coli K230M*	Lee *et al*, 1995
Fwd		9.6	μM	*E. coli Y160F*	Lee *et al*, 1995
Rxn	k_{cat}	76.2	s^-	*E. coli*	Lee *et al*, 1995
		0.85	s^-	*E. coli K230M*	Lee *et al*, 1995
		0.311	s^-	*E. coli Y160F*	Lee *et al*, 1995

Reaction 8:

$$\text{2-oxoglutarate} + \text{CoA} + \text{NAD}^+ \xrightarrow{\text{2-oxoglutarate dehydrogenase}} \text{Succinyl-CoA} + \text{NADH} + \text{CO}_2$$

Enzyme: 2-oxoglutarate dehydrogenase complex

The 2-oxoglutarate dehydrogenase complex catalyzes the irreversible oxidative decarboxylation of 2-oxoglutarate to succinyl-CoA. The complex contains three components: 2-oxoglutarate decarboxylase (E1), lipoamide acyltransferase (E2), and lipoamide dehydrogenase (E3).

Forward Reaction:

The net forward reaction demonstrated normal Michaelis-Menten kinetics (McCormack & Denton, 1981). The kinetic parameters in Table VIII were used with Equation (4) to model the forward reaction.

Table VIII. Kinetic parameters utilized for Reaction 8 in the model.

	Parameter	Value	Units	Organism	Reference
Fwd Rxn	K_m	9.2	µM	*E. coli*	McCormack & Denton, 1981
		10.5	µM	*E. coli*	McCormack & Denton, 1981
	V_m	0.00363	µM /s	*E. coli*	McCormack & Denton, 1981

Reaction 9:

$$\text{Succinyl-CoA} + \text{ADP} + \text{P}^{\text{i}} + \text{H}^+ \xleftrightarrow{\text{Succinyl-CoA synthetase}} \text{Succinate} + \text{ATP} + \text{CoA}$$

Enzyme: Succinyl-CoA synthetase

Succinyl-CoA synthetase catalyzes substrate level phosphorylation in the TCA cycle by converting succinyl-CoA and ADP into succinate and ATP. In *E. coli,* the

enzyme exists as a tetramer and favors adenine over guanine nucleotides. In eukaryotes, guanine nucleotides are preferred (Birney *et al*, 1996). It is a multiple step reaction that uses a covalent enzyme-substrate intermediate. The phosphate group is transferred to the enzyme resulting in a phosphoenzyme that is then used to convert ADP into ATP.

Forward Reaction:

In the forward reaction, enzyme bound succinyl-phosphate is formed as an intermediate. The phosphate group is transferred to a histidine residue and succinate is released as a product. The phosphoenzyme then generates the second product, ATP.

The kinetic mechanism behind this reaction is not well understood. The reaction is similar to many reactions classified as ping-pong, but some studies support a sequential mechanism and the formation of a quaternary structure. Studies indicate that ADP is an allosteric regulator of the enzyme during the forward reaction (Um & Klein, 1993). The reaction displays an unusual catalytic property called substrate synergism. The presence of a substrate for one reaction stimulates another reaction. The exact mechanism for substrate synergism has yet to be defined in terms of an equation (Birney *et al*, 1996; Um & Klein, 1993).

Due to the lack of a kinetic mechanism and parameters, this reaction was modeled by using simple mass-action kinetics. It is hoped that future studies can provide a more accurate kinetic mechanism for this specific reaction.

Reverse Reaction:

The reverse reaction also has unusual catalytic properties, but some studies supported a sequential mechanism and were able to measure some kinetic parameters

(Joyce *et al*, 1999; Luo & Nishimura, 1991; Moffet & Bridger, 1970). An ordered bi-bi mechanism, Equation (3), was used to model the reverse reaction with substrate A as succinate and substrate B as CoA. The parameters shown in Table IX were used for Reaction 9 of the model.

Table IX. Kinetic parameters utilized for Reaction 9 in the model.

	Parameter	Value	Units	Organism	Reference
Fwd Rxn	k	1	s^-	NA	NA
Rev Rxn	K_A	590	µM	*E. coli*	Luo & Nishimura, 1991
		620	µM	*E. coli*	Luo & Nishimura, 1991
		250	µM	*E. coli*	Joyce *et al*, 1999
	K_B	7.6	µM	*E. coli*	Luo & Nishimura, 1991
		18	µM	*E. coli*	Luo & Nishimura, 1991
		4.0	µM	*E. coli*	Joyce *et al*, 1999
	k_{cat}	24.52	s^-	*E. coli*	Joyce *et al*, 1999

Reaction 10:

$$\text{Succinate} + \text{UQH}_2 \xleftrightarrow{\text{Succinate dehydrogenase}} \text{Fumarate} + \text{UQ} + 2\text{H}^+$$

Enzyme: Succinate dehydrogenase

Succinate dehydrogenase catalyzes the oxidation of succinate to fumarate under aerobic conditions. It can also catalyze the reverse reaction, the reduction of fumarate to succinate. Succinate dehydrogenase requires flavins, ubiquinone, or menaquinol as electron donors and acceptors.

Forward Reaction:

The oxidation of succinate to fumarate has demonstrated normal Michaelis-Menten kinetics in studies of *E. coli* (Cecchini *et al*, 2002; Maklashina *et al*, 2006). One

study indicated that succinate dehydrogenase was inhibited by oxaloacetate and malonate, but no mechanism was identified (Maklashina *et al*, 2006). This model utilized a noncompetitive inhibition mechanism, Equation (7), with oxaloacetate as the inhibitor. Kinetic parameters utilized in this model are shown in Table X.

$$\nu = \frac{V_{MAX}[S]}{(K_M + [S]) * \left(1 + I/K_i\right)} = \frac{k_{cat} * [E] * [S]}{(K_M + [S]) * \left(1 + I/K_i\right)} \quad (7)$$

V_{MAX} = k_{cat}*[E] = [µM/s]
K_M = Substrate concentration resulting in $0.5V_{MAX}$ = [µM]
K_i = Inhibitor concentration in $0.5V_{MAX}$ = [µM]
k_{cat} = Maximum number of rxns catalyzed per second = [s^-]
[S] = Concentration of substrate = [µM]
[E] = Concentration of enzyme = [µM]
[I] = Concentration of inhibitor = [µM]

Reverse Reaction:

The reduction of fumarate to succinate has displayed normal Michaelis-Menten kinetics in *E. coli* (Cecchini *et al*, 2002; Maklashina *et al*, 2006). This model utilized Equation (4) to simulate this reaction. Kinetic parameters utilized in this model are shown in Table X.

Table X. Kinetic parameters utilized for Reaction 10 in the model.

	Parameter	Value	Units	Organism	Reference
Fwd Rxn	K_m	110	µM	*E. coli*	Maklashina *et al*, 2006
		2	µM	*E. coli*	Cecchini *et al*, 2002
	K_i	0.07	µM	*E. coli*	Maklashina *et al*, 2006
	k_{cat}	110	s^-	*E. coli*	Maklashina *et al*, 2006
		85	s^-	*E. coli*	Cecchini *et al*, 2002
Rev Rxn	K_m	100	µM	*E. coli*	Maklashina *et al*, 2006
		5	µM	*E. coli*	Cecchini *et al*, 2002
	k_{cat}	2	s^-	*E. coli*	Maklashina *et al*, 2006
		1.7	s^-	*E. coli*	Cecchini *et al*, 2002

Reaction 11:

$$\text{Fumarate} + H_2O \xleftrightarrow{\text{Fumarase}} \text{Malate}$$

Enzyme: Fumarase

Fumarase catalyzes the reaction between fumarate and malate in the TCA cycle. There are three fumarase isozymes in *E. coli*. Fumarase A has the most activity under microaerophilic condition and is inactivated under aerobic conditions. Fumarase B has some activity in microaerophilic and aerobic conditions. Fumarase B also has a higher affinity for malate than fumarate. Fumarase C is highly active under aerobic conditions (Woods *et al*, 1988).

Forward and Reverse Reaction:

No kinetic mechanism was identified for Reaction 11. Normal Michaelis-Menten kinetics were assumed for the forward and reverse reactions. Equation (4) and the kinetic parameters in Table XI were utilized in the model of the forward and reverse reactions.

Table XI. Kinetic parameters utilized for Reaction 11 in the model.

	Parameter	Value	Units	Organism	Reference
Fwd Rxn	K_m	100	µM	*E. coli*	Rose & Weaver, 2004
	k_{cat}	60	s^-	*E. coli*	Rose & Weaver, 2004
Rev Rxn	K_m	300	µM	*E. coli*	Rose & Weaver, 2004
	k_{cat}	129	s^-	*E. coli*	Rose & Weaver, 2004

Reaction 12:

$$\text{Malate} + NAD^+ \xleftrightarrow{\text{Malate dehydrogenase}} \text{Oxaloacetate} + NADH + H^+$$

Enzyme: Malate dehydrogenase

Malate dehydrogenase catalyzes the reversible oxidation of malate to oxaloacetate. The enzyme uses NAD^+ as an electron acceptor. The activity of malate dehydrogenase is lower under anaerobic conditions.

Forward Reaction:

Studies indicate that this reaction follows an ordered bi-bi mechanism (Heyde & Ainsworth, 1968; Muslin *et al*, 1995). Equation (3) was used to model the forward reaction with substrate A as malate and substrate B as NAD^+. The kinetic parameters found in Table XII were utilized for the forward reaction in the model.

Reverse Reaction:

It was assumed that the reverse reaction would also follow an ordered bi-bi mechanism, so Equation (3) was employed to model the reaction with substrate A as oxaloacetate and substrate B as NADH. The kinetic parameters found in Table XII were used to model this reaction.

Table XII. Kinetic parameters utilized for Reaction 12 in the model.

	Parameter	Value	Units	Organism	Reference
Fwd Rxn	K_A	2600	µM	*E. coli*	Muslin *et al*, 1995
	K_B	260	µM	*E. coli*	Muslin *et al*, 1995
	k_{cat}	21	s^-	*E. coli*	Muslin *et al*, 1995
Rev Rxn	K_A	49	µM	*E. coli*	Muslin *et al*, 1995
	K_B	61	µM	*E. coli*	Muslin *et al*, 1995
	k_{cat}	900	s^-	*E. coli*	Muslin *et al*, 1995

Glyoxylate Pathway

The glyoxylate pathway is a shunt in the TCA cycle. It is composed of two reactions catalyzed by the enzymes isocitrate lyase and malate synthase shown in Figure 3. Using additional acetyl-CoA, this pathway can convert isocitrate into malate and succinate bypassing the conversion into 2-oxoglutarate and succinyl-CoA. This shunt generates intermediates to be used elsewhere in the cell, but fails to generate the energy and reducing power that is generated when isocitrate continues through the TCA cycle. The glyoxylate shunt is included in this model to more accurately represent the energy and reducing power generated in the TCA cycle.

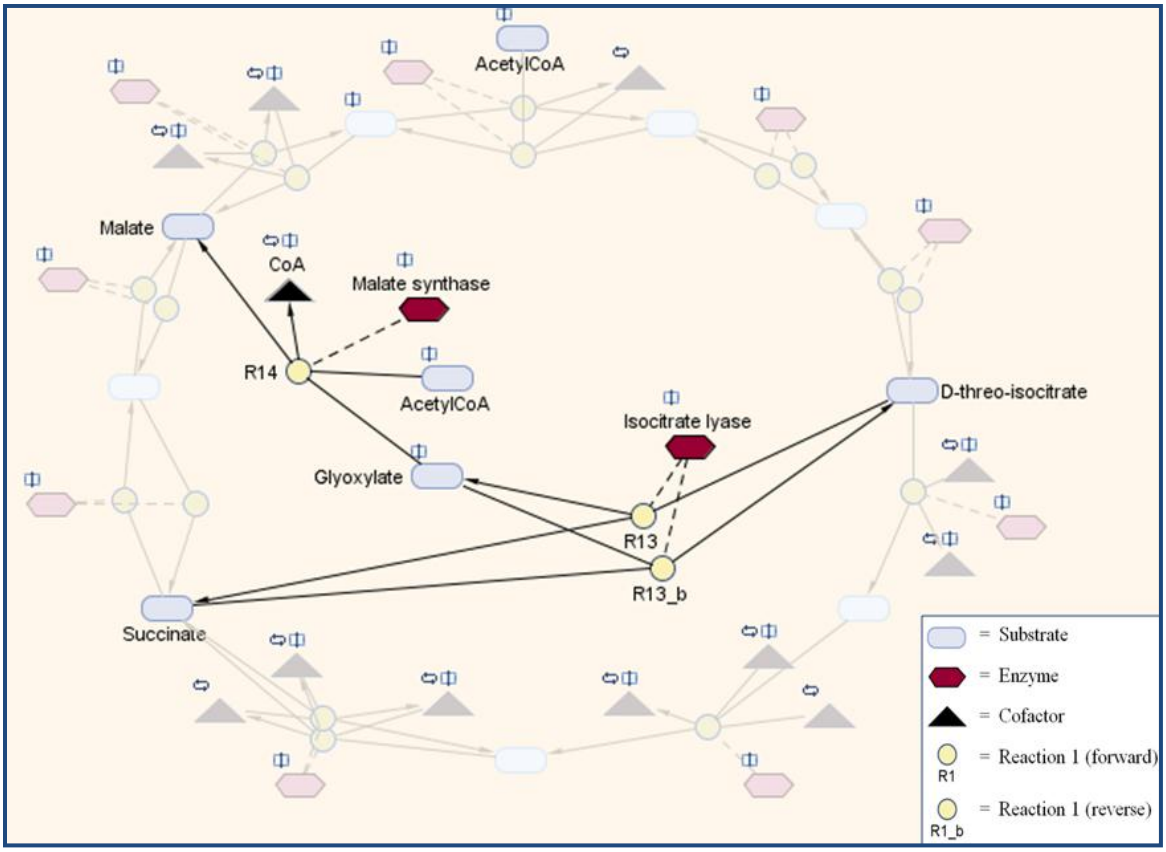

Figure 3. The metabolic pathway for the glyoxylate shunt in the TCA cycle.

Reaction 13:

$$\text{Isocitrate} \xleftrightarrow{\text{Isocitrate lyase}} \text{Glyoxylate} + \text{Succinate}$$

Enzyme: Isocitrate lyase

Isocitrate lyase catalyzes the cleavage of isocitrate into glyoxylate and succinate. This enzyme diverts isocitrate from the TCA cycle into the glyoxylate shunt.

Forward Reaction:

Isocitrate lyase cleaves isocitrate into glyoxylate and succinate in the forward direction. The pH in *E. coli* cells is around 7.3 to 7.6 (Mackintosh & Nimmo, 1988); therefore, the parameters measured at pH = 7.3 were utilized in the model. Phosphoenolpyruvate acts as a non-competitive inhibitor, but the K_i value suggests it is not significant *in vivo*. The species 3-phosphoglycerate is a competitive inhibitor of isocitrate lyase and is more significant due to its higher concentrations in the cell (Mackintosh & Nimmo, 1988). Equation (8) was used to model the competitive inhibition mechanism with 3-phosphoglycerate utilizing the parameters found in Table XIII.

$$\nu = \frac{V_{MAX}[S]}{K_M\left(1+ I/K_i\right)+[S]} = \frac{k_{cat}*[E]*[S]}{K_M\left(1+ I/K_i\right)+[S]} \quad (8)$$

V_{MAX} = k_{cat}*[E] = [µM/s]
K_M = Substrate concentration resulting in $0.5V_{MAX}$ = [µM]
K_i = Inhibitor concentration in $0.5V_{MAX}$ = [µM]
k_{cat} = Maximum number of rxns catalyzed per second = [s^-]
[S] = Concentration of substrate = [µM]
[E] = Concentration of enzyme = [µM]
[I] = Concentration of inhibitor = [µM]

Table XIII. Kinetic parameters utilized for Reaction 13 in the model.

	Parameter	Value	Units	Organism	Reference
Fwd Rxn	K_m	63[a]	µM	*E. coli* ML308	Mackintosh & Nimmo, 1988
		32[b]	µM	*E. coli* ML308	Mackintosh & Nimmo, 1988
	$K_{i,PEP}$	910[a]	µM	*E. coli* ML308	Mackintosh & Nimmo, 1988
		100[b]	µM	*E. coli* ML308	Mackintosh & Nimmo, 1988
	$K_{i,3PG}$	800[a]	µM	*E. coli* ML308	Mackintosh & Nimmo, 1988
		360[b]	µM	*E. coli* ML308	Mackintosh & Nimmo, 1988
	k_{cat}	28.5	s^-	*E. coli* ML308	Robertson & Nimmo, 1995
		19.5	s^-	*C. acremonium*	Perdiguero *et al*, 1995
Rev Rxn	K_A	590	µM	*E. coli* ML308	Mackintosh & Nimmo, 1988
	K_B	130	µM	*E. coli* ML308	Mackintosh & Nimmo, 1988
	k_{cat}	15.7	s^-	*C. acremonium*	Perdiguero *et al*, 1995

a. pH = 7.3
b. pH = 6.8

Reverse Reaction:

Isocitrate lyase condenses glyoxylate and succinate into isocitrate in the reverse reaction. This reaction occurs by a sequential random-order equilibrium mechanism where the substrate binding of glyoxylate and succinate are independent (Mackintosh & Nimmo, 1988). Equation (5) and the parameters in Table XIII were used to model the reaction with substrate A as succinate and substrate B as glyoxylate.

Reaction 14:

$$\text{Glyoxylate} + \text{Acetyl-CoA} + H_2O \xrightarrow{\text{Malate synthase}} \text{Malate} + \text{CoA} + H^+$$

Enzyme: Malate synthase

Malate synthase exists as two isozymes in *E. coli*. Malate synthase A is the enzyme utilized in the glyoxylate shunt in the TCA cycle. Malate synthase A catalyzes

the irreversible reaction of glyoxylate and acetyl-CoA into malate. Malate synthase B catalyzes the synthesis of glyoxylate from glycolate (Molina *et al*, 1994).

Forward Reaction:

Malate synthase catalyzes the Claisen condensation of glyoxylate and acetyl-CoA into a malyl-CoA intermediate. The malyl-CoA intermediate is then cleaved into the two products, malate and CoA. Pyruvate is a competitive inhibitor to malate synthase (Anstrom *et al*, 2003). Studies indicate that this reaction proceeds through a random sequential mechanism with independent substrate binding. Equation (5) and the kinetic parameters shown Table XIV were used to model the reaction with substrate A as glyoxylate and substrate B as acetyl-CoA.

Table XIV. Kinetic parameters utilized for Reaction 14 in the model.

	Parameter	Value	Units	Organism	Reference
Fwd Rxn	K_A	21	µM	*E. coli*	Anstrom *et al*, 2003
		100	µM	*S. cerevisiae*	Durchschlag *et al*, 1981
	K_B	9.0	µM	*E. coli*	Anstrom *et al*, 2003
		83	µM	*S. cerevisiae*	Durchschlag *et al*, 1981
	K_i	1000	µM	*E. coli*	Anstrom *et al*, 2003
	α	1.0	-	*S. cerevisiae*	Durchschlag *et al*, 1981
	k_{cat}	48.1	s^-	*E. coli*	Anstrom *et al*, 2003

Glycolysis/Gluconeogenesis

Glycolysis is the metabolic pathway that breaks down glucose into pyruvate while generating a small amount of energy and reducing power. Glycolysis is composed of ten reactions seen in Figure 4. The enzymes that catalyze these ten reactions are glucokinase, phosphoglucose isomerase, 6-phosphofructokinase, fructose-bisphosphate aldolase, triose phosphate isomerase, glyceraldehyde-3-phosphate dehydrogenase, phosphoglycerate kinase, phosphoglycerate mutase, enolase, and pyruvate kinase. Cofactors that participate in glycolysis are ADP/ATP, $NADH/NAD^+$, and P_i. Glycolysis was included in this model because glucose is a common substrate used to grow cells and produce PHB.

Gluconeogenesis is a metabolic pathway that can convert pyruvate back into glucose. It includes many of the same enzymes as glycolysis. Gluconeogenesis uses five additional enzymes: glucose-1-phosphatase, phosphoglucomutase, fructose-1,6-bisphosphatase, phosphoenolpyruvate carboxykinase, and phosphoenolpyruvate synthetase. Gluconeogenesis includes 12 reactions as shown in Figure 4. Gluconeogenesis was included in this model to account for the conversion of pyruvate into glucose. Gluconeogenesis can occur when the concentrations of acetyl-CoA and citrate are high and the concentration of glucose is low.

Reaction 15:

Forward Reaction:

$$\text{Glucose} + \text{ATP} \xrightarrow{\text{Glucokinase}} \text{Glucose-6-phosphate} + \text{ADP} + \text{P}^{\text{i}}$$

F

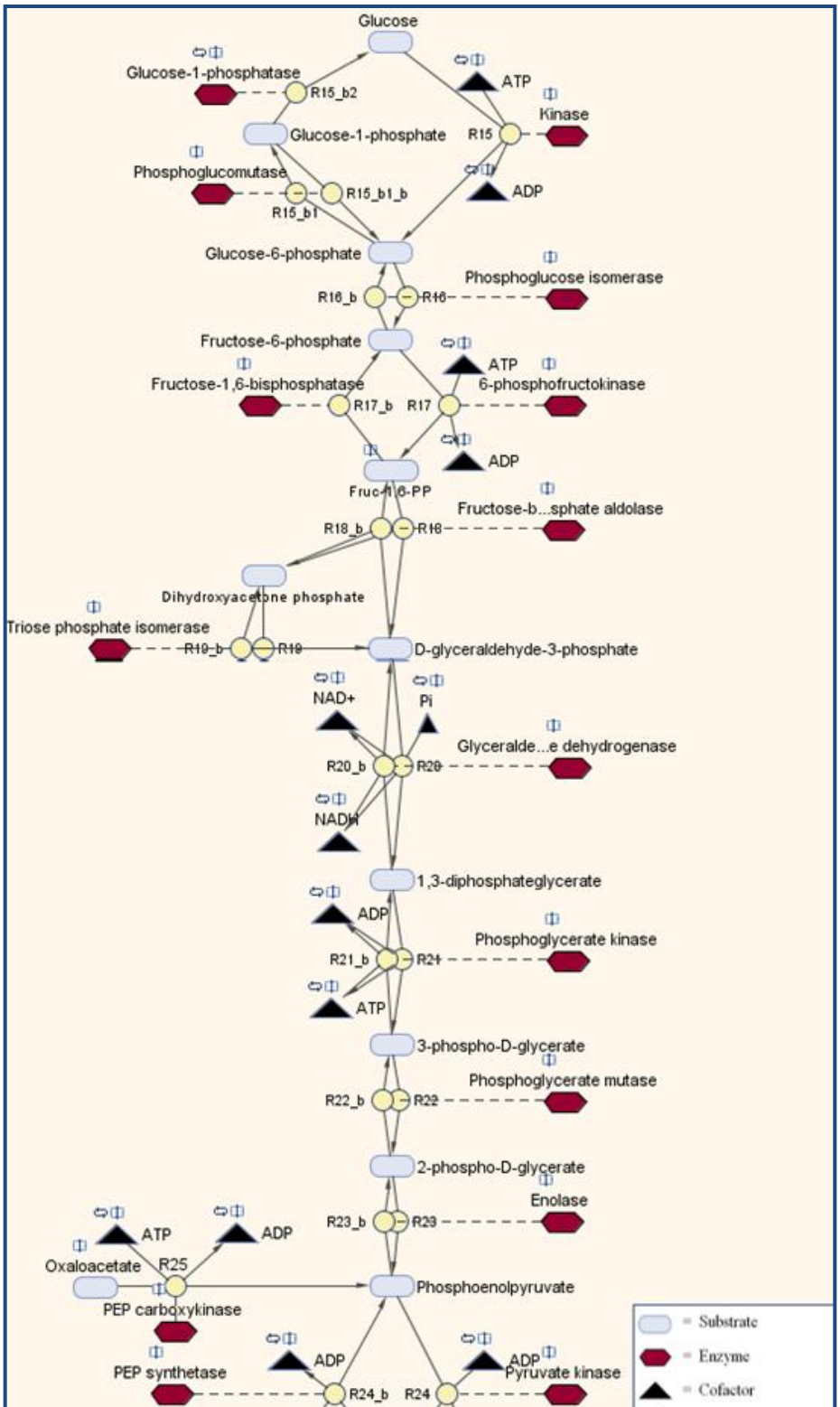
Glucose
Glucose-1-phosphatase
R15_b2
ATP
Kinase
Glucose-1-phosphate
R15
Phosphoglucomutase
R15_b1_b
R15_b1
ADP
Glucose-6-phosphate
Phosphoglucose isomerase
R16_b
R16
Fructose-6-phosphate
ATP
Fructose-1,6-bisphosphatase
R17_b
R17
6-phosphofructokinase
ADP
Fruc-1,6-PP
Fructose-b...sphate aldolase
R18_b
R18
Dihydroxyacetone phosphate
Triose phosphate isomerase
R19_b
R19
D-glyceraldehyde-3-phosphate
NAD+
Pi
Glyceralde...e dehydrogenase
R20_b
R20
NADH
1,3-diphosphateglycerate
ADP
Phosphoglycerate kinase
R21_b
R21
ATP
3-phospho-D-glycerate
Phosphoglycerate mutase
R22_b
R22
2-phospho-D-glycerate
Enolase
R23_b
R23
ATP
ADP
Oxaloacetate
R25
Phosphoenolpyruvate
PEP carboxykinase
PEP synthetase
ADP
R24_b
R24
ADP
Pyruvate kinase
Substrate
Enzyme
Cofactor

igure 4. The metabolic pathway for glycolysis and gluconeogenesis.

The forward reaction is catalyzed by the enzyme glucokinase. Glucokinase phosphorylates glucose into the product glucose-6-phosphate. The reaction requires ATP to proceed. The kinetic mechanism for glucokinase has been studied in several organisms such as *Z. mobilis* and *P. shermanii*. It is hypothesized that the mechanism will be the same in *E. coli* because it is consistent with the crystal structure of the *E. coli* glucokinase. Studies indicate that the mechanism is a preferred order of substrate addition and product release. Glucose is added first followed by ATP (Lunin *et al*, 2004). An ordered bi-bi mechanism, Equation (3), was used to model the forward reaction with the kinetics parameters found in Table XV.

Reverse Reaction:

The conversion of glucose-6-phosphate back into glucose is a two step process that involves two enzymes: phosphoglucomutase and glucose-1-phosphatase.

Step 1:

$$\text{Glucose-6-phosphate} \xleftrightarrow{\text{Phosphoglucomutase}} \text{Glucose-1-phosphate}$$

Step one is a reversible reaction catalyzed by phosphoglucomutase where glucose-6-phosphate is converted into glucose-1-phosphate via the intermediate glucose-1,6-diphosphate. No kinetic data were found for *E. coli* in the direction of glucose-6-phosphate to glucose-1-phosphate, but there was kinetic data from phosphoglucomutase in rat heart cells. Normal Michaelis-Menten kinetics, Equation (4), were assumed and kinetic parameters found in Table XV were utilized in the model.

A thermophilic phosphoglucomutase that was similar to the *E. coli* enzyme demonstrated a ping-pong catalytic mechanism in the direction of glucose-1-phosphate to glucose-6-phosphate (Yoshizaki *et al*, 1971). Other studies have also suggested a ping-pong mechanism (Ray & Roscelli, 1964). It was decided to use normal Michaelis-Menten kinetics for the reverse direction of Step 1 to simplify the model. Equation (4) was utilized along with the kinetic parameters found in Table XV.

Step 2:

$$\text{Glucose-1-phosphate} + H_2O \xrightarrow{\text{Glucose-1-phosphatase}} \text{Glucose} + P^i$$

Step 2 is an irreversible reaction where glucose-1-phosphate is converted into glucose by the enzyme glucose-1-phophatase. Normal Michaelis-Menten kinetics, Equation (4), were used to model the reaction with the parameters found in Table XV.

Table XV. Kinetic parameters utilized for Reaction 15 in the model.

	Parameter	Value	Units	Organism	Reference
Fwd Rxn	K_A	780	µM	*E. coli*	Meyer *et al*, 1997
	K_B	3760	µM	*E. coli*	Meyer *et al*, 1997
	V_m	2.643	µM/s	*E. coli*	Meyer *et al*, 1997
Rev Rxn Step 1 Fwd	K_M	670	µM	Rat heart	Kashiwaya *et al*, 1994
	V_m	1.12	µM/s	Rat heart	Kashiwaya *et al*, 1994
Rev Rxn Step 1 Rev	K_m	60	µM	*E. coli*	Josh & Handler, 1964
		6700	µM	*E. coli*	Dworniczak *et al*, 2008
	V_m	0.001	µM /s	*E. coli*	Dworniczak *et al*, 2008
Rev Rxn Step 2	K_m	240	µM	*E. coli*	Kuznetsova *et al*, 2006
	k_{cat}	1.4	s^-	*E. coli*	Kuznetsova *et al*, 2006

Reaction 16:

$$\text{Glucose-6-phosphate} \xleftrightarrow{\text{Phosphoglucose isomerase}} \text{Fructose-6-phosphate}$$

Enzyme: Phosphoglucose isomerase

Reaction 16 is a reversible reaction catalyzed by the enzyme phosphoglucose isomerase. The enzyme converts glucose-6-phosphate into fructose-6-phosphate or vice versa.

Forward and Reverse Reaction:

A study in *E. coli* indicated that the kinetic mechanism utilized in this reaction was a uni-uni reversible that utilized the Haldane relationship (Ishii *et al*, 2007). Equation (9) and the kinetic parameters shown in Table XVI were used to model this reaction. Glucose-6-phosphate was used as substrate A, and fructose-6-phosphate was used as substrate B. The reverse reaction uses the same kinetics as the forward reaction (Ishii *et al*, 2007); therefore, it was modeled using the same equation and parameters.

$$\nu = \frac{V_{MAX}\left([A] - {[B]}/{K_{eq}}\right)}{K_A\left(1 + {[B]}/{K_B}\right) + [A]} = \frac{k_{cat} * [E] * \left([A] - {[B]}/{K_{eq}}\right)}{K_A\left(1 + {[B]}/{K_B}\right) + [A]} \quad (9)$$

V_{MAX} = k_{cat}*[E] = [µM/s]
K_A = Dissociation constant for substrate A = [µM]
K_B = Dissociation constant for substrate B = [µM]
k_{cat} = Maximum number of rxns catalyzed per second = [s^-]
K_{eq} = Equilibrium constant [unitless]
[A] = Concentration of substrate A = [µM]
[B] = Concentration of substrate B = [µM]
[E] = Concentration of enzyme = [µM]

Table XVI. Kinetic parameters utilized for Reaction 16 in the model.

	Parameter	Value	Units	Organism	Reference
	K_A	3000	µM	*E. coli* K-12	Ishii *et al*, 2007
Fwd	K_B	160	µM	*E. coli* K-12	Ishii *et al*, 2007
Rxn	K_{eq}	0.3	-	*E. coli* K-12	Ishii *et al*, 2007
	V_m	25.18	µM/s	*E. coli* K-12	Ishii *et al*, 2007

Reaction 17:

Forward Reaction:

$$\text{Fructose-6-phosphate} + \text{ATP} \xrightarrow{\text{6-phosphofructokinase}} \text{Fructose-1,6-bisphosphate} + \text{ADP} + 2\text{H}^+$$

Enzyme: 6-phosphofructokinase

The ATP dependent 6-phosphofructokinase catalyzes the phosphorylation of fructose-6-phosphate into fructose-1,6-bisphosphate. An ordered bi-bi reaction mechanism has been proposed for this reaction in *E. coli* with fructose-6-phosphate as substrate A and ATP as substrate B (Campos *et al*, 1984). Equation (3) and the kinetic parameters shown in Table XVII were utilized in the model of the forward direction of Reaction 17.

Reverse Reaction:

$$\text{Fructose-1,6-bisphosphate} + \text{H}_2\text{O} \xrightarrow{\text{Fructose-1,6-bisphosphatase}} \text{Fructose-6-phosphate} + \text{P}^{\text{i}}$$

Enzyme: Fructose-1,6-bisphosphatase

Fructose-1,6-bisphosphatase catalyzes the dephosphorylation of fructose-1,6-bisphosphate to fructose-6-phosphate. There are four major genes that encode for fructose-1,6-bisphosphatase in *E. coli: fbp, yphA, yggF, glpX*. Fbp is the main fructose-1,6-bisphosphatase in the cell. YggF and GlpX are type II fructose-1,6-bisphosphatases.

Hill kinetics have been shown for this reaction in *E. coli* with a cooperativity factor of 2.0 (Brown *et al*, 2009). Equation (6) and the kinetic parameters shown in Table XVII were used to model the reverse direction of Reaction 17. Values for all four

fructose-1,6-bisphosphatases are shown in Table XVII but only values for Fbp were used in the model.

Table XVII. Kinetic parameters utilized for Reaction 17 in the model.

	Parameter	Value	Units	Organism	Reference
Fwd Rxn	K_A	107	µM	*E. coli*	Wang & Kemp, 1999
	K_B	32	µM	*E. coli*	Campos *et al*, 1984
		210	µM	*E. coli*	Wang & Kemp, 1999
		20	µM	*E. coli*	Campos *et al*, 1984
	k_{cat}	82	s^-	*E. coli*	Wang & Kemp, 1999
Rev Rxn	K_m	20[a]	µM	*E. coli*	Brown *et al*, 2009
		2400[b]	µM	*E. coli*	Brown *et al*, 2009
		70[c]	µM	*E. coli*	Brown *et al*, 2009
		100[d]	µM	*E. coli*	Brown *et al*, 2009
	V_m	0.403[a]	µM /s	*E. coli*	Brown *et al*, 2009
		0.16[b]	µM /s	*E. coli*	Brown *et al*, 2009
		0.067[c]	µM /s	*E. coli*	Brown *et al*, 2009
		0.15[d]	µM /s	*E. coli*	Brown *et al*, 2009
	k_{cat}	14.6[a]	s^-	*E. coli*	Brown *et al*, 2009
		5.3[b]	s^-	*E. coli*	Brown *et al*, 2009
		2.5[c]	s^-	*E. coli*	Brown *et al*, 2009
		5.7[d]	s^-	*E. coli*	Brown *et al*, 2009
	n	2.0	-	*E. coli*	Brown *et al*, 2009

a. Fbp fructose-1,6-bisphosphatase
b. YbhA fructose-1,6-bisphosphatase
c. YggF fructose-1,6-bisphosphatase
d. GlpX fructose-1,6-bisphosphatase

Reaction 18:

$$\text{Fructose-1,6-bisphosphate} \xleftrightarrow{\text{Fructose-bisphosphate aldolase}} \text{Dihydroxyacetone phosphate} + \text{Glyceraldehyde-3-phosphate}$$

Enzyme: Fructose-bisphosphate aldolase

Fructose-bisphosphate aldolase catalyzes the aldol cleavage of fructose-1,6-bisphosphate into dihydroxyacetone phosphate and glyceraldehyde-3-phosphate.

Forward Reaction:

Normal Michaelis-Menten kinetics were observed for the cleavage of fructose-1,6-bisphosphate in *E. coli* (Plater *et al*, 1999). Equation (4) and the kinetic parameters shown in Table XVIII were used to model this reaction.

Reverse Reaction:

The reverse reaction proceeds via a ping-pong mechanism (Lambeth & Kushmerick, 2002). Equation (2) and the kinetic parameters in Table XVIII were used to model the reverse reaction in SimBiology. Substrate A was dihydroxyacetone phosphate and substrate B was glyceraldehyde-3-phosphate in the model.

Table XVIII. Kinetic parameters utilized for Reaction 18 in the model.

	Parameter	Value	Units	Organism	Reference
Fwd Rxn	K_m	230	µM	*E. coli*	Plater *et al*, 1999
	k_{cat}	0.07	s^-	*E. coli*	Plater *et al*, 1999
Rev Rxn	K_A	2100	µM	Rabbit	Lambeth & Kushmerick, 2002
	K_B	1100	µM	Rabbit	Lambeth & Kushmerick, 2002
	V_m	1733	µM /s	Rabbit	Lambeth & Kushmerick, 2002

Reaction 19:

$$\text{Dihydroxyacetone phosphate} \xleftrightarrow{\text{Triose phosphate isomerase}} \text{Glyceraldehyde-3-phosphate}$$

Enzyme: Triose phosphate isomerase

Triose phosphate isomerase catalyzes the conversion of dihydroxyacetone phosphate into glyceraldehyde-3-phosphate via a cis-ene-diolate intermediate. Triose phosphate isomerase is considered to be a perfect enzyme.

Forward and Reverse Reaction:

The forward and reverse reactions are expressed by normal Michaelis-Menten kinetics (Nickbarg & Knowles, 1988). Equation (4) and the parameters in Table XIX were used to model the reaction.

Table XIX. Kinetic parameters utilized for Reaction 19 in the model.

	Parameter	Value	Units	Organism	Reference
Fwd Rxn	K_m	2300	µM	*E. coli*	Nickbarg & Knowles, 1988
	K_{eq}	750	µM	*E. coli*	Nickbarg & Knowles, 1988
	k_{cat}	750	s^-	*E. coli*	Nickbarg & Knowles, 1988
Rev Rxn	K_m	320	µM	Rabbit	Lambeth & Kushmerick, 2002
	V_m	200	µM /s	Rabbit	Lambeth & Kushmerick, 2002

Reaction 20:

$$\text{Glyceraldehyde-3-phosphate} + P^i + NAD^+ \xleftrightarrow{\text{Glyceraldehyde-3-phosphate dehydrogenase}} \text{1,3-diphosphateglycerate} + NADH + H^+$$

Enzyme: Glyceraldehyde-3-phosphate dehydrogenase

The enzyme glyceraldehyde-3-phosphate dehydrogenase catalyzes the reversible oxidation of glyceraldehyde-3-phosphate into 1,3-diphosphateglycerate. The cofactor NAD^+ is reduced to NADH during the reaction.

Forward Reaction:

The forward reaction proceeds via a sequential ordered ter-bi mechanism (Wang & Alaupovic, 1980). Ordered ter-bi reactions can be represented by the ordered ter-ter kinetic expression for steady-state and rapid equilibrium kinetics (Purich & Allison, 2000). Equation (10) and the kinetic parameters found in Table XX were used to model

the forward reaction in SimBiology. In the equation, substrate A was NAD^+, substrate B was glyceraldehyde-3-phosphate, and substrate C was inorganic phosphate.

$$v = \frac{V_{MAX}}{\frac{K_{iA}K_{iB}K_{mC}}{[A][B][C]} + \frac{K_{iB}K_{mC}}{[B][C]} + \frac{K_{iA}K_{mB}}{[A][B]} + \frac{K_{mC}}{[C]} + \frac{K_{mB}}{[B]} + \frac{K_{mA}}{[A]} + 1} \quad (10)$$

V_{MAX} = k_{cat}*[E] = [µM/s]
K_A = Dissociation constant for substrate A = [µM]
K_B = Dissociation constant for substrate B = [µM]
K_C = Dissociation constant for substrate C = [µM]
K_{iA} = Binding constant for substrate A = [µM]
K_{iB} = Binding constant for substrate B = [µM]
K_{iC} = Binding constant for substrate C = [µM]
k_{cat} = Maximum number of rxns catalyzed per second = [s^-]
[A] = Concentration of substrate A = [µM]
[B] = Concentration of substrate B = [µM]
[C] = Concentration of substrate C = [µM]
[E] = Concentration of enzyme = [µM]

Table XX. Kinetic parameters utilized for Reaction 20 in the model.

	Parameter	Value	Units	Organism	Reference
Fwd Rxn	K_A	90	µM	Rabbit	Lambeth & Kushmerick, 2002
	K_B	290	µM	*S. mutans*	Crow & Wittenberger, 1979
		2.5	µM	Rabbit	Lambeth & Kushmerick, 2002
	K_C	290	µM	Rabbit	Lambeth & Kushmerick, 2002
	V_m	0.38	µM/s	*S. mutans*	Crow & Wittenberger, 1979
Rev Rxn	K_A	0.8	µM	Rabbit	Lambeth & Kushmerick, 2002
	K_B	3.3	µM	Rabbit	Lambeth & Kushmerick, 2002
	V_m	21.08	µM /s	Rabbit	Lambeth & Kushmerick, 2002

Reverse Reaction:

The reverse reaction has a sequential ordered bi-ter mechanism (Wang & Alaupovic, 1980). Ordered bi-ter reactions can be represented by the ordered bi-bi kinetic expression for steady-state and rapid equilibrium kinetics (Purich & Allison, 2000). Equation (3) and the kinetic parameters found in Table XX were used to model the

forward reaction in SimBiology. Substrate A was set as 1,3-diphosphateglycerate and substrate B was set as NADH.

Reaction 21:

$$\text{1,3-diphosphateglycerate} + \text{ADP} + \text{H}^+ \xleftrightarrow{\text{Phosphoglycerate kinase}} \text{3-phosphoglycerate} + \text{ATP}$$

Enzyme: Phosphoglycerate kinase

Phosphoglycerate kinase catalyzes the phosphoryl group transfer from 1,3-diphosphateglycerate to ADP to form ATP and 3-phosphoglycerate.

Forward Reaction:

The forward reaction catalyzed by phosphoglycerate kinase follows a sequential random bi-bi mechanism (Lavoinne *et al*, 1983). Equation (5) and the kinetic parameters in Table XXI were used to model the reaction. Substrate binding was assumed to be independent with substrate A as 1,3-diphosphateglycerate and substrate B as ADP.

Table XXI. Kinetic parameters utilized for Reaction 21 in the model.

	Parameter	Value	Units	Organism	Reference
Fwd Rxn	K_A	2.2	µM	Rabbit	Lambeth & Kushmerick, 2002
	K_B	50	µM	Pig	Lambeth & Kushmerick, 2002
	V_m	18.7	µM/s	Pig	Lambeth & Kushmerick, 2002
Rev Rxn	K_A	1200	µM	Pig	Lambeth & Kushmerick, 2002
	K_B	360	µM	Rabbit	Lambeth & Kushmerick, 2002
	V_m	18.7	µM/s	Pig	Lambeth & Kushmerick, 2002

Reverse Reaction:

The reverse reaction catalyzed by phosphoglycerate kinase also follows a sequential random bi-bi mechanism (Lavoinne *et al*, 1983). Equation (5) and the kinetic

parameters in Table XXI were used to model the reaction. Substrate binding was assumed to be independent with substrate A as 3-phosphoglycerate and substrate B as ATP.

Reaction 22:

$$\text{3-phosphoglycerate} + \text{H}^+ \xleftrightarrow{\text{Phosphoglycerate mutase}} \text{2-phosphoglycerate}$$

Enzyme: Phosphoglycerate mutase

Phosphoglycerate mutase catalyzes the intramolecular phosphoryl group transfer to form 2-phosphoglycerate from 3-phosphoglycerate. A histidine-phosphoenzyme intermediate is formed during the reaction.

Forward and Reverse Reaction:

No kinetic mechanism was identified in the literature for Reaction 22; therefore, normal Michaelis-Menten kinetics were assumed for the reaction in SimBiology. Equation (4) and the kinetic parameters in Table XXII were used to model Reaction 22.

Table XXII. Kinetic parameters utilized for Reaction 22 in the model.

	Parameter	Value	Units	Organism	Reference
	K_m	200	µM	*E. coli dPGM*	Fraser *et al*, 1999
Fwd		210	µM	*E. coli iPGM*	Fraser *et al*, 1999
Rxn	k_{cat}	330	s^-	*E. coli dPGM*	Fraser *et al*, 1999
		22	s^-	*E. coli iPGM*	Fraser *et al*, 1999
	K_m	190	µM	*E. coli dPGM*	Fraser *et al*, 1999
Rev		97	µM	*E. coli iPGM*	Fraser *et al*, 1999
Rxn	k_{cat}	220	s^-	*E. coli dPGM*	Fraser *et al*, 1999
		10	s^-	*E. coli iPGM*	Fraser *et al*, 1999

Reaction 23:

$$\text{2-phosphoglycerate} \overset{\text{Enolase}}{\longleftrightarrow} \text{Phosphoenolpyruvate} + H_2O + H^+$$

Enzyme: Enolase

Enolase catalyzes the dehydration of 2-phosphoglycerate that produces the high energy compound phosphoenolpyruvate.

Forward and Reverse Reaction:

No kinetic mechanism was identified for Reaction 23. Both reactions were assumed to proceed via normal Michaelis-Menten kinetics. Equation (4) and the kinetic parameters shown in Table XXIII were used to model the reaction in SimBiology.

Table XXIII. Kinetic parameters utilized for Reaction 23 in the model.

	Parameter	Value	Units	Organism	Reference
Fwd Rxn	K_m	100	µM	*E. coli*	Spring & Wold, 1971
		120	µM	Rat	Lambeth & Kushmerick, 2002
	V_m	3	µM/s	*E. coli*	Spring & Wold, 1971
Rev Rxn	K_m	370	µM	Rat	Lambeth & Kushmerick, 2002
	V_m	3.2	µM/s	Rabbit	Lambeth & Kushmerick, 2002

Reaction 24:

Forward Reaction:

$$\text{Phosphoenolpyruvate} + \text{ADP} + 2H^+ \xrightarrow{\text{Pyruvate kinase}} \text{Pyruvate} + \text{ATP}$$

Enzyme: Pyruvate kinase

The forward reaction is catalyzed by pyruvate kinase and has been shown to have a sequential random bi-bi mechanism (Giles *et al*, 1976; Waygood *et al*, 1976). Equation

(5) and the kinetic parameters found in Table XXIV were used to model the reaction in SimBiology. Substrate A was set as phosphoenolpyruvate and substrate B was set as ADP.

Reverse Reaction:

$$\text{Pyruvate} + \text{ATP} + \text{H}_2\text{O} \xrightarrow{\text{Phosphoenolpyruvate synthetase}} \text{Phosphoenolpyruvate} + \text{AMP} + 3\text{H}^+ + \text{P}^{\text{i}}$$

Enzyme: Phosphoenolpyruvate synthetase

The reverse reaction is catalyzed by phosphoenolpyruvate synthetase and proceeds via a ping-pong mechanism (Sigman, 1990). Equation (2) and the values in Table XXIV were used in the model with substrate A as pyruvate and substrate B as ATP.

Table XXIV. Kinetic parameters utilized for Reaction 24 in the model.

	Parameter	Value	Units	Organism	Reference
Fwd Rxn	K_A	25	µM	*E. coli*	Valentini *et al*, 2000
		80	µM	Rat	Lambeth & Kushmerick, 2002
	K_B	280	µM	*E. coli*	Valentini *et al*, 2000
		300	µM	Rat	Lambeth & Kushmerick, 2002
	k_{cat}	103	s^-	*E. coli*	Valentini *et al*, 2000
		110	s^-	*E. coli*	Valentini *et al*, 2000
Rev Rxn	K_A	7050	µM	Rabbit	Lambeth & Kushmerick, 2002
	K_B	820	µM	Rabbit	Lambeth & Kushmerick, 2002
	V_m	24	µM/s	Rabbit	Lambeth & Kushmerick, 2002

Reaction 25:

$$\text{Oxaloacetate} + \text{ATP} \xrightarrow{\text{Phosphoenolpyruvate carboxykinase}} \text{Phosphoenolpyruvate} + \text{CO}_2 + \text{ADP} + \text{H}^+$$

Enzyme: Phosphoenolpyruvate carboxykinase

Phosphoenolpyruvate carboxykinase catalyzes the irreversible conversion of oxaloacetate into phosphoenolpyruvate via a sequential random bi-bi mechanism (Krebs & Bridger, 1980). Equation (5) and the kinetic parameters shown in Table XXV were used to model this reaction in SimBiology. Substrate binding was assumed to be independent with substrate A as oxaloacetate and substrate B as ATP.

Table XXV. Kinetic parameters utilized for Reaction 25 in the model.

	Parameter	Value	Units	Organism	Reference
Fwd Rxn	K_A	670	µM	*E. coli*	Krebs & Bridger, 1980
	K_B	60	µM	*E. coli*	Krebs & Bridger, 1980
	V_m	0.02	µM/s	*E. coli*	Krebs & Bridger, 1980

Acetyl-CoA Synthesis

Acetyl-CoA synthesis is a metabolic pathway composed of one reaction. This reaction is catalyzed by the enzyme complex pyruvate dehydrogenase as shown in Figure 5. This reaction converts pyruvate into acetyl-CoA with the help of the cofactor CoA. This pathway was included in the model because of the use of acetyl-CoA as the starting substrate in the PHB synthesis pathway.

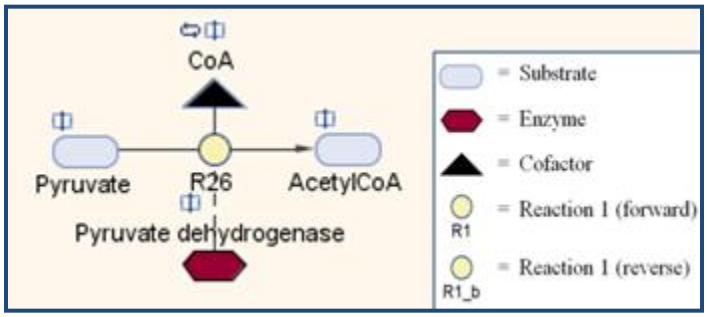

Figure 5. The metabolic pathway for acetyl-CoA synthesis.

Reaction 26:

$$\text{Pyruvate} + \text{CoA} + \text{NAD}^+ \xrightarrow{\text{Pyruvate dehydrogenase}} \text{Acetyl-CoA} + \text{CO}_2 + \text{NADH}$$

Enzyme: Pyruvate dehydrogenase complex

The pyruvate dehydrogenase complex catalyzes an irreversible reaction to produce acetyl-CoA from pyruvate, the product of glycolysis. It is a large, multienzyme complex composed of three distinct types of enzyme. The pyruvate dehydrogenase complex has several catalytic cofactors that include CoA, NAD^+, thiamine pyrophosphate (TPP), lipoamide, and FAD. The complex reaction can be broken down into four steps.

Step 1:

In the first step, pyruvate is decarboxylated after it combines with TPP. This stage of the reaction is catalyzed by the pyruvate dehydrogenase component of the complex (E1). This step exhibits tight-binding inhibition with thiamine 2-thiazolone diphosphate (ThTDP), and with thiamine 2-thiothiazolone diphosphate (ThTTDP) (Liu & Bisswanger, 2003; Nemeria *et al*, 2001).

$$\text{Pyruvate} + \text{TPP} \xrightarrow{\text{E1}} \text{Hydroxyethyl-TPP} + \text{CO}_2$$

Step 2:

In the second step, the hydroxyethyl attached to the TPP is oxidized to form an acetyl group that is transferred to lipoamide. This stage of the reaction is also catalyzed by the pyruvate dehydrogenase component of the complex (E1) (Liu & Bisswanger, 2003; Nemeria *et al*, 2001).

$$\text{Hydroxyethyl-TPP} + \text{Lipoamide} \xrightarrow{\text{E1}} \text{Carbanion of TPP} + \text{Acetyllipoamide}$$

Step 3:

In the third step, the acetyl group is transferred from acetyllipoamide to CoA to form acetyl-CoA. Dihydrolipoyl transacetylase (E2) catalyzes this step (Snoep *et al*, 1992; Willms *et al*, 1967).

$$\text{Acetyllipoamide} + \text{HS-CoA} \xrightarrow{\text{E2}} \text{Dihydrolipoamide} + \text{Acetyl-CoA}$$

Step 4:

In the fourth step, the oxidized lipoamide is regenerated using NAD^+. This stage of the reaction is catalyzed by dihydrolipoyl dehydrogenase (E3) (Allison *et al*, 1988).

$$\text{Dihydrolipoamide} + NAD^+ \xrightarrow{\text{E3}} \text{Lipoamide} + \text{NADH} + H^+$$

Overall Reaction:

Kinetic studies on the pyruvate dehydrogenase complex from the bovine kidney have demonstrated that the overall reaction fits a random bi-bi mechanism as well as the Theorell-Chance mechanism (Butterworth *et al*, 1975).

In *E. coli*, studies have shown that the first step catalyzed by the E1 component of the enzyme complex is the rate-limiting step (Liu & Bisswanger, 2003). Michaelis-Menten kinetic parameters have been determined for the overall reaction in *E. coli.* Equation (4) and the parameters in Table XXVI were used to model the overall reaction in SimBiology.

Table XXVI. Kinetic parameters utilized for Reaction 26 in the model.

	Parameter	Value	Units	Organism	Reference
	K_m	321[a]	µM	*E. coli*	Liu & Bisswanger, 2003
Fwd		356[b]	µM	*E. coli*	Liu & Bisswanger, 2003
Rxn	V_m	6.263[a]	µM/s	*E. coli*	Liu & Bisswanger, 2003
		3.682[b]	µM/s	*E. coli*	Liu & Bisswanger, 2003

a. H_2O as solvent
b. D_2O as solvent

TRANSCRIPTIONAL NETWORK

The transcriptional network associated with the enzymes in the selected metabolic pathways was included in the model. Enzymes are synthesized through the transcription and translation of genes. Cells regulate the amount of enzymes synthesized depending upon the needs of the cell. It is undesirable to waste energy synthesizing enzymes that are not needed. Transcription factors are regulatory proteins that can repress or induce transcription of genes. Cells use transcription factors to dynamically regulate the intracellular concentration of enzymes (Lehninger *et al*, 2008).

The first step in modeling the transcriptional network was to identify all the genes that contribute to the synthesis of the 30 enzymes used in Reactions 1-26. After the genes were known, then the next step was to determine which promoters initiated transcription of each gene. Next, the transcription factors associated with each promoter were identified. Only promoters that interact with transcription factors were included in the model. An equation was developed to calculate the rate of enzyme synthesis based on promoter activity and the concentrations of each transcription factor. Each promoter was represented by a reaction in the SimBiology model.

Ligand binding was also included in the model. Ligands that bind to each transcription factor were identified. Rules were used in SimBiology to calculate the concentration of active transcription factors based on the concentration of ligands. Reactions were also included to account for the degradation of enzymes that occurs in the cell. The end result of these equations and rules was a dynamic model of the concentration of 30 enzymes based on a transcriptional network.

Enzyme Genes and Promoters

The enzyme genes were determined using the EcoCyc database (ecocyc.org) and the RegulonDB database (regulondb.ccg.unam.mx) for *E. coli* K12. These databases were used to identify the promoters that initiate transcription of each gene, and the regulatory proteins that activate or repress the transcription of each gene.

β-ketothiolase:

The gene *phaA* encodes for the enzyme β-ketothiolase that catalyzes Reaction 1. The gene *phaA* is not naturally found in *E. coli*. The plasmid pBHR68 shown in Figure 6 has been used to insert *phaA, phaB,* and *phaC* into *E. coli* (Linton, 2010). These three genes are transcribed using the *lac* promoter shown in Figure 6. The transcription factors Crp, H-NS, and LacI help regulate *lac* as shown in Figure 7.

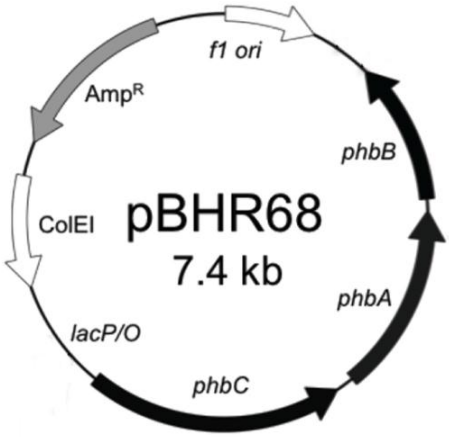

Figure 6. Summary diagram of the pBHR68 plasmid (Spiekermann *et al*, 1999).

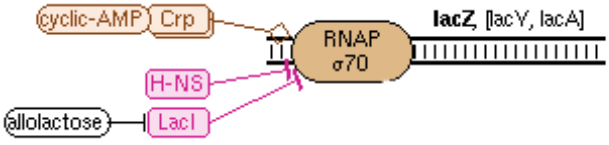

Figure 7. Transcription regulation summary diagram for the *lac* promoter from EcoCyc.

Acetoacetyl-CoA Reductase:

The gene *phaB* encodes for the enzyme acetoacetyl-CoA reductase that catalyzes Reaction 2. The gene *phaB* is not found in the *E. coli* genome and is inserted using the plasmid pBHR68 shown in Figure 6. The promoter associated with *phaB* is the *lac* promoter. Figure 7 shows how Crp, H-NS, and LacI regulate the transcription of *phaB.*

Poly-β-hydroxybutyrate Polymerase:

The gene *phaC* encodes for the enzyme poly-β-hydroxybutyrate polymerase that catalyzes Reaction 3. The gene *phaC* is added into *E. coli* by using the plasmid pBHR68 shown in Figure 6. The *lac* promoter and the three transcription factors shown in Figure 7 (Crp, H-NS, and LacI) regulate the transcription of *phaC.*

Citrate Synthase:

Citrate synthase is the enzyme that catalyzes Reaction 4, and it is encoded in the *E. coli* genome by the gene *gltA.* The transcription factors that regulate the transcription of *gltA* are Crp, IHF, and ArcA as shown in Figure 8. Figure 9 illustrates that there are two promoters for *gltA,* but only the promoter *gltAp1* is affected by the transcription factors. Therefore, only the promoter *gltAp1* was included in the model.

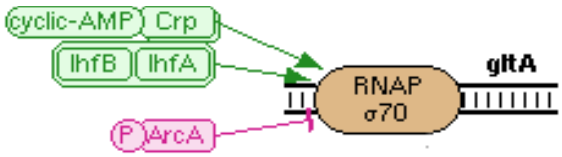

Figure 8. Transcription regulation summary diagram for the gene *gltA* from EcoCyc.

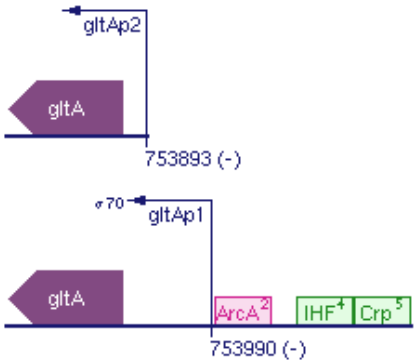

Figure 9. Promoters and transcription factors for the gene *gltA* from EcoCyc.

Citrate Hydro-lyase:

The gene *acnA* encodes for the aconitase A enzyme that can catalyze Reaction 5 as citrate hydro-lyase. Figure 10 shows that transcription of *acnA* is regulated by the transcription factors Crp, FruR, MarA, Rob, SoxS, ArcA, and Fnr. These transcription factors activate or repress the promoter activity of *acnAp2* as shown in Figure 11.

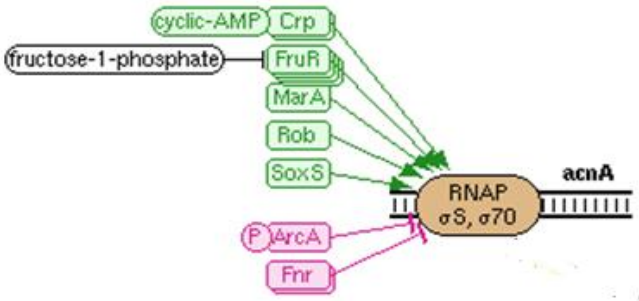

Figure 10. Transcription regulation summary diagram for the gene *acnA* from EcoCyc.

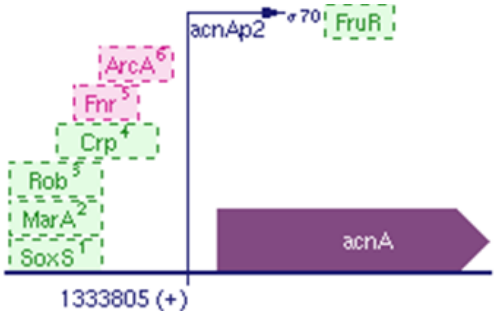

Figure 11. Promoter and transcription factors for the gene *acnA* from EcoCyc.

The aconitase B enzyme that can also function as citrate hydro-lyase is encoded by the gene *acnB*. Four transcription factors (Crp, ArcA, Fis, and FruR) regulate transcription of *acnB* as illustrated by Figure 12. This gene is transcribed with the help of two promoters (*acnBp* and *acnBp2*) as shown in Figure 13. However, the transcription factors only regulate *acnBp* so the promoter *acnBp2* was not included in the model.

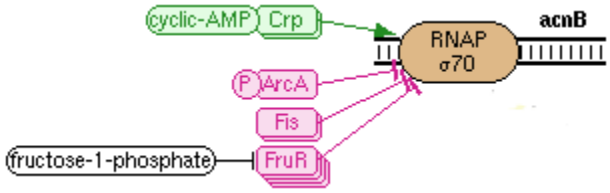

Figure 12. Transcription regulation summary diagram for the gene *acnB* from EcoCyc.

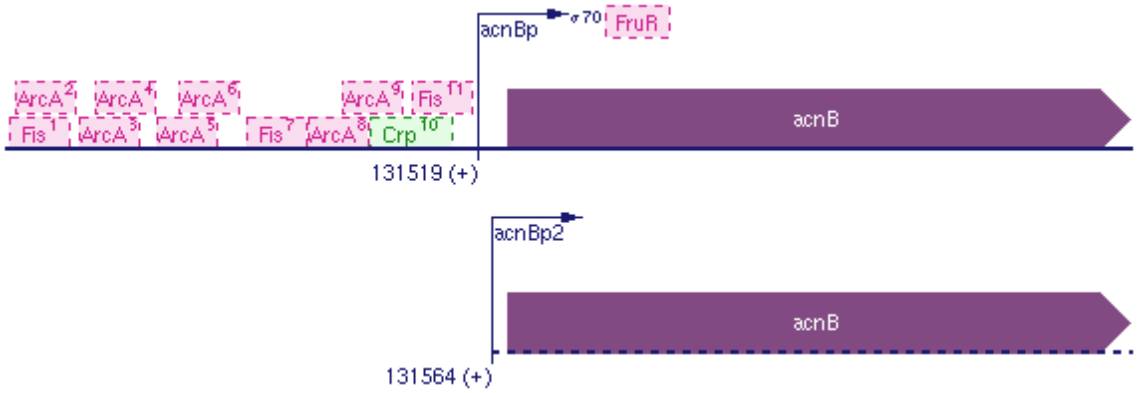

Figure 13. Promoters and transcription factors for the gene *acnB* from EcoCyc.

Isocitrate Hydro-lyase:

Aconitase A is encoded by *acnA* and can also function as the enzyme isocitrate hydro-lyase that catalyzes Reaction 6. See Figure 10 and Figure 11 for the promoter and transcription factors involved with *acnA*.

The gene *acnB* encodes for the aconitase B enzyme that can also function as isocitrate hydro-lyase. See Figure 12 for the transcription factors regulating *acnB* and see Figure 13 for the promoters involved in the transcription of *acnB*.

Isocitrate Dehydrogenase:

Isocitrate dehydrogenase catalyzes Reaction 7 and is encoded by the gene *icd.* Transcription factors FruR and ArcA regulate the transcription of *icd* as illustrated by Figure 14. ArcA represses the promoter *icdAp1* and FruR activates the promoter *icdAp2* as shown in Figure 15. Both promoters, *icdAp1* and *icdAp2,* were included in the model.

Figure 14. Transcription regulation summary diagram for the gene *icd* from EcoCyc.

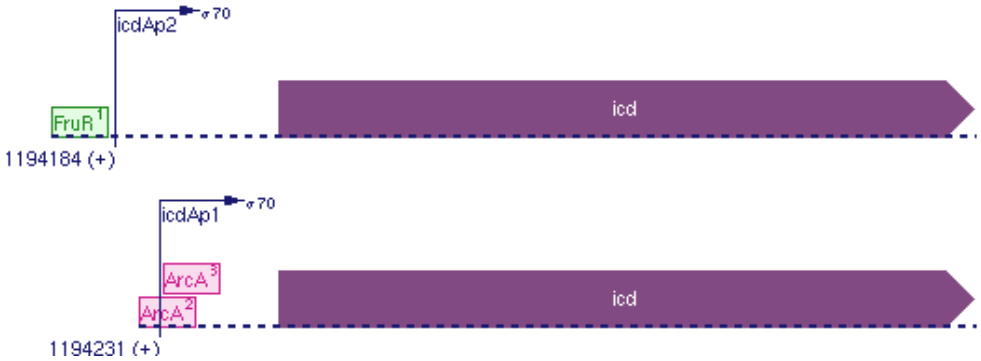

Figure 15. Promoters and transcription factors for the gene *icd* from EcoCyc.

2-Oxoglutarate Dehydrogenase:

The gene *sucA* encodes for the 2-oxoglutarate decarboxylase subunit of 2-oxoglutarate dehydrogenase. This enzyme catalyzes Reaction 8 in the model. Transcription of *sucA* is regulated by Crp, Fur, ArcA, Fnr, and IHF as shown in Figure 16. The promoter *sucAp* starts the transcription of *sucA* as illustrated by Figure 17.

The gene *sucB* encodes for the second subunit of 2-oxoglutarate dehydrogenase: dihydrolipoyltranssuccinylase. The gene *sucB* is regulated by the same transcription factors and promoters as *sucA* seen in Figure 16 and Figure 17.

Figure 16. Transcription regulation summary diagram for the genes *sucA*, *sucB*, *sucC*, and *sucD* from EcoCyc.

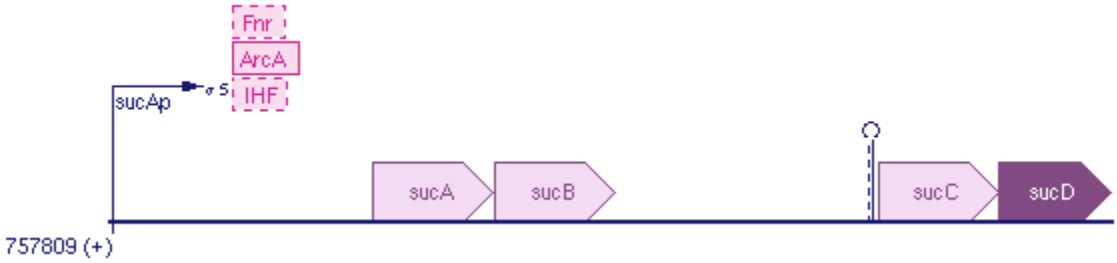

Figure 17. Promoter and transcription factors for the genes *sucA*, *sucB*, *sucC*, and *sucD* from EcoCyc.

Lipoamide dehydrogenase is the third subunit of 2-oxoglutarate dehydrogenase and is encoded by the gene *lpd.* This gene is regulated by the transcription factors Fis, Crp, Fnr, Fur, ArcA, FruR, and PdhR as shown in Figure 18. The gene *lpd* has two promoters initiating transcription: *pdhRp* and *lpdAp.* The promoter *pdhRp* is affected by the transcription factors Crp, Fnr, and PdhR. The promoter *lpdAp* is regulated by ArcA, Crp, Fis, Fnr, and Fur as illustrated in Figure 19.

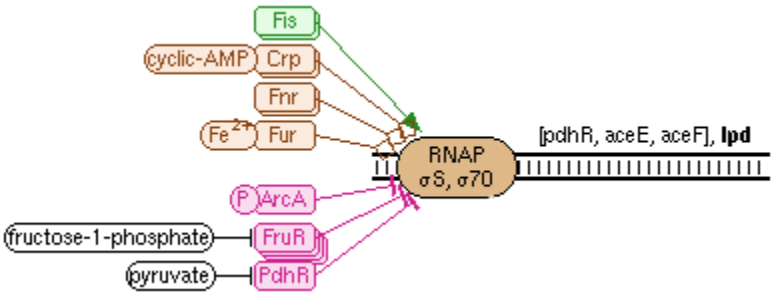

Figure 18. Transcription regulation summary diagram for the gene *lpd* from EcoCyc.

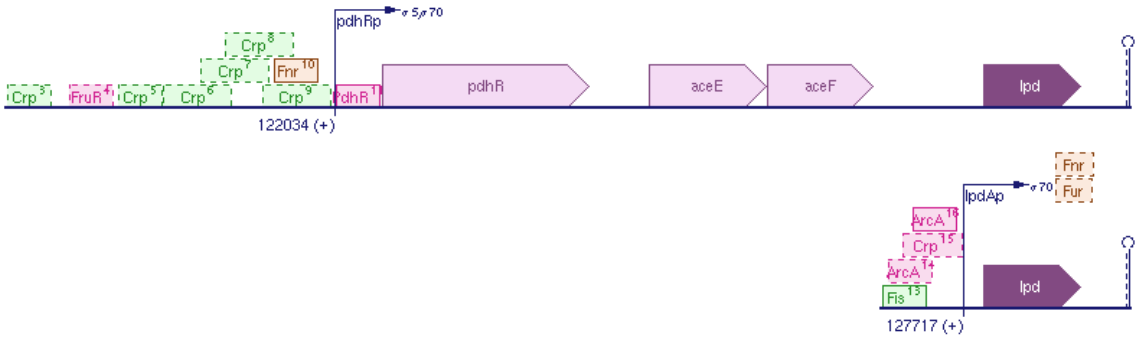

Figure 19. Promoters and transcription factors for the gene *lpd* from EcoCyc.

Succinyl-CoA Synthetase:

The enzyme succinyl-CoA synthetase is encoded by the genes *sucC* and *sucD.* This enzyme catalyzes Reaction 9 in the model. These genes are regulated by the same transcription factors and promoters as *sucA* and *sucB.* Figure 16 shows the transcription regulation summary diagram and Figure 17 shows the promoters used to regulate transcription of *sucC* and *sucD.*

Succinate Dehydrogenase:

The genes *sdhA, sdhB, sdhC,* and *sdhD* encode for the enzyme succinate dehydrogenase that catalyzes Reaction 10. These four genes are regulated by Crp, Fur, ArcA, and Fnr as seen in Figure 20. The promoters *sdhCp* and *sdhDp2* are involved in the transcription of these four genes. Figure 21 shows that the promoter *sdhCp* is regulated by ArcA, Crp, Fur, and Fnr while the promoter *sdhDp2* is only regulated by Crp. Both promoters were included in the model of the transcriptional network.

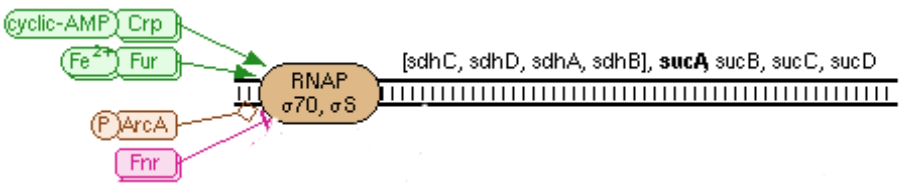

Figure 20. Transcription regulation summary diagram for the genes *sdhA, sdhB, sdhC,* and *sdhD* from EcoCyc.

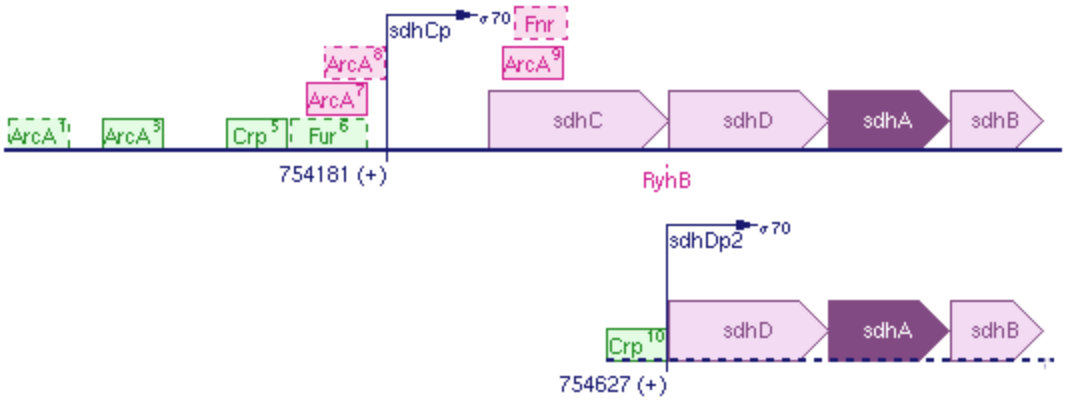

Figure 21. Promoters and transcription factors for the genes *sdhA*, *sdhB*, *sdhC*, and *sdhD* from EcoCyc.

Fumarase:

The gene *fumA* encodes for the fumarase A enzyme that catalyzes Reaction 11. Figure 22 shows the transcription factors that regulate the transcription of *fumA.* ArcA Crp, and Fnr regulate *fumA* through the promoter *fumAp* as shown in Figure 23.

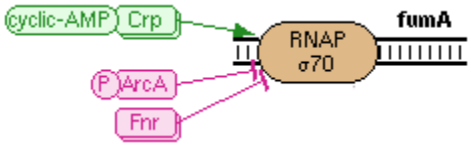

Figure 22. Transcription regulation summary diagram for the gene *fumA* from EcoCyc.

Figure 23. Promoter and transcription factors for the gene *fumA* from EcoCyc.

Fumarase B is encoded by the gene *fumB* and can also catalyze Reaction 11. The transcriptional regulation of *fumB* is more complex than *fumA.* Figure 24 shows that ArcA, Crp, DcuR, Fnr, Fur, Fis, and NarL are all involved in regulating the transcription

of *fumB*. The seven transcription factors regulate the transcription of *fumB* through three promoters shown in Figure 25. Transcription factors ArcA, Fis, Fnr, and Fur are involved with the promoter *fumBp*. Transcription factors Crp, Fnr, and NarL affect the promoter *dcuBp*. The transcription factor DcuR activates promoter activity of *dcuBp2*.

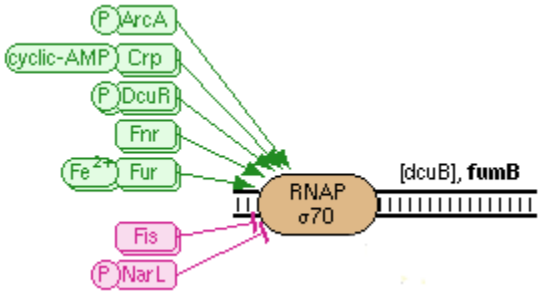

Figure 24. Transcription regulation summary diagram for the gene *fumB* from EcoCyc.

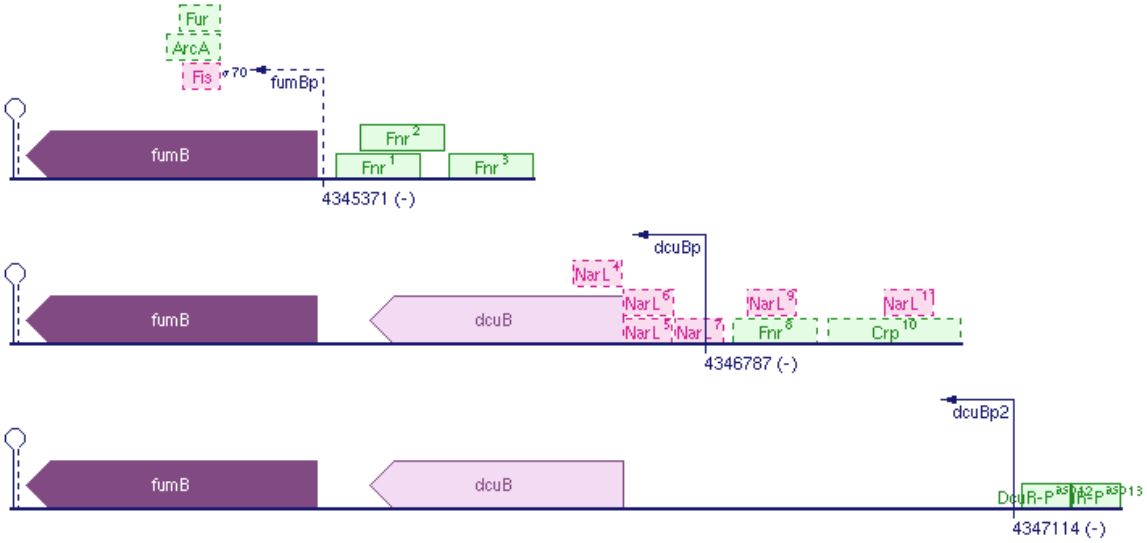

Figure 25. Promoters and transcription factors for the gene *fumB* from EcoCyc.

The gen *fumC* encodes for fumarase C that can also catalyze Reaction 11. This gene is regulated by seven transcription factors shown in Figure 26: MarA, Rob, SoxR, SoxS, ArcA, Fnr, and Fur. These seven transcription factors regulate *fumC* through the promoter *fumCp* shown in Figure 27.

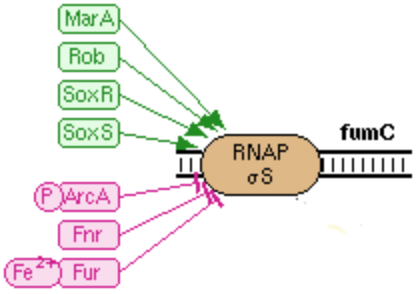

Figure 26. Transcription regulation summary diagram for the gene *fumC* from EcoCyc.

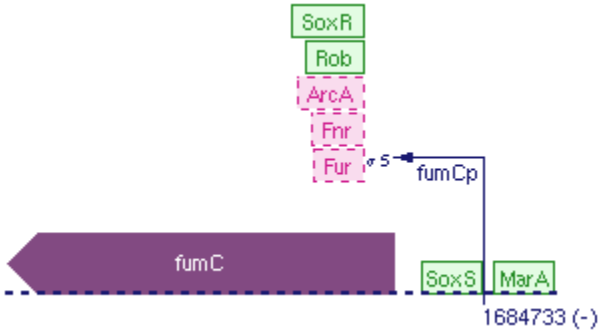

Figure 27. Promoter and transcription factors for the gene *fumC* from EcoCyc.

Malate Dehydrogenase:

Malate dehydrogenase catalyzes Reaction 12 and is encoded in the *E. coli* genome by the gene *mdh.* The transcription factors Crp, DpiA, ArcA, and FlhCD regulate the transcription of *mdh* as shown in Figure 28. Two promoters, *mdhp1* and *mdhp2*, are involved in the transcription of *mdh* as illustrated by Figure 29. All four transcription factors impact *mdhp1*, whereas only DpiA affects *mdhp2.*

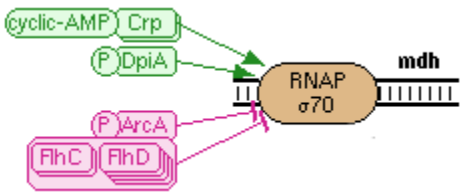

Figure 28. Transcription regulation summary diagram for the gene *mdh* from EcoCyc.

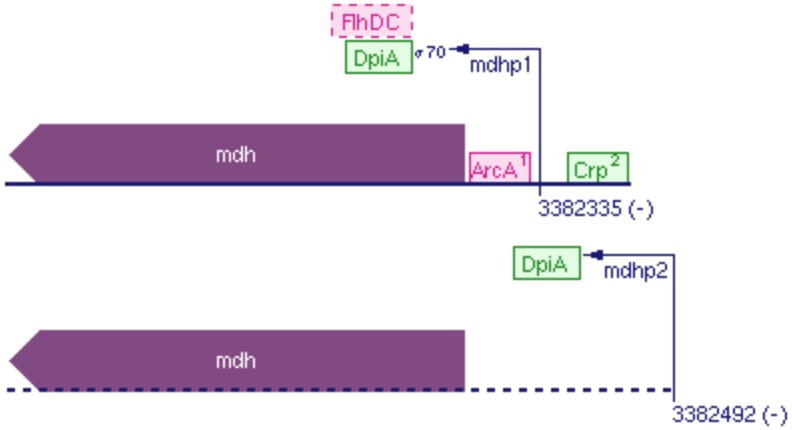

Figure 29. Promoters and transcription factors for the gene *mdh* from EcoCyc.

Isocitrate Lyase:

Isocitrate lyase catalyzes Reaction 13 and is encoded by the gene *aceA.* The transcription factors FruR, IHF, ArcA, Crp, and IclR regulate the transcription of *aceA* as shown by Figure 30. These five transcription factors regulate transcription of *aceA* through their interaction with the promoter *aceBp* shown in Figure 31.

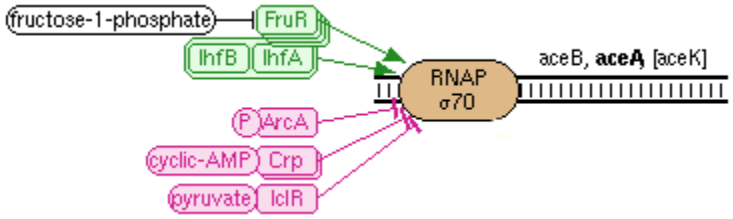

Figure 30. Transcription regulation summary diagram for the genes *aceA* and *aceB* from EcoCyc.

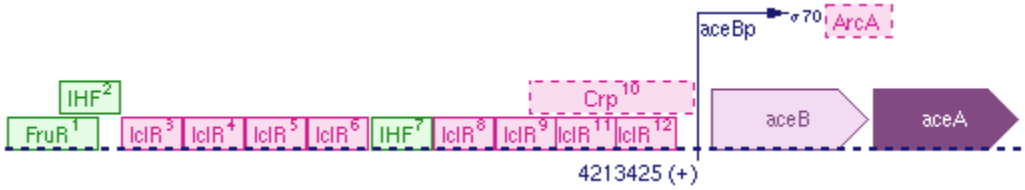

Figure 31. Promoter and transcription factors for the genes *aceA* and *aceB* from EcoCyc.

Malate Synthase:

Malate synthase A is the enzyme that catalyzes Reaction 14 and is encoded by the gene *aceB.* The transcription of *aceB* is under the same regulation as *aceA.* Figure 30 shows the five transcription factors and Figure 31 shows the promoter involved in the transcription of *aceB.*

Malate synthase G can also catalyze Reaction 14. This isozyme is encoded by the gene *glcB.* This gene is regulated by the transcription factors GlcC, IHF, and ArcA as shown in Figure 32. There are two promoters involved in the transcription of *glcB*: *glcBp* and *glcDp*. Figure 33 shows that only the promoter *glcDp* is affected by the transcription factors; therefore, only *glcDp* was included in the model.

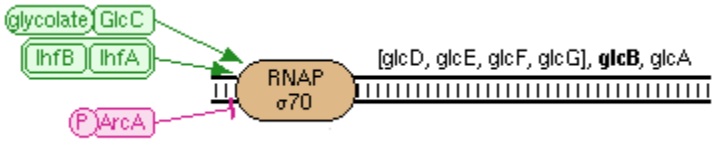

Figure 32. Transcription regulation summary diagram for the gene *glcB* from EcoCyc.

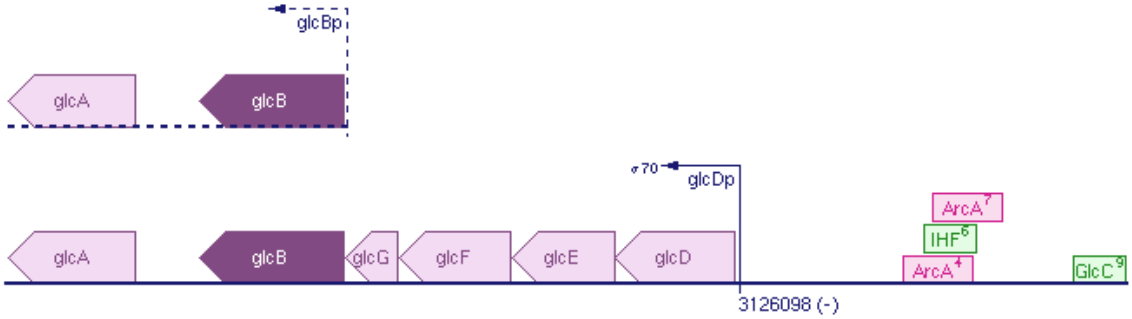

Figure 33. Promoters and transcription factors for the gene *glcB* from EcoCyc.

Glucokinase:

The enzyme glucokinase catalyzes Reaction 15 in the model. This enzyme is encoded by the gene *glk.* The transcription of *glk* is regulated by the transcription factor

FruR as shown in Figure 34. FruR represses the promoter activity of *glkp* as shown in Figure 35. The promoter *glkp1* is not affected by transcription factors and was not included in the model.

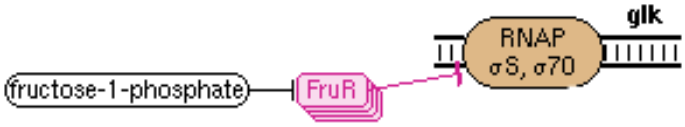

Figure 34. Transcription regulation summary diagram for the gene *glk* from EcoCyc.

Figure 35. Promoters and transcription factor for the gene *glk* from EcoCyc.

Phosphoglucomutase:

The gene *pgm* encodes the enzyme phosphoglucomutase that catalyzes the first step in the reverse direction of Reaction 15. This gene is regulated by HU as shown in Figure 36. HU represses the activity of the *seqAp* promoter as shown in Figure 37.

Figure 36. Transcription regulation summary diagram for the gene *pgm* from EcoCyc.

Figure 37. Promoter and transcription factor for the gene *pgm* from EcoCyc.

Glucose-1-Phosphatase:

Glucose-1-phosphatase catalyzes second step in the reverse direction of Reaction 15. This enzyme is encoded by the gene *yihX*. Figure 38 and Figure 39 show that no transcription factors are known to regulate transcription of *yihX*. Therefore, this gene was not included in the transcriptional network model.

Figure 38. Transcription regulation summary diagram for the gene *yihX* from EcoCyc.

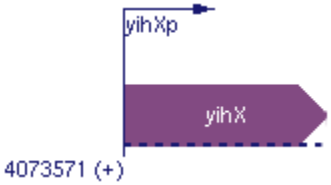

Figure 39. Promoter for the gene *yihX* from EcoCyc.

Phosphoglucose Isomerase:

Phosphoglucose isomerase catalyzes Reaction 16 and is encoded by the gene *pgi*. Transcription of *pgi* is regulated by the transcription factor SoxS as shown in Figure 40. SoxS interacts with the promoter *pgip* as shown in Figure 41.

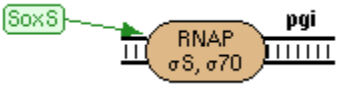

Figure 40. Transcription regulation summary diagram for the gene *pgi* from EcoCyc.

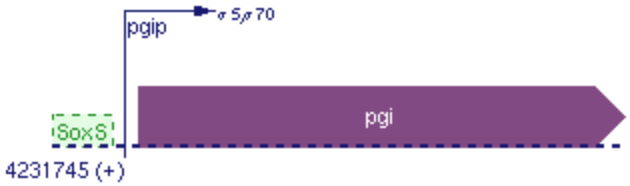

Figure 41. Promoter and transcription factor for the gene *pgi* from EcoCyc.

6-Phosphofructokinase:

The gene *pfkA* encodes for the enzyme 6-phospofructokinase that catalyzes Reaction 17. This gene is regulated by the transcription factor FruR as shown in Figure 42. The promoters *pfkAp1* and *pfkAp2* initiate transcription of *pfkA* as seen in Figure 43. Only *pfkAp2* interacts with FruR. Therefore, the promoter *pfkAp1* was not included in the model.

Figure 42. Transcription regulation summary diagram for the gene *pfkA* from EcoCyc.

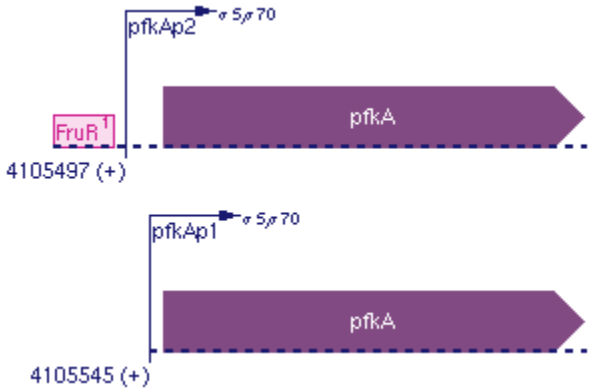

Figure 43. Promoters and transcription factor for the gene *pfkA* from EcoCyc.

The gene *pfkB* also encodes for 6-phosphofructokinase. However, as seen in Figure 44 and Figure 45, there are no transcription factors associated with the regulation

of *pfkB.* Therefore, this gene was not included in the model of the transcriptional network.

Figure 44. Transcription regulation summary diagram for the gene *pfkB* from EcoCyc.

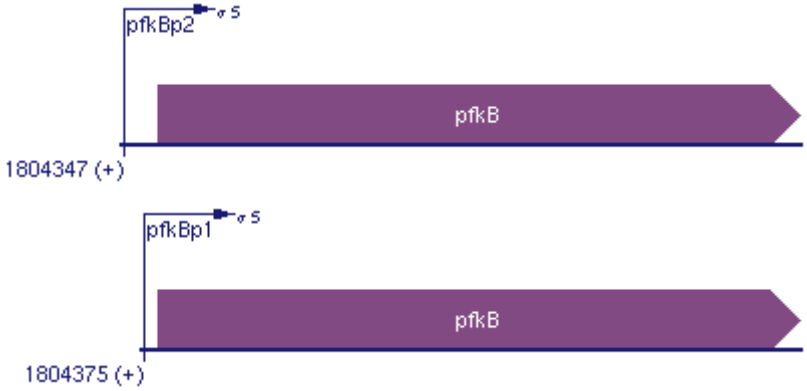

Figure 45. Promoters for the gene *pfkB* from EcoCyc.

Fructose-1,6-Bisphosphatase:

The enzyme fructose-1,6-bisphosphatase that catalyzes the reverse direction of Reaction 17 is encoded by the gene *glpX*. The transcription factors Crp and GlpR regulate the transcription of *glpX* shown in Figure 46. GlpR and Crp regulate the gene by interacting with the promoter *glpFp* shown in Figure 47.

Figure 46. Transcription regulation summary diagram for the gene *glpX* from EcoCyc.

Figure 47. Promoter and transcription factors for the gene *glpX* from EcoCyc.

The gene *ybhA* also encodes for the enzyme fructose-1,6-bisphosphatase. However, as seen in Figure 48 and Figure 49, no transcription factors or promoters are known to regulate *ybhA.* Therefore, the gene *ybhA* was not included in the model.

Figure 48. Transcription regulation summary diagram for the gene *ybhA* from EcoCyc.

Figure 49. The gene *ybhA* from EcoCyc.

Another gene, *yggF,* also encodes for fructose-1,6-bisphosphatase. But, similar to the gene *ybhA*, no transcription factors or promoters have been identified for *yggF* as illustrated by Figure 50 and Figure 51.

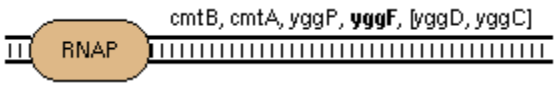

Figure 50. Transcription regulation summary diagram for the gene *yggF* from EcoCyc.

Figure 51. The gene *yggF* from EcoCyc.

Fructose-1,6-bisphosphatase is encoded by another gene, *fbp*. Figure 52 and Figure 53 illustrate that no transcription factors or promoters are currently known to regulate *fbp*.

Figure 52. Transcription regulation summary diagram for the gene *fbp* from EcoCyc.

Figure 53. The gene *fbp* from EcoCyc.

Fructose-Bisphosphate Aldolase:

Fructose-bisphosphate aldolase is the enzyme that catalyzes Reaction 18 and is encoded by the gene *fbaA*. The transcription factors Crp and FruR regulate the transcription of *fbaA* as shown in Figure 54. Four promoters are known to be associated with the transcription of *fbaA*: *epdp*, *pgkp1*, *pgkp2*, and *pgkp3*. Figure 55 shows that only the promoter *epdp* is affected by the transcription factors FruR and Crp. Therefore, *epdp* was the only promoter included in the model.

Fructose-bisphosphate aldolase is also encoded by the gene *fbaB*. The gene *fbaB* is regulated by the transcription factor FruR as shown in Figure 56. FruR interacts with the promoter *fbaBp* as shown in Figure 57. The promoter *fbaBp* was included in the transcriptional network model for the enzyme fructose-bisphosphate aldolase.

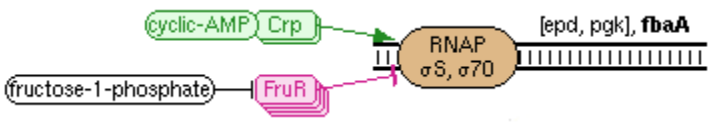

Figure 54. Transcription regulation summary diagram for the gene *fbaA* from EcoCyc.

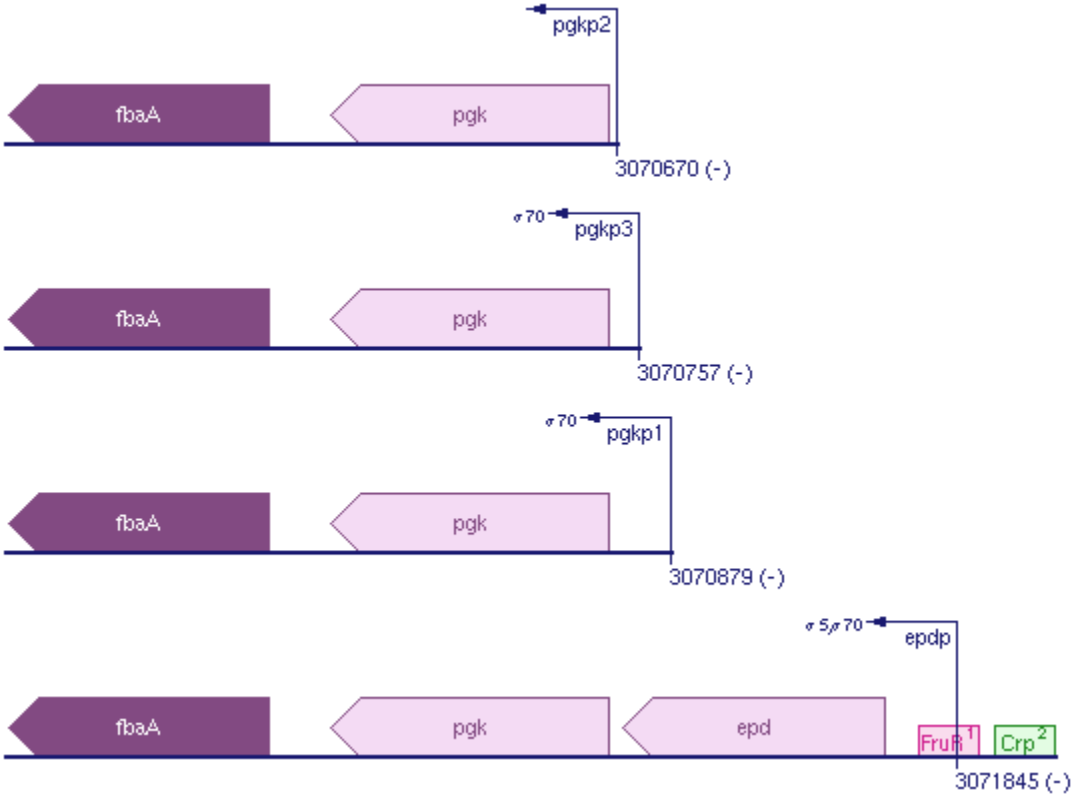

Figure 55. Promoters and transcription factors for the gene *fbaA* from EcoCyc.

Figure 56. Transcription regulation summary diagram for the gene *fbaB* from EcoCyc.

Figure 57. Promoter and transcription factor for the gene *fbaB* from EcoCyc.

Triose Phosphate Isomerase:

The gene *tpiA* encodes for the enzyme triose phosphate isomerase that catalyzes Reaction 19. The gene *tpiA* is regulated by the transcription factor FruR as shown in

Figure 58. There are two promoters that initiate transcription of *tpiA*, but only the promoter *tpiAp2* interacts with transcription factors as illustrated by Figure 59. Therefore, only the promoter *tpiAp2* was included in the transcriptional network model.

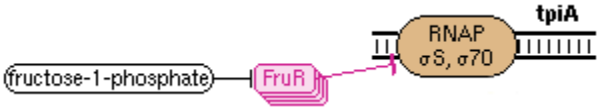

Figure 58. Transcription regulation summary diagram for the gene *tpiA* from EcoCyc.

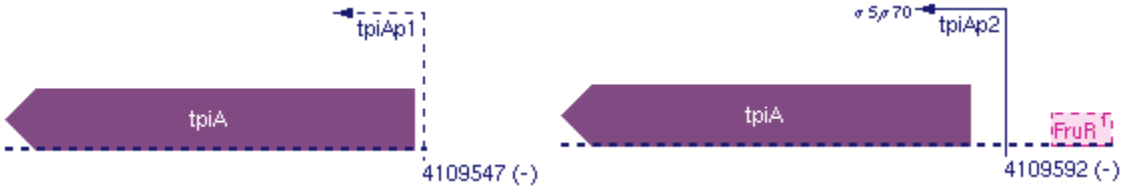

Figure 59. Promoters and transcription factor for the gene *tpiA* from EcoCyc.

Glyceraldehyde-3-Phosphate Dehydrogenase:

The enzyme glyceraldehyde-3-phosphate dehydrogenase catalyzes Reaction 20 and is encoded by the gene *gapA*. The transcription factors Crp and FruR regulate the transcription of *gapA* as shown in Figure 60. There are four promoters for the gene *gapA* as shown in Figure 61. Only the promoters *gapAp1* and *gapAp3* interact with Crp and FruR; therefore, only *gapAp1* and *gapAp3* were included in the model.

The genes *gapC1* and *gapC2* also encode for the enzyme glyceraldehyde-3-phosphate dehydrogenase that catalyzes Reaction 20. The transcription of these two genes is regulated by the protein Fnr as shown in Figure 62. Fnr regulates the transcription of *gapC1* and *gapC2* through its interaction with the promoter *gapC_1p* shown in Figure 63.

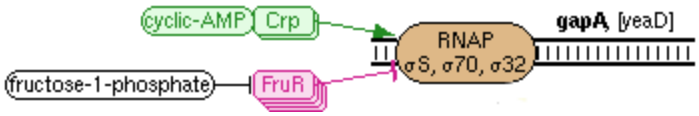

Figure 60. Transcription regulation summary diagram for the gene *gapA* from EcoCyc.

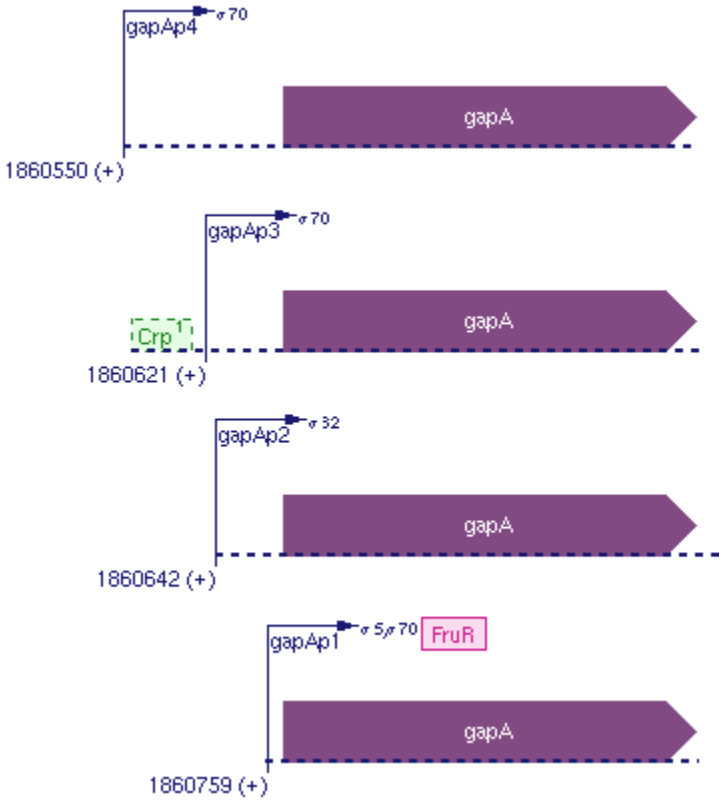

Figure 61. Promoters and transcription factors for the gene gapA from EcoCyc.

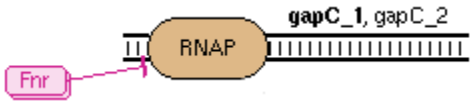

Figure 62. Transcription regulation summary diagram for the genes *gapC1* and *gapC2* from EcoCyc.

Figure 63. Promoter and transcription factor for the genes *gapC1* and *gapC2* from EcoCyc.

Phosphoglycerate Kinase:

The gene *pgk* encodes for the enzyme phosphoglycerate kinase that catalyzes Reaction 21. The transcription of *pgk* is regulated by Crp and FruR as shown in Figure 64. Four promoters initiate transcription of *pgk* as shown in Figure 65. Only the promoter *epdp* is regulated; therefore, it was the only promoter included in the model.

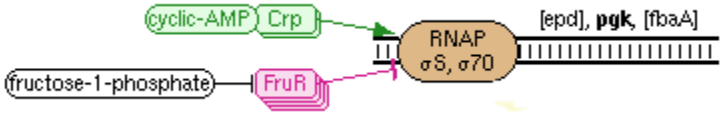

Figure 64. Transcription regulation summary diagram for the gene *pgk* from EcoCyc.

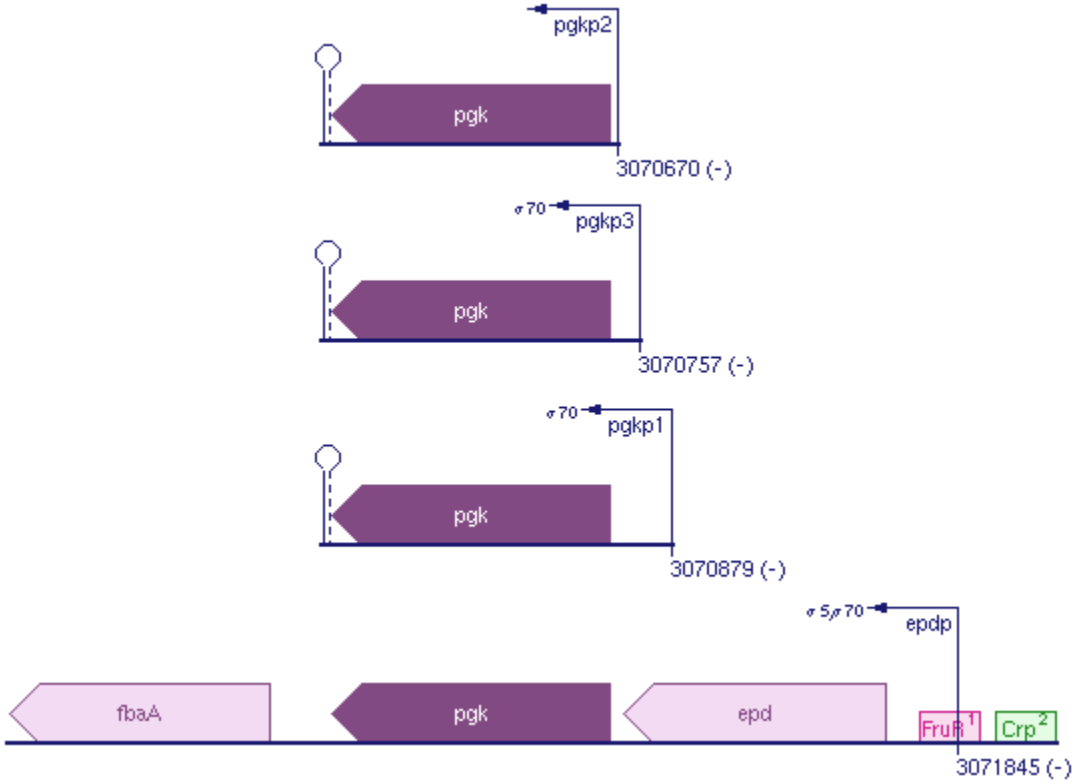

Figure 65. Promoters and transcription factors for the gene *pgk* from EcoCyc.

Phosphoglycerate Mutase:

Phosphoglycerate mutase catalyzes Reaction 22 and is encoded by the gene *gpmM*. This gene is regulated by the transcription factor FruR as shown in Figure 66. FruR regulates transcription of *gpmM* through its interactions with the promoter *gpmMp* as shown in Figure 67.

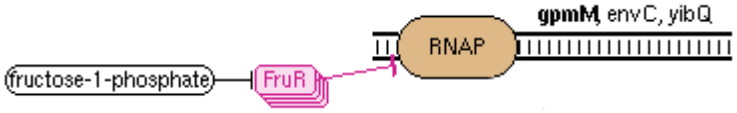

Figure 66. Transcription regulation summary diagram for the gene *gpmM* from EcoCyc.

Figure 67. Promoter and transcription factor for the gene *gpmM* from EcoCyc.

The gene *ytjC* also encodes for the enzyme phosphoglycerate mutase. However, as seen in Figure 68 and Figure 69, there are no known promoters and transcription factors that regulate *ytjC*. Therefore, the gene *ytjC* was not included in the model.

Figure 68. Transcription regulation summary diagram for the gene *ytjC* from EcoCyc.

Figure 69. The gene *ytjC* from EcoCyc.

Another gene that encodes for phosphoglycerate mutase is *gpmA*. The transcription of the gene *gpmA* is regulated by Fur through the promoter *gmpAp* as

illustrated in Figure 70 and Figure 71. Since the second promoter *gmpAp2* does not interact with transcription factors, only the promoter *gmpAp* was included in the model.

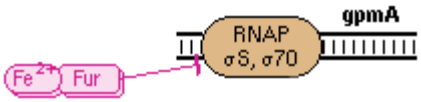

Figure 70. Transcription regulation summary diagram for the gene *gpmA* from EcoCyc.

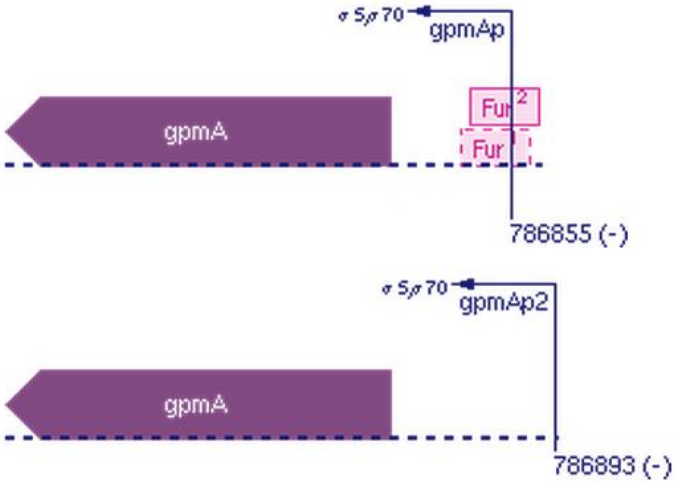

Figure 71. Promoters and transcription factors for the gene *gpmA* from EcoCyc.

Enolase:

The gene *eno* encodes for the enzyme enolase that catalyzes Reaction 23 in the model. The transcription of *eno* is regulated by the transcription factor FruR as shown in Figure 72. There are nine promoters that have been identified to initiate transcription of *eno* as shown in Figure 73. Out of the nine promoters, only the promoters *enop1*, *enop2*, and *enop3* interact with the transcription factor FruR. Therefore, only the promoters *enop1*, *enop2*, and *enop3* were included in the transcriptional network model.

Figure 72. Transcription regulation summary diagram for the gene *eno* from EcoCyc.

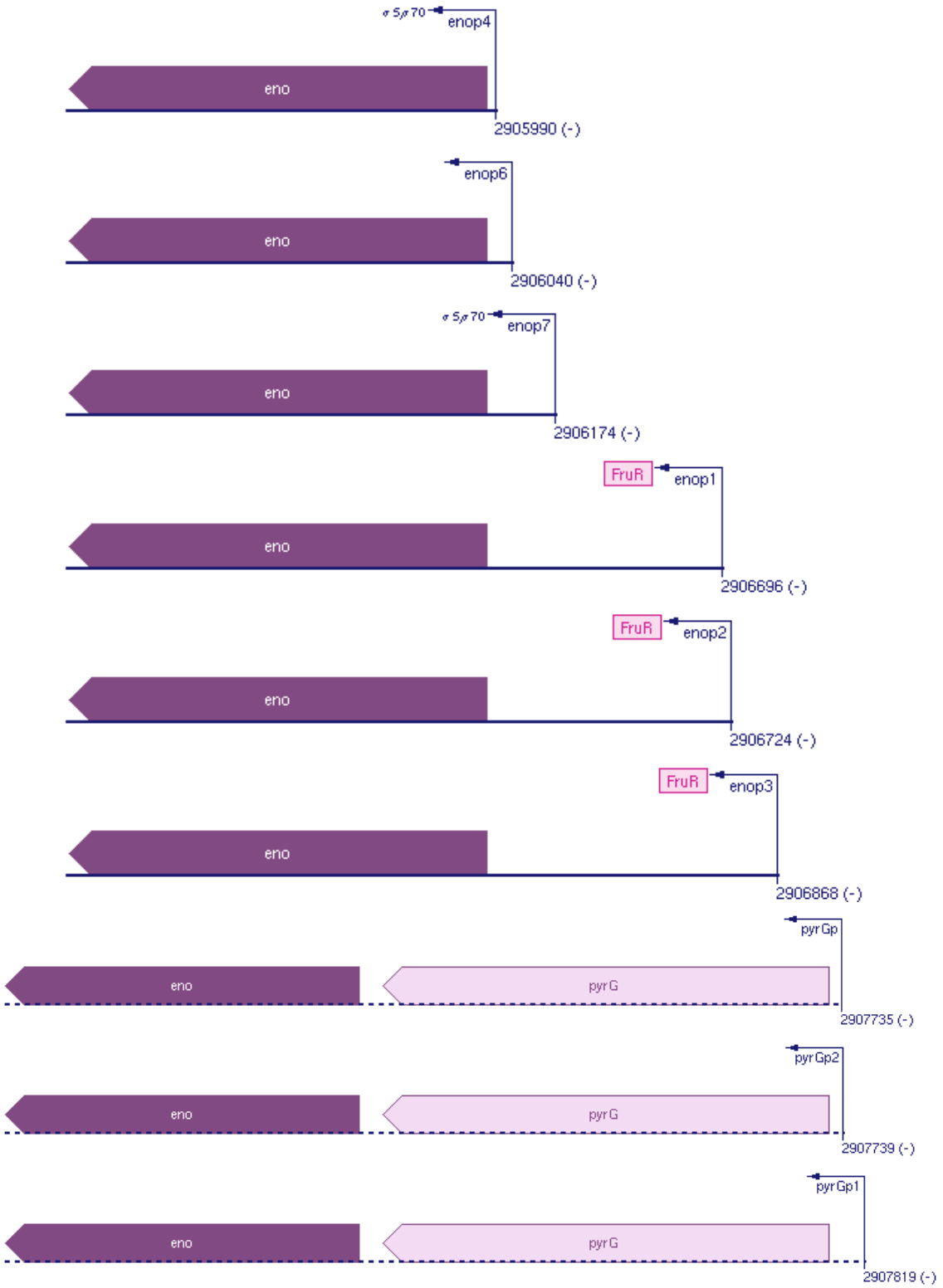

Figure 73. Promoters and transcription factor for the gene *eno* from EcoCyc.

Pyruvate Kinase:

The enzyme pyruvate kinase catalyzes the forward direction of Reaction 24 and is encoded by the gene *pykF*. The transcription of *pykF* is regulated by the protein FruR as illustrated by Figure 74. The promoters *pykFp*, *pykFp1*, *pykFp2*, and *pykFp3* initiate transcription of *pykF* as shown in Figure 75. The only promoter that interacts with FruR is *pykFp*; therefore, the promoter *pykFp* was the only one included in the transcriptional network model.

Figure 74. Transcription regulation summary diagram for the gene *pykF* from EcoCyc.

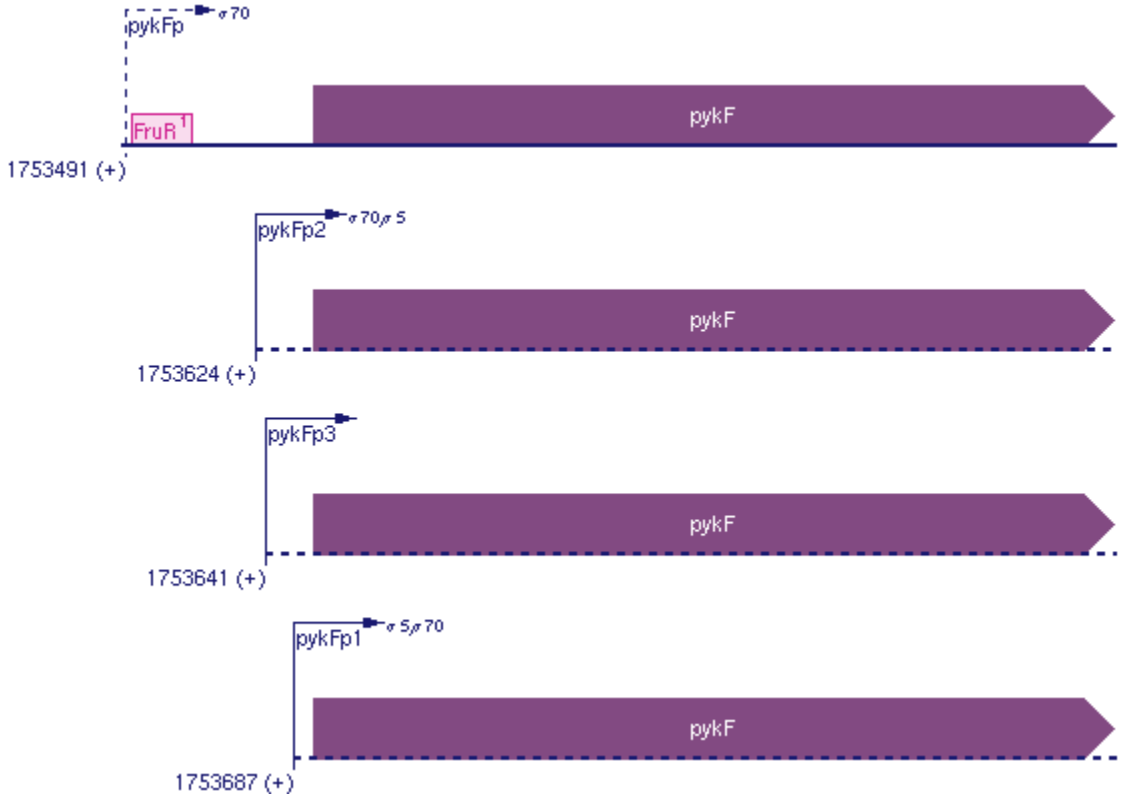

Figure 75. Promoters and transcription factor for the gene *pykF* from EcoCyc.

Pyruvate kinase is also encoded by the gene *pykA*. As seen in Figure 76, there are no transcription factors known to regulate the transcription of *pykA*. Two promoters, *pykAp1* and *pykAp2*, are known to initiate transcription of *pykA* as shown in Figure 77. Since there are no transcription factors involved, the gene *pykA* was not included in the transcriptional network model.

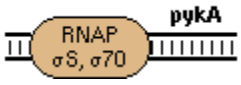

Figure 76. Transcription regulation summary diagram for the gene *pykA* from EcoCyc.

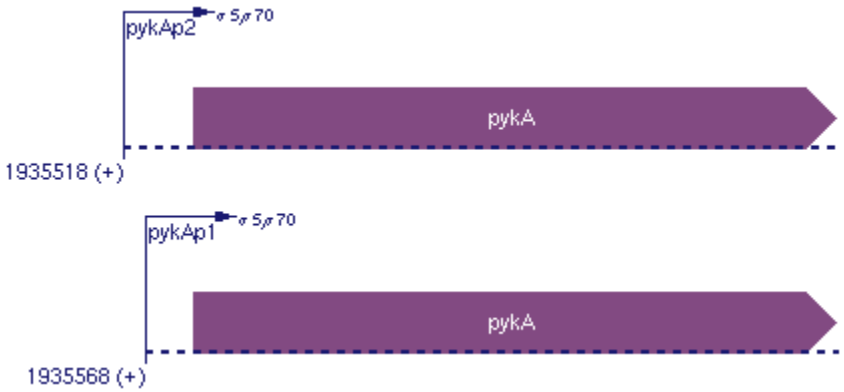

Figure 77. Promoters for the gene *pykA* from EcoCyc.

Phosphoenolpyruvate Synthetase:

The gene *ppsA* encodes for the enzyme phosphoenolpyruvate synthetase that catalyzes the reverse direction of Reaction 24. Figure 78 shows that FruR is the only transcription factor that regulates *ppsA.* FruR interacts with the promoter *ppsp* as illustrated by Figure 79.

Figure 78. Transcription regulation summary diagram for the gene *ppsA* from EcoCyc.

Figure 79. Promoter and transcription factor for the gene *ppsA* from EcoCyc.

Phosphoenolpyruvate Carboxykinase:

The gene *pck* encodes for the enzyme phosphoenolpyruvate carboxykinase that catalyzes Reaction 25. Transcription of the gene *pck* is regulated by the protein FruR as shown in Figure 80. FruR regulates transcription by interacting with the promoter *pckp* as shown in Figure 81.

Figure 80. Transcription regulation summary diagram for the gene *pck* from EcoCyc.

Figure 81. Promoter and transcription factor for the gene *pck* from EcoCyc.

Pyruvate Dehydrogenase:

The enzyme pyruvate dehydrogenase is a complex composed of three subunits. The first subunit is encoded by the gene *aceE*. Figure 82 shows that transcription of *aceE* is regulated by the proteins Crp, Fnr, ArcA, FruR, NsrR, and PdhR. The *pdhRp* and *aceEp* promoters interact with these transcription factors as illustrated by Figure 83. Both *pdhRp* and *aceEp* were included in the model.

The second subunit of pyruvate dehydrogenase is encoded by the gene *aceF*. The gene *aceF* is in the same operon as the gene *aceE*. See Figure 82 and Figure 83 for the transcription factors and promoters that regulate transcription of *aceF*.

The gene *lpd* codes for the third subunit of pyruvate dehydrogenase that is also a subunit of the enzyme 2-oxoglutarate dehydrogenase. See Figure 18 and Figure 19 for the transcription factors and promoters that regulate *lpd*.

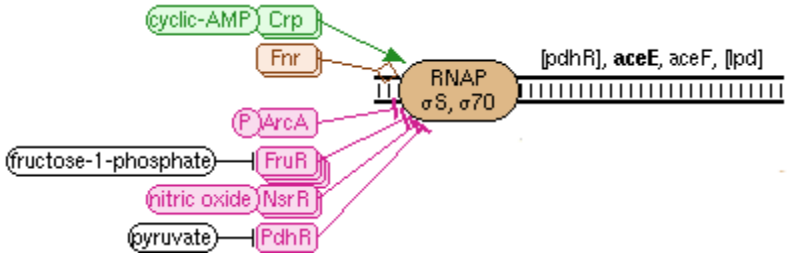

Figure 82. Transcription regulation summary diagram for the genes *aceE* and *aceF* from EcoCyc.

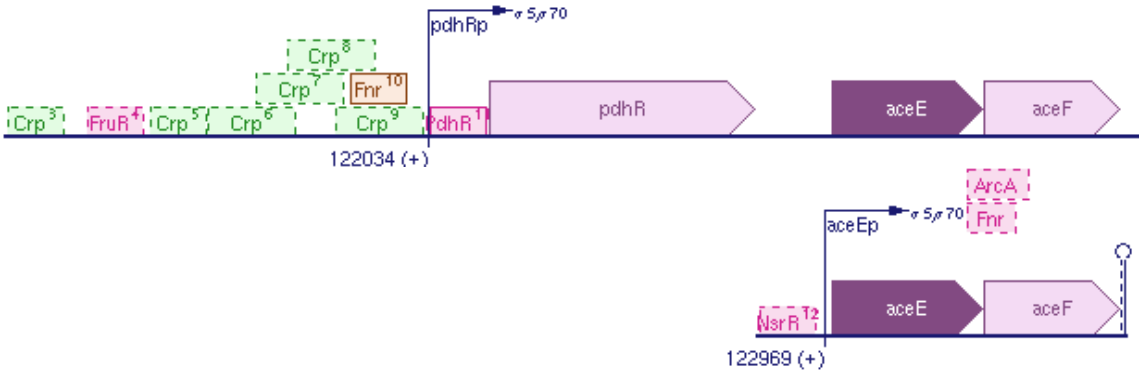

Figure 83. Promoters and transcription factors for the genes *aceE* and *aceF* from EcoCyc.

Transcription Regulatory Proteins

Transcription regulatory proteins are proteins that have a DNA binding domain and regulate the transcription of genes. When the DNA binding domain is accessible, these proteins bind to the DNA near promoters. If the regulatory protein is a repressor, it interferes with the ability of the RNA polymerase to bind to the promoter and initiate

transcription. If the protein is an activator, it increases the binding affinity between RNA polymerase and the promoter in order to upregulate transcription of a gene (Lehninger *et al*, 2008).

Transcription factors can be turned off or on through ligand binding. Ligand binding induces a conformational shift that can either open or close the DNA binding domain of the protein (Lehninger *et al*, 2008). In order to correctly model the transcriptional network, it was important to understand when and how the regulatory proteins became active transcription factors. This section explains the interactions with ligands and the specific regulatory proteins identified in this model. A summary chart of the transcription factors used in this model is available in Appendix A.

ArcA:

ArcA is a transcriptional regulatory protein that is capable of binding to DNA when phosphorylated by the kinase ArcB. Phosphorylated ArcA acts as a repressor by binding to promoters or activator binding sites (Jeon *et al*, 2001). ArcA-P is a transcriptional repressor for many of the TCA cycle and glyoxylate enzymes under anaerobic conditions (Gunsalus & Park, 1994). ArcA acts as a transcriptional activator for a small number of genes by being part of a nucleoprotein complex (Sawers & Suppmann, 1992).

Crp:

The Crp transcriptional regulator, also known as CAP, can bind to DNA only when activated by cAMP. In the absence of glucose, cAMP-Crp levels rise allowing more Crp to bind to DNA (Ishizuka *et al*, 1994). Crp generally acts as a transcriptional

activator by binding upstream of the polymerase binding site. However, it can also act as a repressor by occupying the binding site of an activator protein or by interfering with the promoter region (Kolb *et al*, 1993; Liu *et al*, 2004).

DcuR:

The DcuR regulatory protein is activated for DNA binding through phosphorylation by kinase DcuS. Upon phosphorylation of an aspartate residue, DcuR dimerizes and is capable of binding to DNA to activate transcription (Golby *et al*, 1999).

DpiA:

DpiA is a transcriptional regulator that can bind to DNA when phosphorylated on an aspartate residue. It binds to DNA sequences rich in A and T nucleotides. DpiA-P is a transcriptional activator of malate dehydrogenase when citrate is available in an anaerobic environment (Yamamoto *et al*, 2008).

Fis:

Fis is a small protein capable of tight binding to DNA when dimerized (Finkel & Johnson, 1992). One study indicated that approximately 21% of genes are regulated by Fis (Cho *et al*, 2008). Fis requires no modifications to bind to DNA.

FlhDC:

FlhD and FlhC are proteins that can form the heterotetramer FlhD2C2. As a heterotetramer, FlhDC can bind to DNA and act as a transcriptional repressor or activator. No inducer has been observed for FlhDC (Stafford *et al*, 2005).

Fnr:

Fnr is a protein that activates genes needed for anaerobic metabolism and represses genes used for aerobic metabolism. The concentration of Fnr remains approximately the same under aerobic and anaerobic conditions (~3.7 μM) (Sutton *et al*, 2004). The DNA-binding activity of Fnr is regulated by oxygen. In the absence of oxygen, a [4Fe-4S] cluster binds to Fnr allowing the protein to dimerize. As a dimer, Fnr can bind to DNA and activate or repress transcription. In the presence of oxygen, the [4Fe-4S] cluster is oxidized into [2Fe-2S] that destabilizes the dimer (Sutton *et al*, 2004).

FruR:

FruR is a transcriptional regulator also known as Cra. Unmodified FruR can bind to DNA and can activate transcription of genes in the TCA cycle, the glyoxylate pathways, and gluconeogenesis. FruR acts as a repressor for genes involved in glycolysis. Fructose-1,6-bisphosphate and fructose-1-phosphate can bind with FruR and prevent FruR from binding to DNA (Ramseier *et al*, 1995).

Fur:

Fur is a transcriptional activator and repressor that can only bind to DNA with the cofactor Fe^{2+}. Fur is a regulator of many genes including some involved in the TCA cycle, glycolysis, and gluconeogenesis (Mills & Marletta, 2005).

GlcC:

GlcC is a dual transcriptional regulator that can bind to DNA when induced by glycolate. It regulates genes needed when glycolate is the main carbon source (Pellicer *et al*, 1999).

GlpR:

GlpR is a transcriptional repressor that can bind to DNA in its unmodified form. Binding of either glycerol or glycerol-3-phosphate to GlpR causes a conformational shift that interferes with DNA binding (Lin, 1976).

H-NS:

Histone-like nucleoid structuring protein (H-NS) is a small DNA-binding protein used to condense and supercoil DNA. It acts as a transcription factor for several genes, and has so far only been identified as a repressor with no inducer (Oshima *et al*, 2006).

HU:

HU is a transcriptional dual regulator. It is a small DNA-binding protein similar to histones and helps supercoil DNA. It can bind to DNA and act as a transcriptional activator or repressor without an inducer (Oberto *et al*, 2009).

IclR:

IclR is a transcriptional repressor that regulates enzymes in the glyoxylate shunt. Pyruvate and glyoxylate can bind to IclR. Pyruvate stabilizes the active tetrameric form that can bind to DNA while glyoxylate stabilizes the inactive dimer form that cannot bind to DNA (Lorca *et al*, 2007).

IHF:

IHF is a protein that is highly abundant in cells, and is used as both a transcriptional repressor and activator. IHF often stabilizes correct nucleoprotein complexes and can facilitate the formation of loops near the promoter. It is a heterodimer

protein that binds to A/T rich sequences of DNA. IHF requires no inducer to bind to DNA (Azam *et al*, 1999).

LacI:

LacI is an inducible transcriptional repressor for the *lac* operon. Unmodified LacI can bind to DNA at two operators forming a repressor loop to reduce transcription. Allolactose, or IPTG, can bind to LacI and cause a conformational shift that prevents LacI from binding to DNA (Lewis, 2005).

MarA:

MarA is a dual transcriptional regulator similar to SoxS and Rob. MarA binds to a specific DNA sequence known as the sox-mar-rob box. MarA requires no inducer to bind to DNA (Martin *et al*, 2008).

NarL:

NarL is a nitrate/nitrite response regulator that can activate and repress transcription of genes needed for nitrate respiration and other pathways. In the presence of nitrate or nitrite, the kinase NarX phosphorylates NarL. Phosphorylated NarL is capable of binding to DNA. In the absence of nitrate and nitrite, NarL is inactivated by dephosphorylation (Schröder *et al*, 1994).

NsrR:

NsrR is a nitrate-sensitive repressor that regulates at least 30 genes. NsrR can only bind to DNA with the cofactor [2Fe-2S] cluster. If nitric oxide (NO) binds to the [2Fe-

2S] cluster, then NsrR can no longer bind to DNA (Tucker *et al*, 2008). Ammonium nitrate is a usable nitrogen source for PHB production (Khanna & Srivastava, 2005).

PdhR:

PdhR is a transcriptional repressor for genes coding the pyruvate dehydrogenase and 2-oxoglutarate dehydrogenase complexes. Unmodified PdhR can bind to DNA to repress transcription. Pyruvate can bind to PdhR and cause a conformational shift that prevents PdhR from binding to target promoters (Quail & Guest, 1995).

Rob:

Rob is a transcriptional activator similar to SoxS and MarA and binds to the sox-mar-rob box. No inducer is needed for Rob to bind to DNA (Martin *et al*, 2008).

SoxR:

SoxR is a transcriptional activator that is activated by the cofactor [2Fe-2S] cluster. SoxR can bind to DNA with or without [2Fe-2S], but is only able to activate transcription with the presence of a [2Fe-2S] cluster (Gaudu & Weiss, 1996).

SoxS:

SoxS is a transcriptional activator sensitive to superoxide and nitric oxide. SoxS is similar to Rob and MarA and binds to the sox-mar-rob box DNA sequence (Martin *et al*, 2008). Activity of SoxS is controlled solely by its concentration (Griffith *et al*, 2004).

Transcriptional Network Equations

The metabolic pathways modeled consist of many enzymatic reactions. These enzymatic reactions are intrinsically dependent upon the concentration of the enzymes. The concentration of enzymes in a cell is dependent upon the quantity being transcribed and translated from the DNA coupled with the rate of enzyme degradation. Expressions were used to relate enzyme concentration to promoter activity and transcription factors. The concentration of transcription factors was related to the frequency of ligand binding. Enzyme degradation was correlated to the amino acid on the N-terminus of the enzyme's polypeptide. The following equations were used to model the concentration of enzymes based on their transcriptional network.

Enzyme Concentration:

An equation was needed to correlate the amount of enzyme synthesized to its transcription factors and promoters. Equation (11) describes enzyme concentration as a function of the concentration of a single transcription factor (Ronen *et al*, 2002; Zaslaver *et al*, 2004). However, enzymes are usually regulated by multiple transcription factors.

$$\frac{dE}{dt} = \frac{\beta}{1+\left(TF/k\right)^{H}} \tag{11}$$

E = Enzyme concentration
β = Promoter activity (unrepressed/inactivated)
TF = Transcription factor concentration
k = Effective affinity of the transcription factor (Conc. for half maximal repression/activation)
H = Hill coefficient of cooperativity
H > 0 = repression
H < 0 = activation

Equation (11) was modified as part of this thesis development to include terms for multiple transcription factors affecting one promoter. Equation (12) was the result and it relates enzyme concentration to the concentrations of *n* transcription factors. This equation calculates the enzyme concentration based on all of the activators and repressors that interact with the promoter that initiates transcription of the enzyme's gene.

$$\frac{dE}{dt} = \frac{\beta}{1+\left({TF_1}/{k_1}\right)^{H_1}+\left({TF_2}/{k_2}\right)^{H_2}+\cdots+\left({TF_n}/{k_n}\right)^{Hn}} \quad (12)$$

E = Enzyme concentration
β = Promoter activity (unrepressed/inactivated)
TF_n = Transcription factor *n* concentration
k_n = Effective affinity of transcription factor *n* (Conc. for half maximal repression/activation)
H_n = Hill coefficient of cooperativity
H > 0 = repression
H < 0 = activation

Each promoter found to be regulated by transcription factors was represented by a reaction as shown in Figure 84. The rate for each promoter reaction was based on Equation (12). Forty promoters were used to model the transcription of 29 enzymes as seen in Figure 84. The transcription factors that regulate each promoter are shown as substrates to the promoter reactions, with enzymes shown as products of the reaction. Eight of the promoters initiate transcription of more than one enzyme, so multiple enzymes are shown as products of those reactions. Thirteen of the enzymes are impacted by multiple promoters, so they are shown as products of multiple promoter reactions. Table XXVII contains values from the literature that were used for the transcription factor terms in Equation (12) for each promoter reaction.

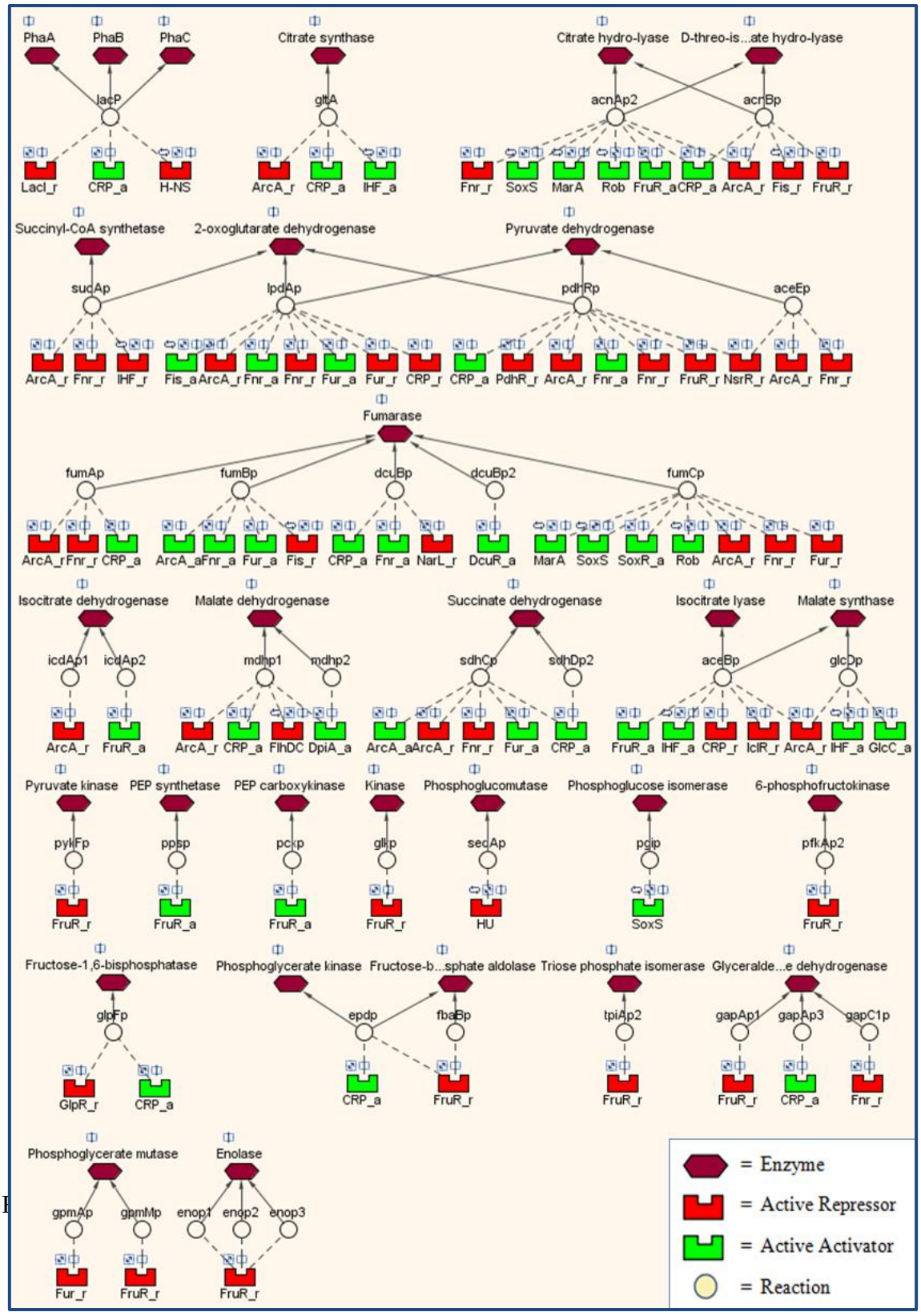
PhaA
PhaB
PhaC
lacP
LacI_r
CRP_a
H-NS
Citrate synthase
gltA
ArcA_r
CRP_a
IHF_a
Citrate hydro-lyase
D-threo-is...ate hydro-lyase
acnAp2
acnBp
Fnr_r
SoxS
MarA
Rob
FruR_a
CRP_a
ArcA_r
Fis_r
FruR_r
Succinyl-CoA synthetase
2-oxoglutarate dehydrogenase
Pyruvate dehydrogenase
sucAp
lpdAp
pdhRp
aceEp
ArcA_r
Fnr_r
IHF_r
Fis_a
ArcA_r
Fnr_a
Fnr_r
Fur_a
Fur_r
CRP_r
CRP_a
PdhR_r
ArcA_r
Fnr_a
Fnr_r
FruR_r
NsrR_r
ArcA_r
Fnr_r
Fumarase
fumAp
fumBp
dcuBp
dcuBp2
fumCp
ArcA_r
Fnr_r
CRP_a
ArcA_a
Fnr_a
Fur_a
Fis_r
CRP_a
Fnr_a
NarL_r
DcuR_a
MarA
SoxS
SoxR_a
Rob
ArcA_r
Fnr_r
Fur_r
Isocitrate dehydrogenase
Malate dehydrogenase
Succinate dehydrogenase
Isocitrate lyase
Malate synthase
icdAp1
icdAp2
mdhp1
mdhp2
sdhCp
sdhDp2
aceBp
glcDp
ArcA_r
FruR_a
ArcA_r
CRP_a
FlhDC
DpiA_a
ArcA_a
ArcA_r
Fnr_r
Fur_a
CRP_a
FruR_a
IHF_a
CRP_r
IclR_r
ArcA_r
IHF_a
GlcC_a
Pyruvate kinase
PEP synthetase
PEP carboxykinase
Kinase
Phosphoglucomutase
Phosphoglucose isomerase
6-phosphofructokinase
pykFp
ppsp
pckp
glkp
secAp
pgip
pfkAp2
FruR_r
FruR_a
FruR_a
FruR_r
HU
SoxS
FruR_r
Fructose-1,6-bisphosphatase
Phosphoglycerate kinase
Fructose-b...sphate aldolase
Triose phosphate isomerase
Glyceralde...e dehydrogenase
glpFp
epdp
fbaBp
tpiAp2
gapAp1
gapAp3
gapC1p
GlpR_r
CRP_a
CRP_a
FruR_r
FruR_r
FruR_r
CRP_a
Fnr_r
Phosphoglycerate mutase
Enolase
gpmAp
gpmMp
enop1
enop2
enop3
Fur_r
FruR_r
FruR_r
= Enzyme
= Active Repressor
= Active Activator
= Reaction

F

Table XXVII. Transcription factor concentrations [TF] and effective affinity values (k_n).

TF	[TF] µM	k_n	Organism	Reference
ArcA	NA	0.25-0.6	*E. coli*	Shen & Gunsalus, 1997
Crp	3.3-9.4	NA	*E. coli*	Ishizuka *et al*, 1993
DcuR	0.7-1.7	6	*E. coli*	Abo-Amer *et al*, 2004
Fis	0.17	NA	*E. coli*	Azam *et al*, 1999
Fnr	3.7	NA	*E. coli*	Sutton *et al*, 2004
Fur	8.3-16.6	NA	*E. coli*	Zheng *et al*, 1999
H-NS	13	NA	*E. coli*	Azam *et al*, 1999
HU	50	NA	*E. coli*	Azam *et al*, 1999
IHF	42	NA	*E. coli*	Azam *et al*, 1999
LacI	0.033	NA	*E. coli*	Zheng *et al*, 1999
MarA	0.067	0.02	*E. coli*	Martin *et al*, 1996
NarL	NA	0.9-1.4	*E. coli*	Darwin *et al*, 1997
NsrR	NA	0.02	*N. gonorrhoeae*	Isabella *et al*, 2009
PdhR	0.61	0.005	*E. coli*	Quail & Guest, 1995
Rob	17	NA	*E. coli*	Azam *et al*, 1999
SoxR	0.17	0.045	*E. coli*	Hidalgo & Demple, 1994 Pomposiello & Demple, 2001
SoxS	0.2	0.015	*E. coli*	Li & Demple, 1994 Martin *et al*, 1996

Active Transcription Factor Concentration:

Transcription factors are proteins with DNA binding domains that allow the protein to regulate transcription of certain genes. The DNA binding domain can be made more or less accessible by the binding of ligands to the transcription factor. The concentration of active transcription factor is the amount of the transcription factor that has the DNA binding domain accessible. Equation (13) shows how the fraction of bindings sites bound with a ligand is dependent upon the ligand concentration.

$$\theta = \frac{[L]}{[L]+K_d} \tag{13}$$

L = Ligand concentration
K_d = Dissociation constant
θ = Fraction of binding sites bound with ligand

The transcription factors FruR, GlpR, PdhR, LacI, and IclR have DNA binding domains that are made less accessible when a specific ligand binds to the transcription factor. For these transcription factors, Equation (14) was used to calculate the active transcription factor concentration in the model. In the model, Equations (13) and (14) were entered as Rules to calculate the active concentration of FruR, GlpR, PdhR, LacI, and IclR at each time step.

$$TF_A = (1-\theta)*[TF] \quad (14)$$

TF_A = Active transcription factor concentration
θ = Fraction of binding sites bound with ligand
TF = Total transcription factor concentration

ArcA, CRP, DcuR, DpiA, Fnr, Fur, GlcC, IclR, NarL, NsrR, and SoxR are transcription factors that need a specific ligand bound in order to open up the DNA binding domain. Equations (13) and (15) were used to calculate the active transcription factor concentration in the model for transcription factors that require ligand-binding. Rules were used to evaluate the two equations at each time step for these 11 transcription factors.

$$TF_A = \theta*[TF] \quad (15)$$

TF_A = Active transcription factor concentration
θ = Fraction of binding sites bound with ligand
TF = Total transcription factor concentration

The DNA binding domains have not yet been found to be affected by ligand-binding for the transcription factors Fis, FlhDC, H-NS, HU, IHF, MarA, Rob, and SoxS.

The active transcription factor concentration was set equal to the total transcription factor concentration for these regulatory proteins. Table XXVIII shows values found in the literature for ligand concentrations that were used in the model. The model diagram for the interactions between transcription factors and ligands is shown in Figure 85.

Table XXVIII. Known values for ligand concentrations used in the model.

Ligand	[L] µM	Organism	Reference
cAMP	10-70	*E. coli*	Makman & Sutherland, 1965
	28	*E. coli*	Krishna *et al*, 2009
Glycerol	4200	*S. cerevisiae*	Hynne *et al*, 2001
IPTG	100	*E. coli*	Linton, 2010
P_i	2440	*H. sapiens*	Nazaret *et al*, 2009
	7000	*T. brucei*	Helfert *et al*, 2001
	6500	*S. cerevisiae*	Teusink *et al*, 2000
	12000	*S. cerevisiae*	Nielsen *et al*, 1998

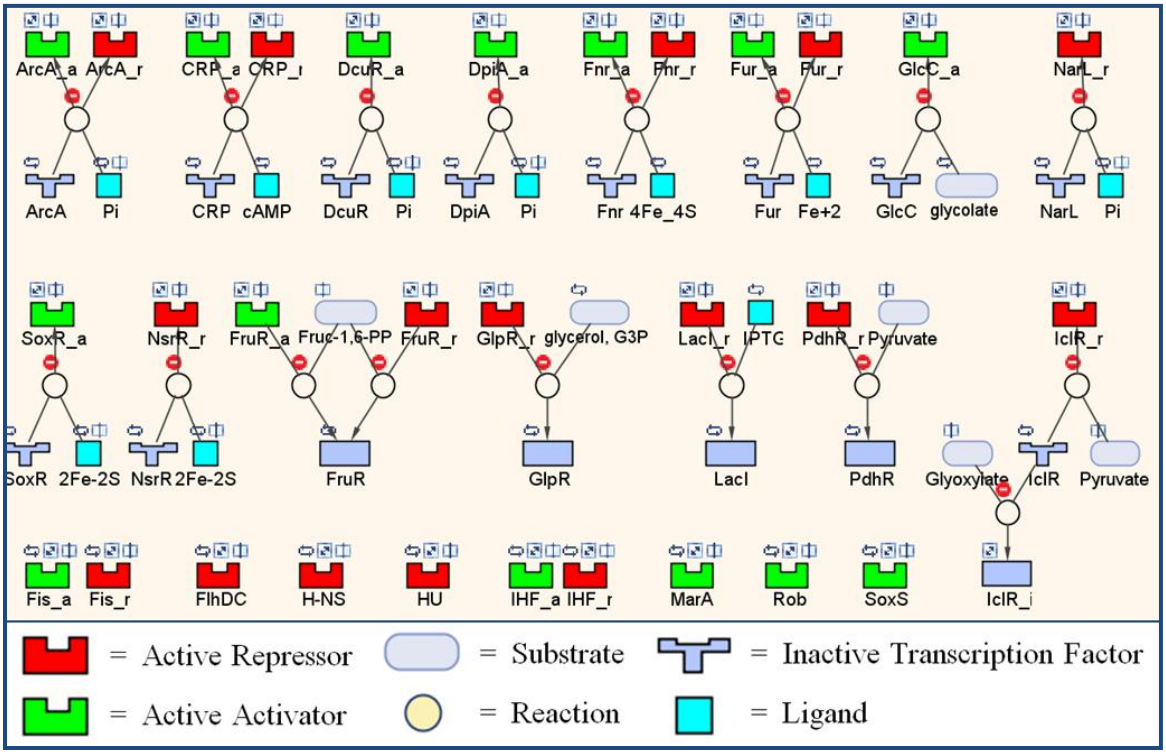

Figure 85. SimBiology model diagram of ligand and transcription factor interactions.

Enzyme Degradation:

The intracellular concentration of an enzyme is dependent upon the amount synthesized and degraded. Enzyme synthesis is represented in this model by the transcriptional network. Degradation reactions were added to the model to prevent constant accumulation of enzyme concentrations.

Degradation reactions were modeled using simple-mass action kinetics with the rate constant calculated from the enzyme half-life as shown in Equation (16). Enzyme half-lives were estimated based on the N-end rule (Varshavsky, 1997). Enzyme half-lives have a rough correlation with the amino acid on the N-terminus of the polypeptide chain.

$$r = \frac{\ln(2)}{\tau} \tag{16}$$

r = Degradation rate
τ = Enzyme half-life

The N-terminal amino acid was determined for each enzyme and the degradation rate was calculated from the half-life determined from the N-end rule. Figure 86 shows the model diagram for the enzyme degradation reactions. Because degradation rates are only estimates, these values were adjusted later on to achieve the best fit to published models.

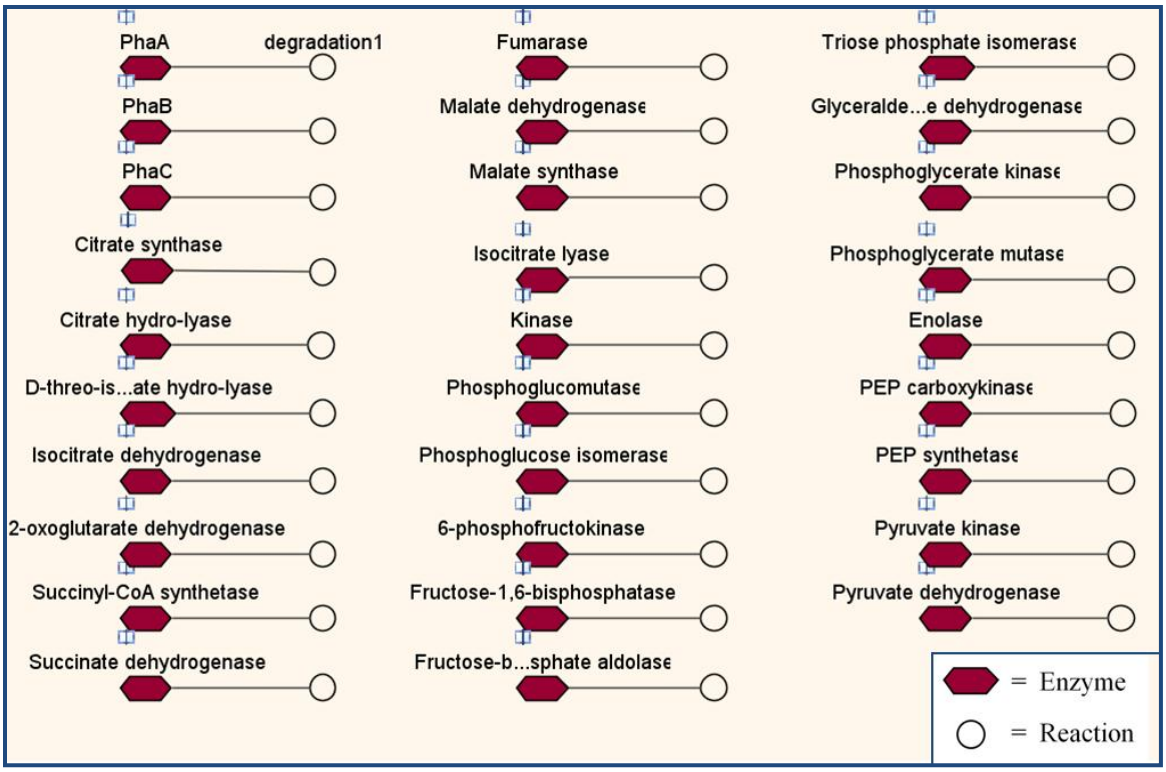

Figure 86. SimBiology model diagram of enzyme degradation reactions.

METABOLIC PROFILING

Introduction

Metabolic profiling is the process of monitoring the concentration of specific metabolites over time. The resulting data can be used to adjust parameters in order to create a more accurate model of the metabolic pathways in a specific strain of bacteria. Metabolic profiling requires culture samples to be quenched at specific time intervals. Quenching provides metabolic concentrations at a given time. One of the most common quenching methods is to shock the samples with a cold-buffered aqueous methanol mixture (Bajad *et al*, 2006; Buchholz *et al*, 2001; Dettmer *et al*, 2006; Lu *et al*, 2008; Mashego *et al*, 2007; Ohashi *et al*, 2007).

After sample preparations, metabolite concentrations can be determined through combinations of liquid chromatography (LC), gas chromatography (GC), mass spectrometry (MS), capillary electrophoresis (CE), and nuclear magnetic resonance (NMR) (Bajad *et al*, 2006; Buchholz *et al*, 2001; Dettmer *et al*, 2006; Lu *et al*, 2008; Mashego *et al*, 2007; Ohashi *et al*, 2007). Liquid chromatography combined with mass spectrometry (LC-MS) is effective because it can use a small sample volume to determine the concentrations of many metabolites simultaneously. One study was able to analyze the concentration of 69 metabolites from a single sample (Bajad *et al*, 2006).

The data obtained from metabolic profiling can be incorporated into the predictive model to allow a more precise simulation of the metabolic pathways under analysis. Metabolic profiling can continue to be used in the iterative process of genetically engineering an optimized PHB producing strain of bacteria.

Materials and Methods

Strains and Culture Methods:

E. coli XL1-Blue cells containing the pBHR68 plasmid have been shown to accumulate as much as 55% of their cell dry weight as bio-plastic (Linton, 2010). Analysis of the metabolomics was conducted on samples from this cell line and a control study was performed using untransformed *E. coli* XL1-Blue cells. The control study used the same procedures outlined below with the exception of adding ampicillin to the growth media.

Cells were pre-cultured by inoculating 5 mL of M9 growth media with 50 µL of a frozen glycerol stock. The M9 growth media was supplemented with 50 µg/mL ampicillin for selection of cells harboring the pBHR68 plasmid. Cultures were grown for 10 hours and then used to inoculate a second culture in 5 mL of M9 growth media (1:100 v/v). The second culture was grown for 10 hours and then used to inoculate a third culture in 5 mL of M9 growth media (1:100 v/v). The third culture was grown for 10 hours and then used to inoculate 150 mL M9 growth media (1:100 v/v) containing 1% (w/v) glucose and 50 µg/mL ampicillin. Cells were grown to stationary phase, and then isopropyl β-D-1-thiogalactopyranoside (IPTG) was added to a final concentration of 0.1 mM. Additional glucose, 15 mL of 7.5% (w/v) glucose solution, was added 5 hours after inoculation. Starting 5 hours after inoculation, 0.5 mL samples were taken every 15 minutes until cell growth reached stationary phase. Absorbance of the cultures was recorded at 600 nm every 30 minutes to monitor cell growth.

Quenching and Sample Preparation:

The samples were quenched for metabolic activity by adding 2.5 mL of -50^{o} C aqueous methanol (60% v/v) containing 70 mM Hepes buffer (Bajad *et al*, 2006). Samples were sonicated for 2 minutes while kept on ice in order to lyse the cells. Samples were lyophilized using a speed vacuum and then re-suspended in 300 µL of quenching fluid in order to concentrate the samples. Then the samples were centrifuged for 10 minutes at 10,286g. Cell pellets were discarded and then the supernatant was stored at -80^{o} C. All samples were stored for future analysis by high performance liquid chromatography and mass spectrometry (HPLC-MS). Recommended analytical methods for HPLC-MS are outlined in Appendix B.

Results

Growth curves obtained from the optical density for the two strains of *E. coli* are shown in Figure 87. After IPTG was added, the strain with the pBHR68 plasmid showed slower cell growth than the other strain as seen in Figure 87. Slower cell growth after induction by IPTG is consistent with the hypothesis that energy is being diverged from normal cellular functions in order to synthesize PHB.

Metabolic profiling data was not obtained due to the unavailability of a functioning mass-spectrometer. Metabolic profiling samples were stored at -80^{o} C for future analysis. It was anticipated that the metabolic profiling data would be used to better fit the predictive model to the specific strain of *E. coli* under study. Because this data was unavailable, the model was fit to nine published models and to preliminary PHB production data as shown in the next chapter.

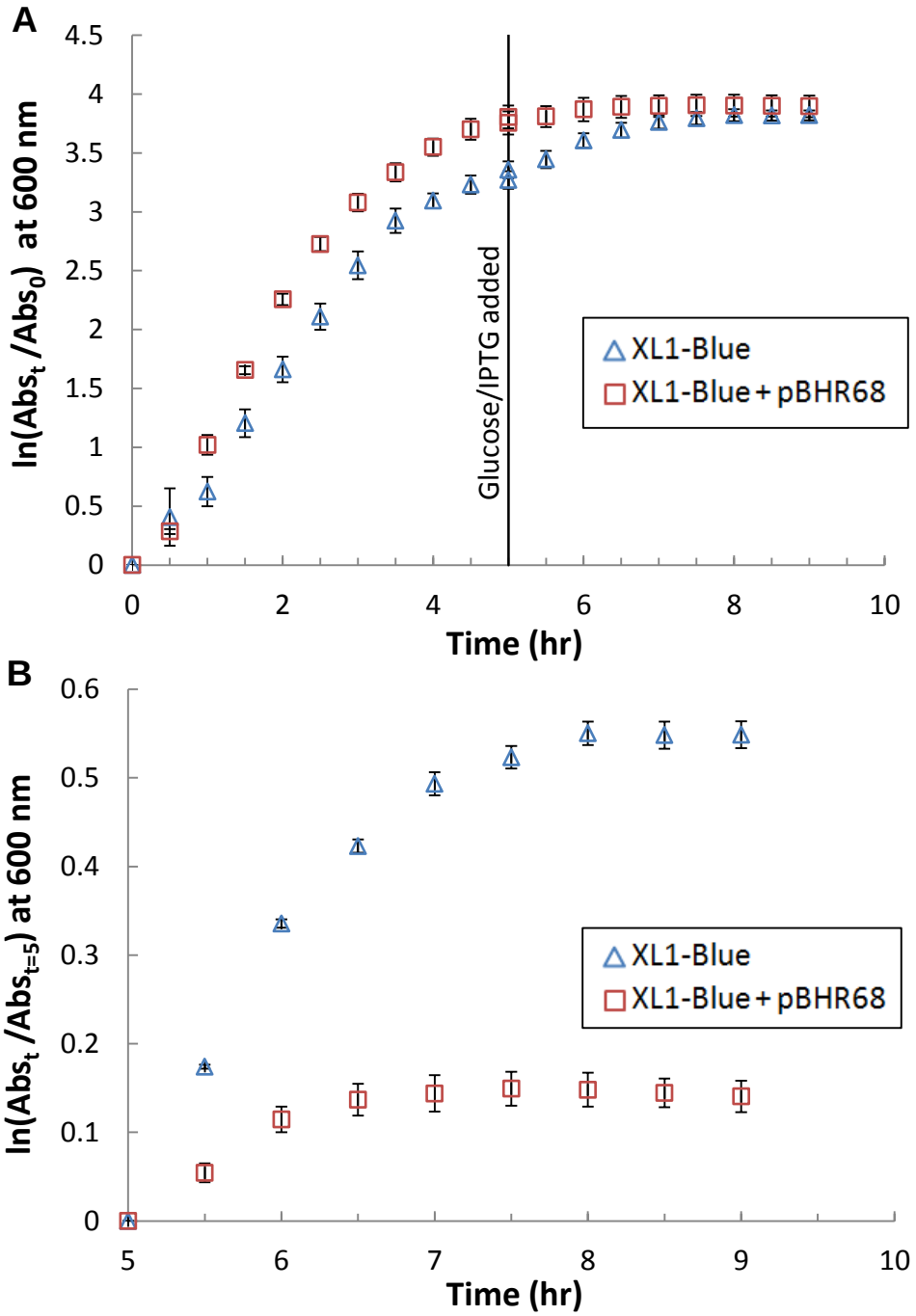

Figure 87. Natural log of the absorbance at time t divided by (A) the initial absorbance reading and (B) absorbance reading at t = 5 hr plotted over time. Absorbance was read at 600 nm. At t = 5 hr, 15 mL of 5 x glucose solution was added to both cultures and IPTG was added to a final concentration of 0.1 mM in the XL1-Blue + pBHR68 culture. Error bars represent standard error with n = 3.

SIMULATIONS AND RESULTS

Comparing Model with Literature

The glycolysis and TCA portions of the SimBiology model were validated using published models found in the BioModels database at http://www.ebi.ac.uk/biomodels-main/publ-models.do. This database is a compilation of published models assembled by the European Bioinformatics Institute. Out of 366 curated BioModels, seven were identified as glycolysis models and two were identified as TCA cycle models. These nine models were used to validate the glycolysis pathway and the TCA cycle modeled in SimBiology.

Glycolysis BioModels:

Seven BioModels including 42, 61, 64, 71, 172, 176, and 177 were used to validate the glycolysis portion of the predictive model. The online simulator in the BioModels database was used to run simulations of the species in glycolysis. The SimBiology model was adjusted to match its steady-state concentrations with the steady-state concentrations of the glycolysis intermediates simulated in the BioModels. The first two BioModels (42 and 61) modeled glycolytic oscillations observed in synchronous cultures. The SimBiology model is not a model for synchronous cultures; therefore, the SimBiology model was adjusted to match the average steady-state concentrations of the glycolysis species for these two BioModels.

The SimBiology model needed to be altered to accurately match these seven BioModels. The BioModels do not account for PHB synthesis; therefore, the PHB synthesis pathway was shut off in the model by inactivating the forward and reverse

directions of Reaction 1. To account for diffusion of extracellular glucose into the cell, Reaction 0 was created using simple mass action kinetics. Reaction 27 was added to account for pyruvate used elsewhere in the cell and Reaction 28 was created to account for acetyl-CoA used in pathways not included in the model. Reactions 27 and 28 were modeled using simple mass action kinetics.

None of the BioModels accounted for the transcriptional network. Therefore, the transcriptional network portion of the SimBiology model was inactivated by holding the enzyme concentrations constant. All of the seven BioModels identified above simulated continuous cultures, so the concentration of extracellular glucose was held constant in the predictive model. The concentrations of ATP, ADP, NAD^+, and NADH were also held constant during simulation. Initial concentrations of glycolysis substrates were changed to match the initial values used in each BioModel. The value zero was used for any initial concentration not specified in the BioModel. The values for Reaction 0, Reaction 27, Reaction 28, and the glycolysis enzyme concentrations were adjusted until the SimBiology simulations matched the simulations from the BioModel.

Reaction 0:

$$\mathrm{Glucose}_{\mathrm{extracellular}} \xrightarrow{\text{Diffusion}} \mathrm{Glucose}_{\mathrm{intracellular}}$$

Reaction 27:

$$\mathrm{Pyruvate} \rightarrow \mathrm{Null}$$

Reaction 28:

$$\text{Acetyl-CoA} \rightarrow \mathrm{Null}$$

BioModel 42 - Nielsen 1998 Glycolysis:

BioModel 42 is a glycolysis model for *S. cerevisiae* (Nielsen *et al*, 1998). This model simulates observed oscillations in a continuous-flow, stirred tank reactor. Glycolytic oscillations in yeast are a result of a synchronous culture. BioModel 42 used the initial concentrations shown in Table XXIX. In order to fit the SimBiology model to BioModel 42, the values in Table XXIX were used as initial concentrations in the SimBiology model.

Twelve variables were adjusted in order to match the simulations between the SimBiology model and BioModel 42. Two of the variables were reaction rates for Reaction 0 and Reaction 27. The other ten variables were the glycolysis enzyme concentrations. Table XXIX shows the enzyme concentrations and reaction rates used to successfully fit the model. Figure 88 and Figure 89 visually compare the simulations from BioModel 42 with the adjusted SimBiology model.

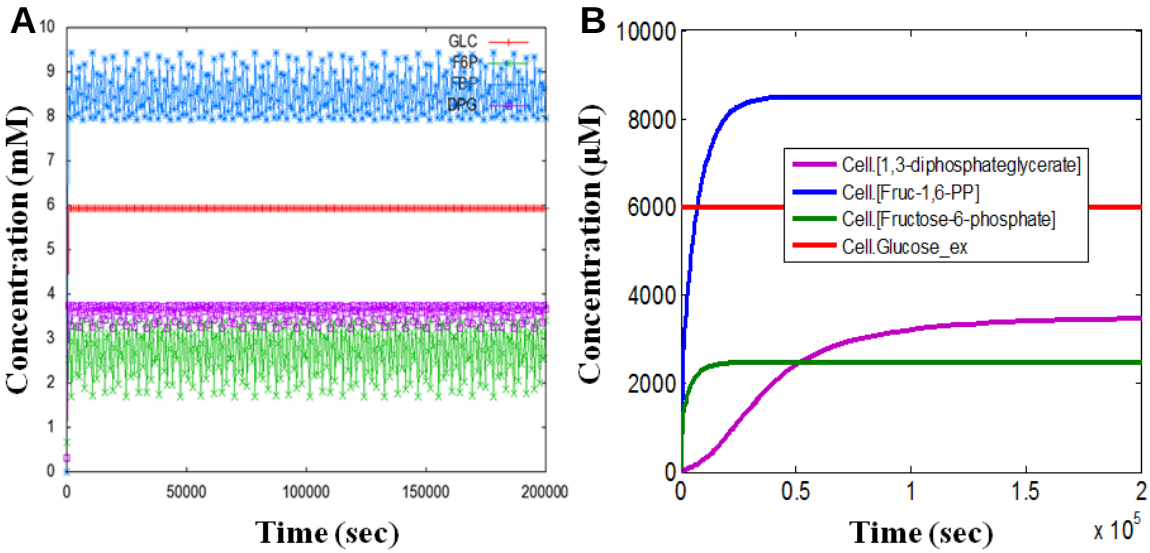

Figure 88. Simulations from (A) BioModel 42 and (B) SimBiology model for the species glucose, fructose-6-phosphate, fructose-1,6-bisphosphate, and 1,3-diphosphoglycerate.

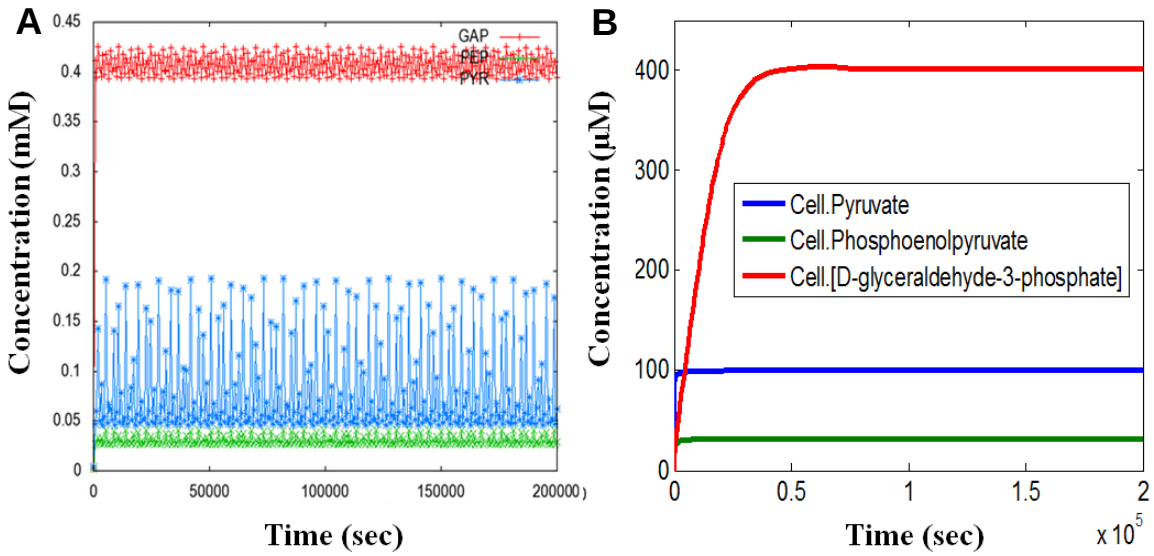

Figure 89. Simulations from (A) BioModel 42 and (B) SimBiology model for the species glyceraldehyde-3-phosphate, phosphoenolpyruvate, and pyruvate.

Table XXIX. Initial substrate concentrations, enzyme concentrations, and reaction rates used to compare the SimBiology model to BioModel 42.

	Species	Value	Unit	Reference
Initial Concentrations of Glycolysis Substrates	GLC_ex	6000	µM	Nielsen *et al*, 1998
	GLC	11.3	µM	Nielsen *et al*, 1998
	G6P	0	µM	----
	F6P	659	µM	Nielsen *et al*, 1998
	FBP	7.7	µM	Nielsen *et al*, 1998
	GAP	1.9	µM	Nielsen *et al*, 1998
	DHAP	0	µM	----
	DPG	299	µM	Nielsen *et al*, 1998
	3PG	0	µM	----
	2PG	0	µM	----
	PEP	2.1	µM	Nielsen *et al*, 1998
	PYR	4.2	µM	Nielsen *et al*, 1998
Enzyme Concentrations Used to Fit Model	KIN	310	µM	----
	PGI	50	µM	----
	6PFK	0.8328	µM	----
	FBA	880.33	µM	----
	TPI	0.56	µM	----
	GAD	351.7	µM	----
	PGK	6.65045	µM	----
	PGM	2.06	µM	----
	ENO	420	µM	----
	PYK	2.52	µM	----
Reaction Rates Used to Fit Model	R0	0.01	µM/s	----
	R27	1.17	µM/s	----

BioModel 61 - Hynne 2001 Glycolysis:

BioModel 61 is another model for glycolysis in *S. cerevisiae* (Hynne *et al*, 2001). Similar to BioModel 42, this model simulates glycolytic oscillations in yeast. BioModel 61 used the initial species concentrations found in Table XXX. The values in Table XXX were used as initial substrate concentrations to fit the SimBiology model to BioModel 61

Many different values for ten enzymes and two reaction rates were tried in order to successfully fit the model to BioModel 61. Table XXX shows the combination of values that resulted in a successful fit to BioModel 61. The matching simulations between the model and BioModel 61 are shown in Figure 90, Figure 91, and Figure 92.

BioModel 61 did not have simulations available for the species 2-phosphoglycerate and 3-phosphoglycerate. The average simulation value from the other BioModels for 2-phosphoglycerate was 0.062 mM. The average simulation value for 3-phosphoglycerate was 0.48 mM. For these two species, the SimBiology model was fit to match the average values as shown in Figure 93.

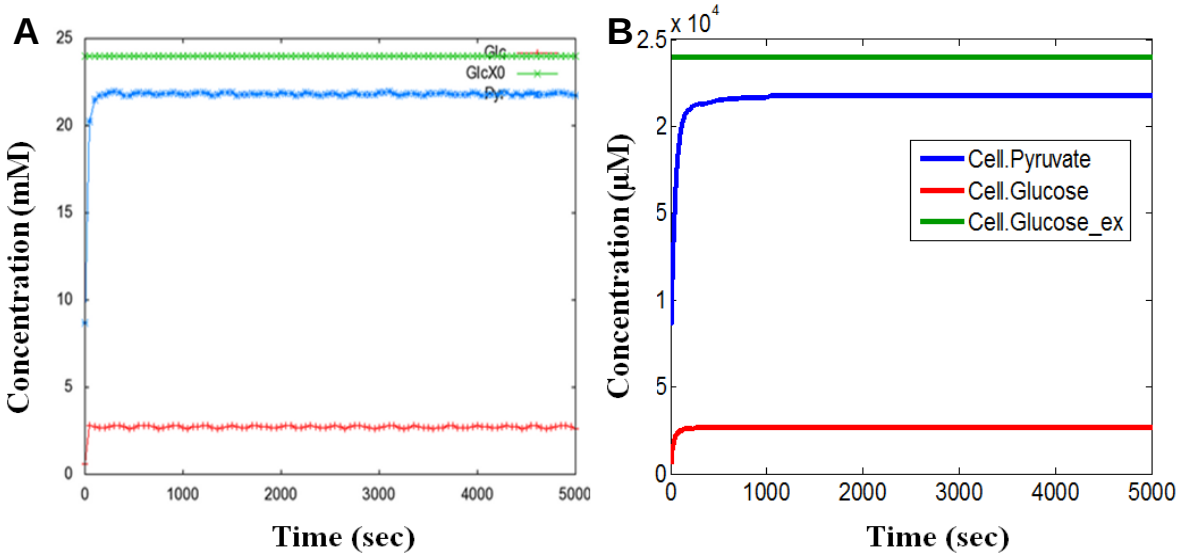

Figure 90. Simulations from (A) BioModel 61 and (B) SimBiology model for the species glucose intracellular, glucose extracellular, and pyruvate.

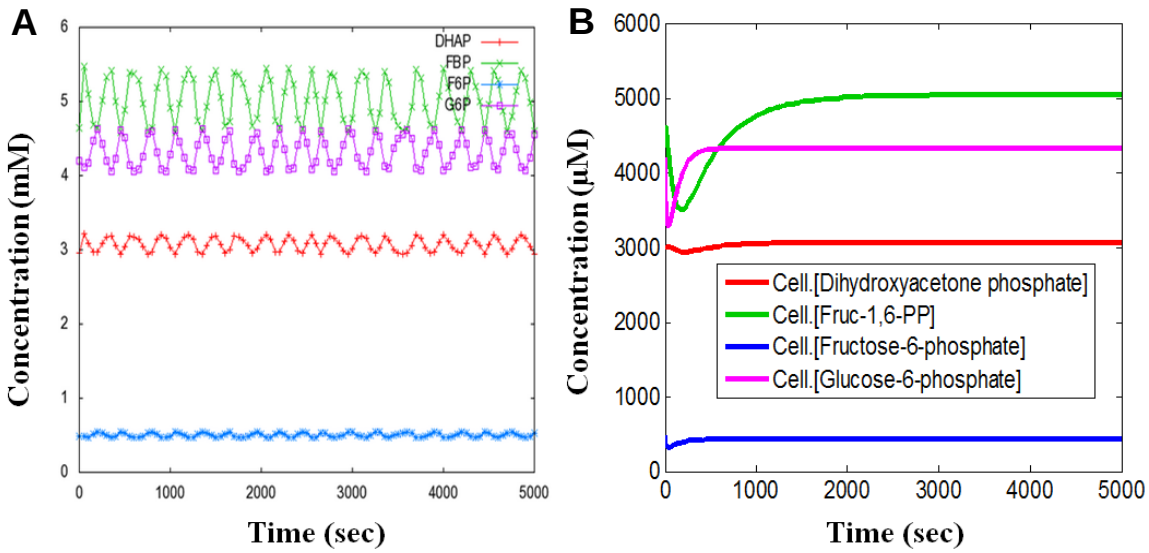

Figure 91. Simulations from (A) BioModel 61 and (B) SimBiology model for the species dihydroxyacetone phosphate, fructose-1,6-bisphophosphate, fructose-6-phosphate, and glucose-6-phosphate.

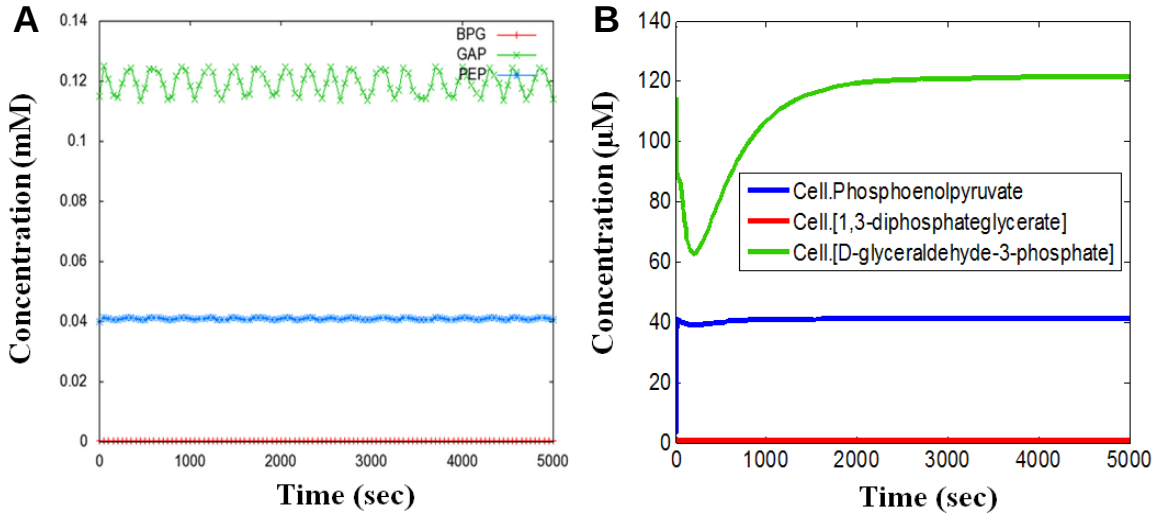

Figure 92. Simulations from (A) BioModel 61 and (B) SimBiology model for the species 1,3-diphosphoglycerate, glyceraldehyde-3-phosphate, and phosphoenolpyruvate.

BioModel 64 – Teusink 2000 Glycolysis:

BioModel 64 is another glycolysis model for *S. cerevisiae* (Teusink *et al*, 2000). This model simulates steady-state fluxes in a continuous fed reactor. Unlike BioModel 42 and 61, this BioModel does not model glycolytic oscillations. The initial species concentrations in Table XXXI were used in BioModel 64 and in the SimBiology model.

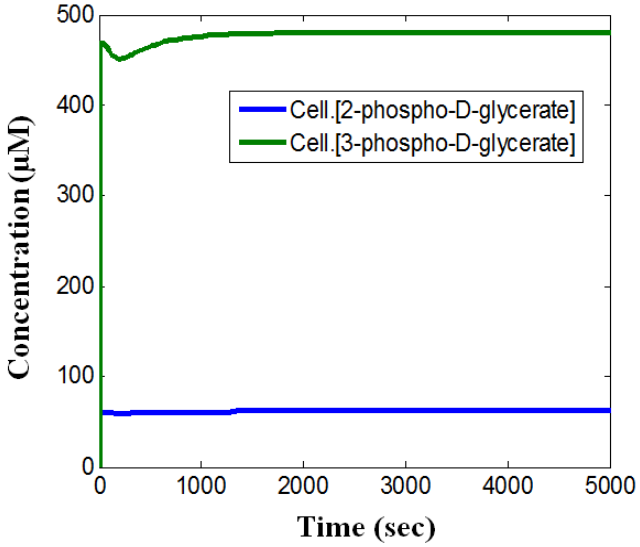

Figure 93. Simulation from SimBiology model for the species 2-phosphoglycerate and 3-phosphoglycerate. BioModel 61 had no simulations for these species.

Table XXX. Initial substrate concentrations, enzyme concentrations, and reaction rates used to compare the SimBiology model to BioModel 61.

	Species	Value	Unit	Reference
Initial Concentrations of Glycolysis Substrates	GLC_ex	24000	µM	Hynne *et al*, 2001
	GLC	573	µM	Hynne *et al*, 2001
	G6P	4200	µM	Hynne *et al*, 2001
	F6P	490	µM	Hynne *et al*, 2001
	FBP	4640	µM	Hynne *et al*, 2001
	GAP	115	µM	Hynne *et al*, 2001
	DHAP	2950	µM	Hynne *et al*, 2001
	DPG	0.27	µM	Hynne *et al*, 2001
	3PG	0	µM	----
	2PG	0	µM	----
	PEP	40	µM	Hynne *et al*, 2001
	PYR	8700	µM	Hynne *et al*, 2001
Enzyme Concentrations Used to Fit Model	KIN	310	µM	----
	PGI	50	µM	----
	6PFK	4.0	µM	----
	FBA	3585	µM	----
	TPI	0.56	µM	----
	GAD	1427	µM	----
	PGK	150	µM	----
	PGM	2.06	µM	----
	ENO	420	µM	----
	PYK	9.0	µM	----
Reaction Rates Used to Fit Model	R0	0.01	µM/s	----
	R27	0.022	µM/s	----

Different combinations of enzyme concentrations and reaction rate values were simulated in the SimBiology model. The values found in Table XXXI were a successful combination that resulted in a good fit to BioModel 64. Figure 94 and Figure 95 show how closely the SimBiology model simulations matched the BioModel 64 simulations.

BioModel 64 had no simulations available for glyceraldehyde-3-phosphate and dihydroxyacetone phosphate. The average concentration for glyceraldehyde-3-phosphate from other BioModels was 2.14 mM. The average concentration for dihydroxyacetone phosphate from BioModels 71, 172, 176, and 177 was 0.032 mM. The SimBiology model was adjusted to match these average values as shown in Figure 96.

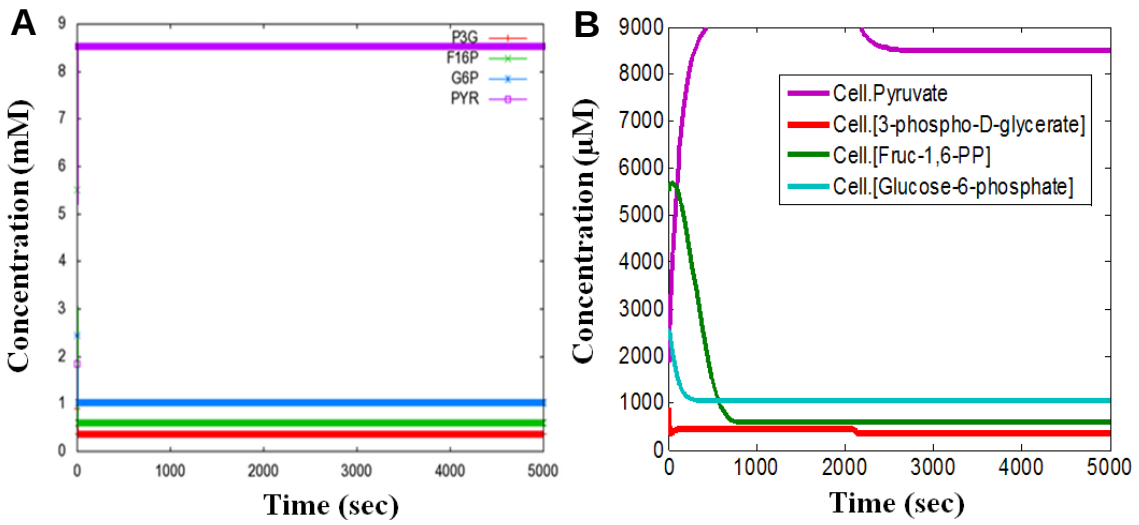

Figure 94. Simulations from (A) BioModel 64 and (B) SimBiology model for the species 3-phosphoglycerate, fructose-1,6-bisphosphate, glucose-6-phosphate, and pyruvate.

BioModel 71 - Bakker 2001 Glycolysis:

BioModel 71 simulates glycolysis in the protist species *T. brucei* (Helfert *et al*, 2001). Like the other glycolysis BioModels, this one also models a continuous fed reactor. Initial substrate concentrations in the SimBiology model were set to match the initial concentrations in BioModel 71 shown in Table XXXII.

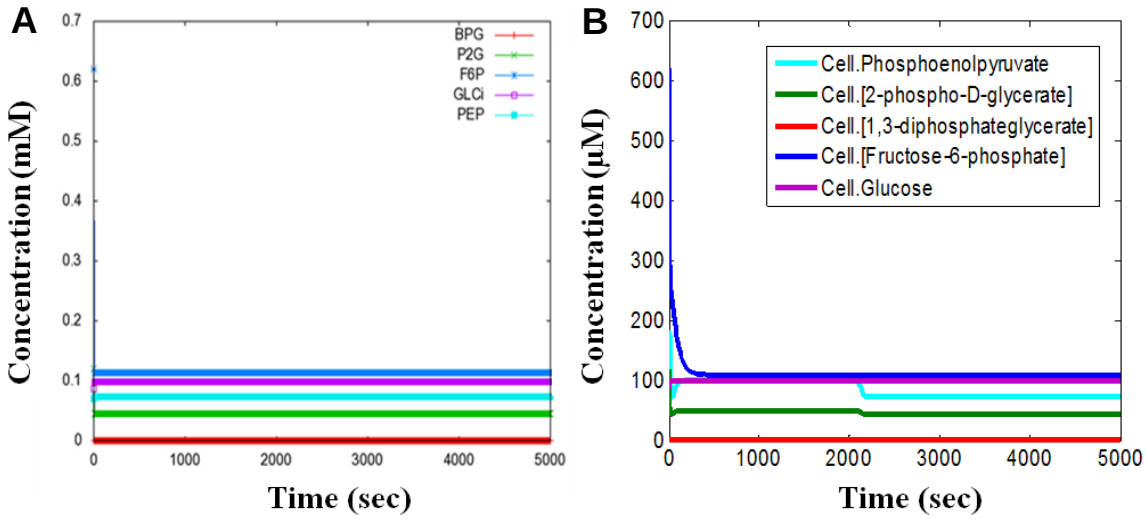

Figure 95. Simulations from BioModel 64 for the species 1,3-diphosphoglycerate, 2-phosphoglycerate, fructose-6-phosphate, glucose intracellular, and phosphoenolpyruvate.

Table XXXI. Initial substrate concentrations, enzyme concentrations, and reaction rates used to compare the SimBiology model to BioModel 64.

	Species	Value	Unit	Reference
Initial Concentrations of Glycolysis Substrates	GLC_ex	50000	µM	Teusink *et al*, 2000
	GLC	87	µM	Teusink *et al*, 2000
	G6P	2450	µM	Teusink *et al*, 2000
	F6P	620	µM	Teusink *et al*, 2000
	FBP	5510	µM	Teusink *et al*, 2000
	GAP	0	µM	----
	DHAP	0	µM	----
	DPG	0	µM	----
	3PG	900	µM	Teusink *et al*, 2000
	2PG	120	µM	Teusink *et al*, 2000
	PEP	70	µM	Teusink *et al*, 2000
	PYR	1850	µM	Teusink *et al*, 2000
Enzyme Concentrations Used to Fit Model	KIN	354	µM	----
	PGI	14.22	µM	----
	6PFK	1.05	µM	----
	FBA	790	µM	----
	TPI	0.11	µM	----
	GAD	250	µM	----
	PGK	34	µM	----
	PGM	0.377	µM	----
	ENO	86.0	µM	----
	PYK	1.245	µM	----
Reaction Rates Used to Fit Model	R0	0.0008	µM/s	----
	R27	0.00799	µM/s	----

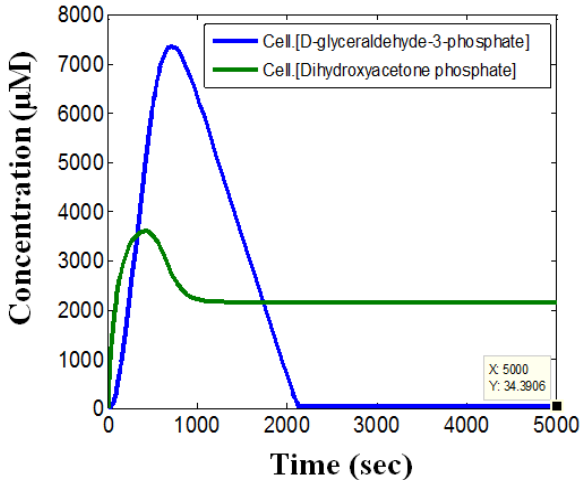

Figure 96. Simulation from SimBiology model for the species glyceraldehyde-3-phosphate and dihydroxyacetone phosphate. BioModel 64 had no simulations for these species.

The values of the glycolysis enzymes and the reaction rates of Reaction 0 and Reaction 27 were adjusted to fit the model to BioModel 71. The values that resulted in a successful fit are found in Table XXXII. The best fit was determined by comparing each glycolysis substrate simulation between BioModel 71 and the SimBiology model. Figure 97, Figure 98, and Figure 99 show how the simulations of BioModel 71 compare with the simulations of the SimBiology model.

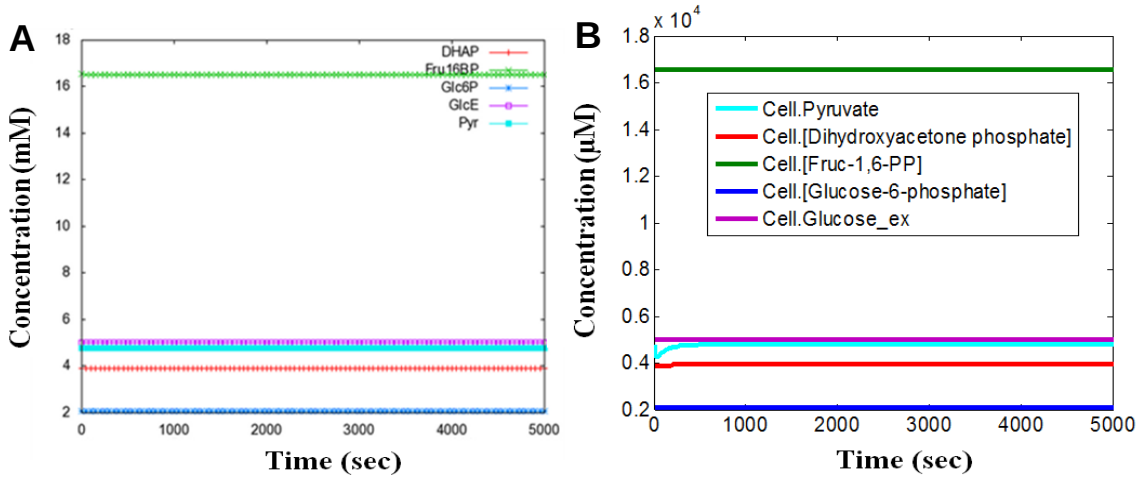

Figure 97. Simulations from (A) BioModel 71 and (B) SimBiology model for the species dihydroxyacetone phosphate, fructose-1,6-bisphosphate, glucose-6-phosphate, extracellular glucose, and pyruvate.

Table XXXII. Initial substrate concentrations, enzyme concentrations, and reaction rates used to compare the SimBiology model to BioModel 71.

	Species	Value	Unit	Reference
Initial Concentrations of Glycolysis Substrates	GLC_ex	50000	µM	Helfert *et al*, 2001
	GLC	34	µM	Helfert *et al*, 2001
	G6P	2072	µM	Helfert *et al*, 2001
	F6P	512	µM	Helfert *et al*, 2001
	FBP	16537	µM	Helfert *et al*, 2001
	GAP	39.9	µM	Helfert *et al*, 2001
	DHAP	3899	µM	Helfert *et al*, 2001
	DPG	32.7	µM	Helfert *et al*, 2001
	3PG	0	µM	----
	2PG	0	µM	----
	PEP	0	µM	Helfert *et al*, 2001
	PYR	4774	µM	Helfert *et al*, 2001
Enzyme Concentrations Used to Fit Model	KIN	1200	µM	----
	PGI	78.5	µM	----
	6PFK	0.805	µM	----
	FBA	724.23	µM	----
	TPI	0.1059	µM	----
	GAD	309.5	µM	----
	PGK	5.919	µM	----
	PGM	0.3977	µM	----
	ENO	87.1	µM	----
	PYK	1.2015	µM	----
Reaction Rates Used to Fit Model	R0	0.01	µM/s	----
	R27	0.01846	µM/s	----

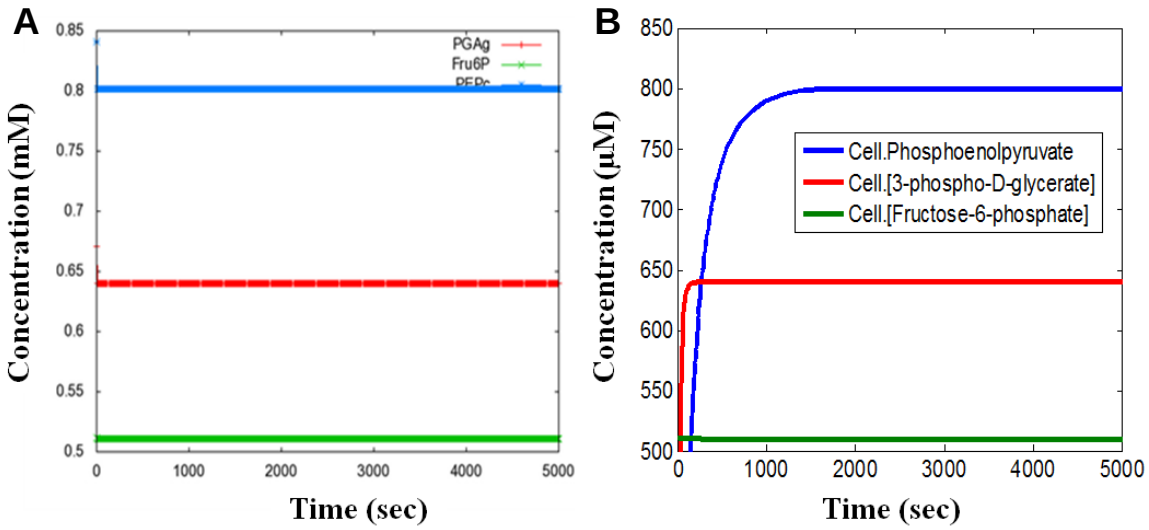

Figure 98. Simulations from (A) BioModel 71 and (B) SimBiology model for the species 3-phosphoglycerate, fructose-6-phosphate, and phosphoenolpyruvate.

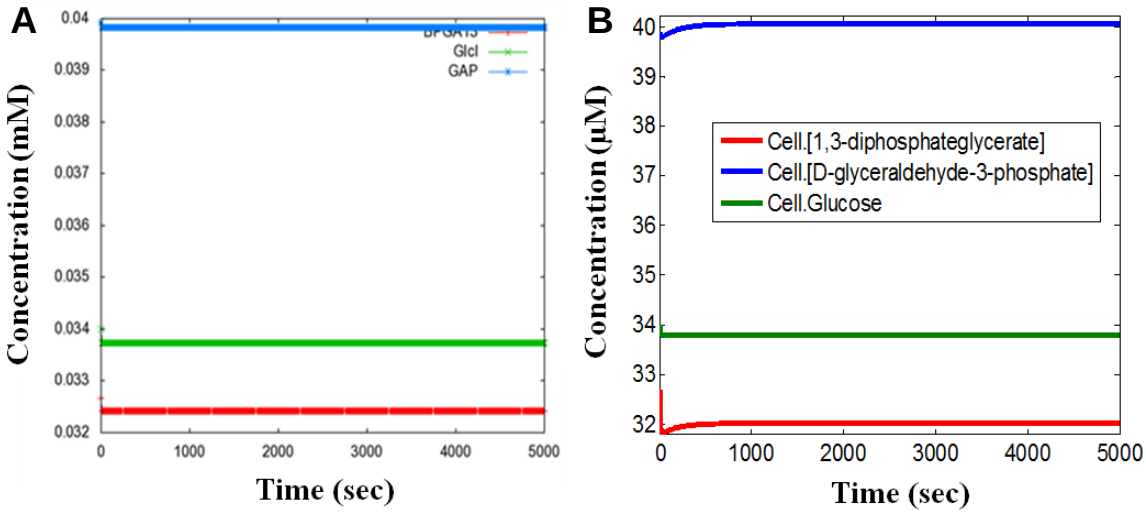

Figure 99. Simulations from (A) BioModel 71 and (B) SimBiology model for the species 1,3-diphosphoglycerate, intracellular glucose, and glyceraldehyde-3-phosphate.

BioModel 71 had no simulation available for 2-phosphoglycerate. The SimBiology simulation of 2-phosphoglycerate was fitted to the average concentration from the other BioModels. Figure 100 shows how the simulation matches the average value of 0.62 mM for 2-phosphoglycerate.

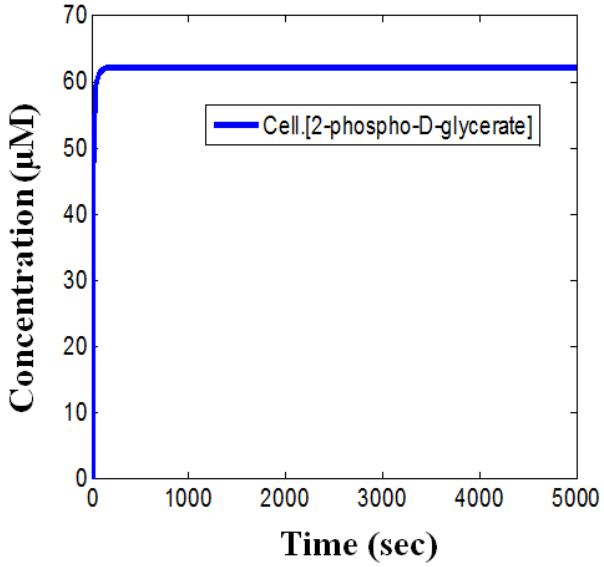

Figure 100. Simulation from SimBiology model for the species 2-phosphoglycerate. BioModel 71 had no simulations available for this species.

BioModel 172 - Pritchard 2002 Glycolysis:

BioModel 172 is a model of *S. cerevisiae* glycolysis (Pritchard & Kell, 2002). Similar to BioModel 64, this model does not simulate glycolytic oscillations in yeast. BioModel 172 is a model for a continuous fed reactor. Initial species concentrations used in BioModel 172 were also used in the SimBiology model and are shown in Table XXXIII. Enzyme concentrations and reaction rates were varied in the SimBiology model in order to find a successful fit to BioModel 172. The best fit came from the values in Table XXXIII.

Comparison of species simulations between BioModel 172 and the SimBiology model are shown in Figure 101, Figure 102, and Figure 103. These figures show closely matched simulations for all 11 glycolysis species that BioModel 172 can simulate.

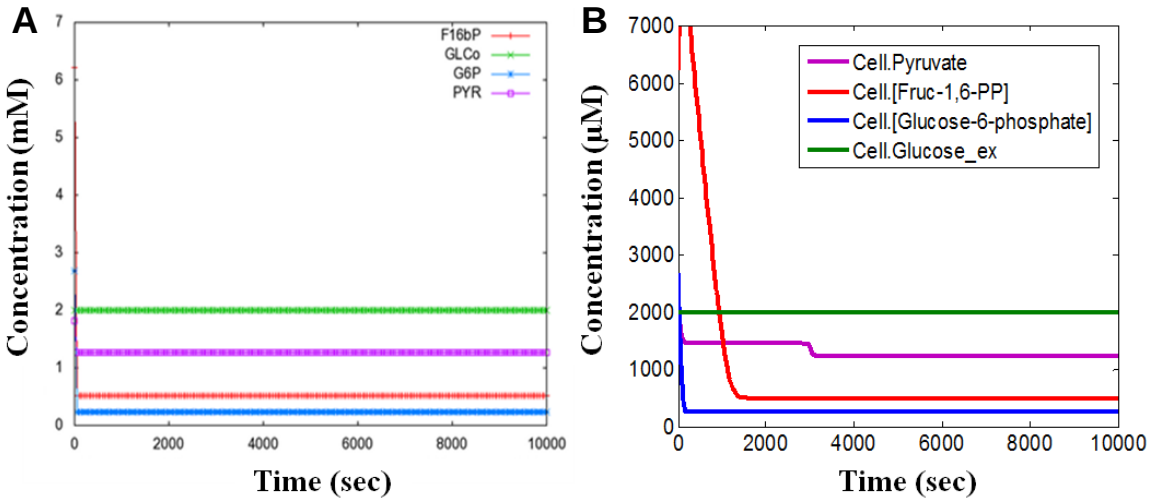

Figure 101. Simulations from (A) BioModel 172 and (B) SimBiology model for the species fructose-1,6-bisphosphate, extracellular glucose, glucose-6-phosphate, and pyruvate.

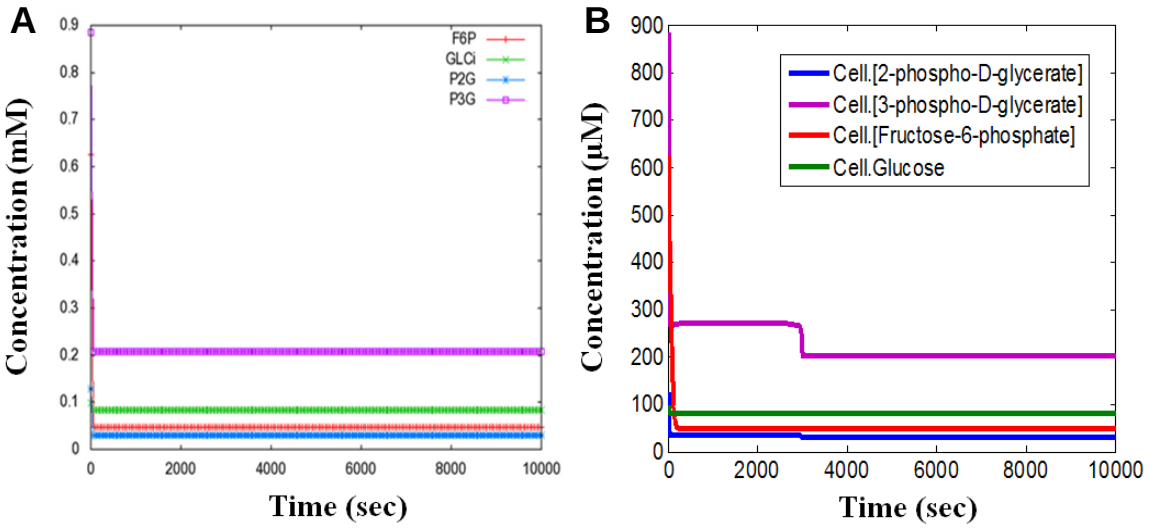

Figure 102. Simulations from (A) BioModel 172 and (B) SimBiology model for the species fructose-6-phosphate, intracellular glucose, 2-phosphoglycerate, and 3-phosphoglycerate.

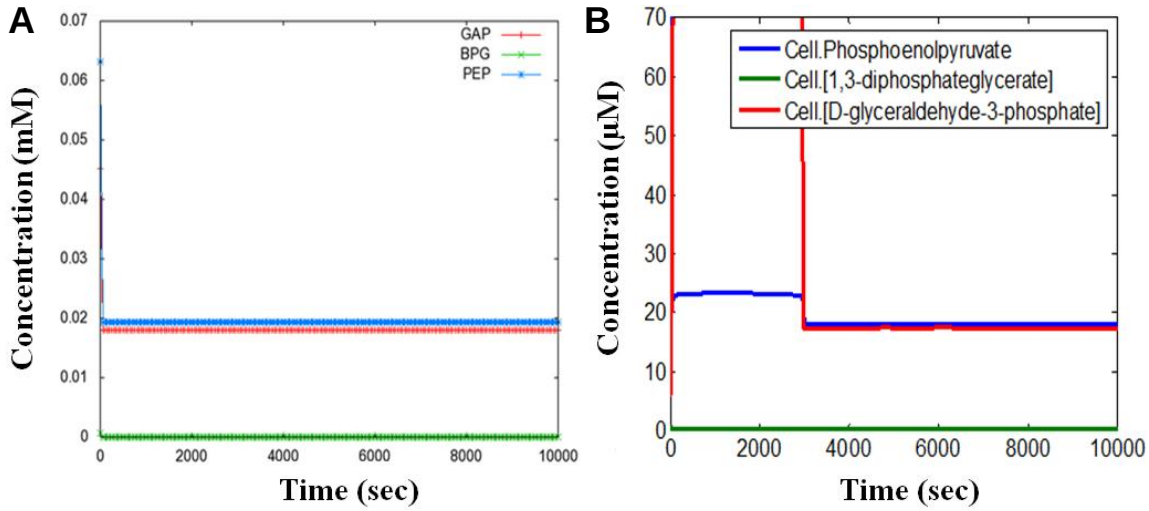

Figure 103. Simulations from (A) BioModel 172 and (B) SimBiology model for the species glyceraldehyde-3-phosphate, 1,3-diphosphoglycerate, and phosphoenolpyruvate.

BioModel 172 had no simulation available for dihydroxyacetone phosphate. The simulation for dihydroxyacetone phosphate in the SimBiology model was matched to an average concentration from other BioModels. BioModels 176 and 177 had an average concentration of 0.785 mM for dihydroxyacetone phosphate. Figure 104 shows the SimBiology simulation of dihydroxyacetone phosphate to be close to this value.

Table XXXIII. Initial substrate concentrations, enzyme concentrations, and reaction rates used to compare the SimBiology model to BioModel 172.

	Species	Value	Unit	Reference
Initial Concentrations of Glycolysis Substrates	GLC_ex	2000	µM	Pritchard & Kell, 2002
	GLC	97.7	µM	Pritchard & Kell, 2002
	G6P	2675	µM	Pritchard & Kell, 2002
	F6P	625	µM	Pritchard & Kell, 2002
	FBP	6221	µM	Pritchard & Kell, 2002
	GAP	45.2	µM	Pritchard & Kell, 2002
	DHAP	0	µM	----
	DPG	0.74	µM	Pritchard & Kell, 2002
	3PG	886	µM	Pritchard & Kell, 2002
	2PG	128	µM	Pritchard & Kell, 2002
	PEP	63	µM	Pritchard & Kell, 2002
	PYR	1815	µM	Pritchard & Kell, 2002
Enzyme Concentrations Used to Fit Model	KIN	207.4	µM	----
	PGI	40.0	µM	----
	6PFK	0.835	µM	----
	FBA	417.2	µM	----
	TPI	0.105	µM	----
	GAD	133.4	µM	----
	PGK	63.9	µM	----
	PGM	0.241	µM	----
	ENO	58.0	µM	----
	PYK	1.11	µM	----
Reaction Rates Used to Fit Model	R0	0.01	µM/s	----
	R27	0.0242	µM/s	----

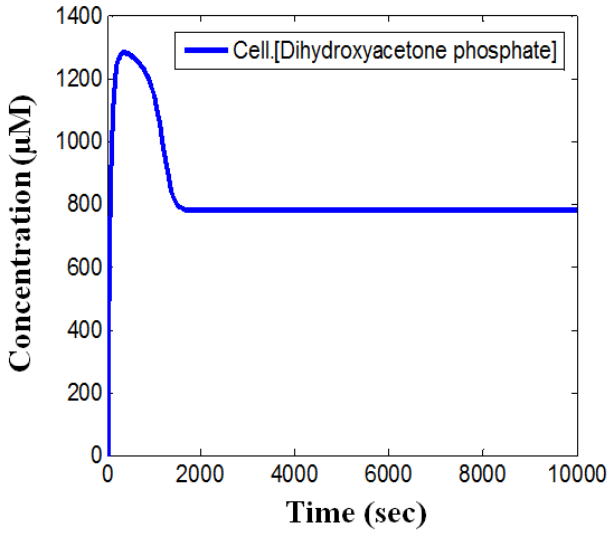

Figure 104. Simulation from SimBiology model for the species dihydroxyacetone phosphate. BioModel 172 had no simulations available for this species.

BioModel 176 - Conant 2007 WGD Glycolysis 2A3AB:

BioModel 176 is also a simulation of glycolysis in the species *S. cerevisiae* (Conant & Wolfe, 2007). This BioModel is based on a continuous fed reactor and does not model glycolytic oscillations in yeast. Table XXXIV shows the initial species concentrations from BioModel 176 that were also used in the SimBiology model. The best fit to BioModel 176 was achieved by adjusting the twelve variables shown in Table XXXIV until the SimBiology simulations matched the simulations from BioModel 176.

BioModel 176 had simulations available for all of the glycolysis species. The best fit to BioModel 176 used the values found in Table XXXIV for the enzyme concentrations and reaction rates. The simulations from this best fit are shown next to the simulations from BioModel 176 in Figure 105 and Figure 106.

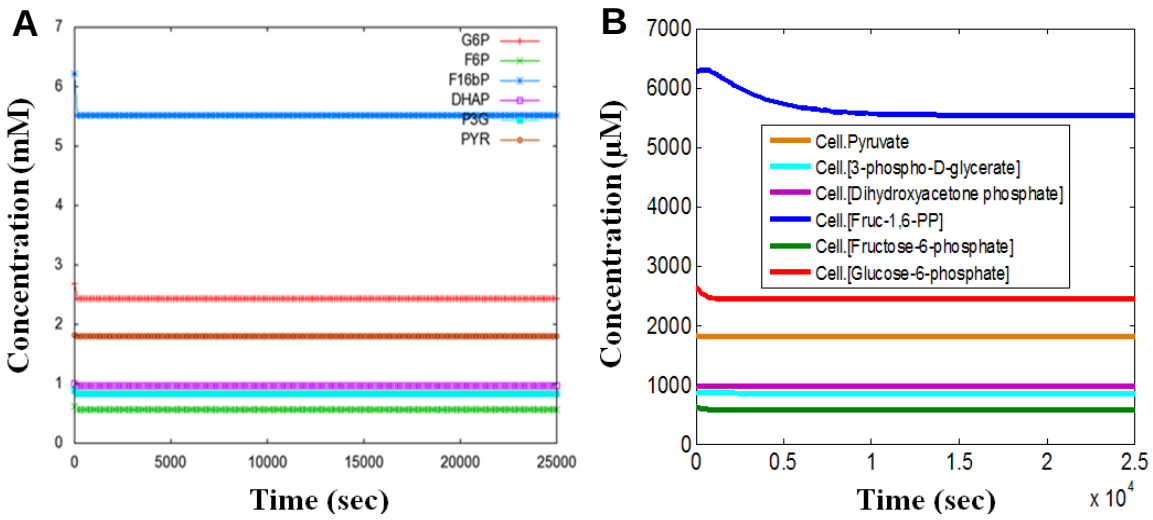

Figure 105. Simulations from (A) BioModel 176 and (B) SimBiology model for the species glucose-6-phosphate, fructose-6-phosphate, fructose-1,6-bisphosphate, dihydroxyacetone phosphate, 3-phosphoglycerate, and pyruvate.

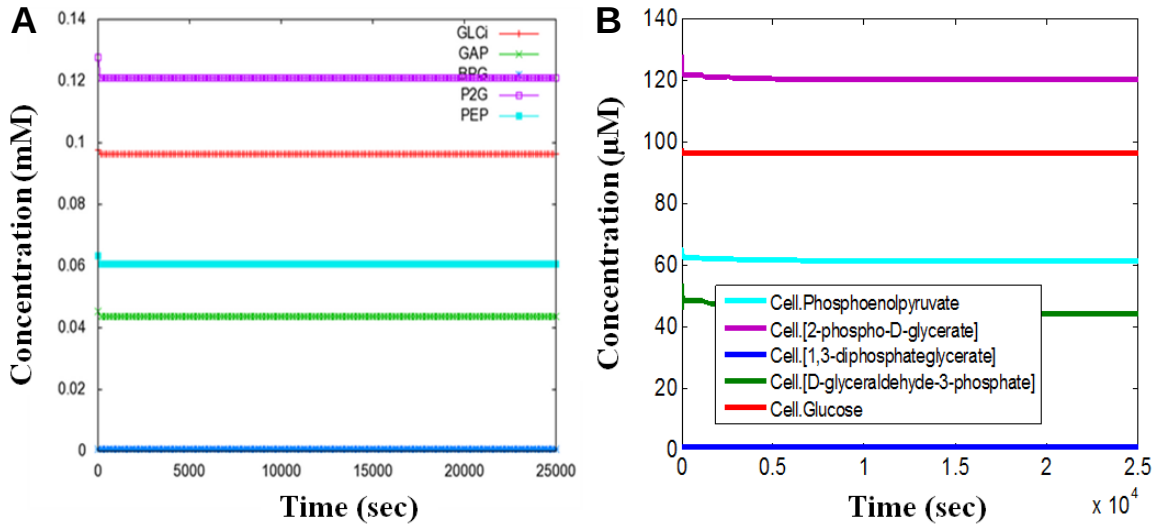

Figure 106. Simulations from (A) BioModel 176 and (B) SimBiology model for the species intracellular glucose, glyceraldehyde-3-phosphate, 1,3-diphosphoglycerate, 2-phosphoglycerate, and phosphoenolpyruvate.

Table XXXIV. Initial substrate concentrations, enzyme concentrations, and reaction rates used to compare the SimBiology model to BioModel 176.

	Species	Value	Unit	Reference
Initial Concentrations of Glycolysis Substrates	GLC_ex	50000	µM	Conant & Wolfe, 2007
	GLC	97.7	µM	Conant & Wolfe, 2007
	G6P	2675	µM	Conant & Wolfe, 2007
	F6P	625	µM	Conant & Wolfe, 2007
	FBP	6221	µM	Conant & Wolfe, 2007
	GAP	45.2	µM	Conant & Wolfe, 2007
	DHAP	1004	µM	Conant & Wolfe, 2007
	DPG	0.74	µM	Conant & Wolfe, 2007
	3PG	886	µM	Conant & Wolfe, 2007
	2PG	128	µM	Conant & Wolfe, 2007
	PEP	63.2	µM	Conant & Wolfe, 2007
	PYR	1815	µM	Conant & Wolfe, 2007
Enzyme Concentrations Used to Fit Model	KIN	454.8	µM	-----
	PGI	60	µM	-----
	6PFK	0.79	µM	-----
	FBA	0.744	µM	-----
	TPI	0.2248	µM	-----
	GAD	307.9	µM	-----
	PGK	23.45	µM	-----
	PGM	0.3752	µM	-----
	ENO	61.1	µM	-----
	PYK	1.642	µM	-----
Reaction Rates Used to Fit Model	R0	0.001	µM/s	-----
	R27	0.0496	µM/s	-----

BioModel 177 - Conant 2007 Glycolysis 2C:

BioModel 177 is based on the same study for *S. cerevisiae* as BioModel 176 (Conant & Wolfe, 2007). The main difference between models is that BioModel 177 includes acetyl-CoA synthesis from pyruvate. This is the only glycolysis BioModel that simulates acetyl-CoA. In order to fit simulations of acetyl-CoA to the BioModel, Reaction 28 was added to account for acetyl-CoA that is used elsewhere in the cell. Reaction 28 uses simple mass action kinetics, and the rate value was adjusted to achieve the best fit to the simulations from BioModel 177.

Initial substrate concentrations in the SimBiology model were set equal to initial concentrations used in BioModel 177. These values are shown in Table XXXV. The best fit to BioModel 177 was found by varying the values for the ten glycolysis enzymes and the three reaction rates for Reaction 0, Reaction 27, and Reaction 28. The values that resulted in the best fit are shown in Table XXXV.

Simulations for each glycolysis substrate and acetyl-CoA were compared between the SimBiology model and BioModel 177. The simulation values of acetyl-CoA, pyruvate, and fructose-1,6-bisphosphate were very similar between the models as shown in Figure 107. Comparable values were seen between the models for the rest of the species as shown in Figure 108, Figure 109, and Figure 110.

Target Values in Glycolysis for the SimBiology Model:

Comparisons with the seven glycolysis BioModels resulted in a distribution of enzyme concentrations, reaction rates, and initial species concentrations that could be used in the final SimBiology model. Figure 111 shows box plots representing the range of values used for the initial species concentrations in glycolysis. Ten outliers out of 84

values were identified in these box plots. Outliers were removed and then an average value was calculated for each species. Table XXXVI shows the resulting averages that were used in the final SimBiology model for initial species concentrations.

The distribution of rate values for Reaction 0 and Reaction 27 are shown by the box plots in Figure 112. One outlier out of 14 values was identified and removed before average values were calculated. Table XXXVI shows the resulting averages that were used as reaction rates in the final SimBiology model.

Table XXXV. Initial substrate concentrations, enzyme concentrations, and reaction rates used to compare the SimBiology model to BioModel 177.

	Species	Value	Unit	Reference
Initial Concentrations of Glycolysis Substrates	GLC_ex	50000	µM	Conant & Wolfe, 2007
	GLC	97.7	µM	Conant & Wolfe, 2007
	G6P	2675	µM	Conant & Wolfe, 2007
	F6P	625	µM	Conant & Wolfe, 2007
	FBP	6221	µM	Conant & Wolfe, 2007
	GAP	45.2	µM	Conant & Wolfe, 2007
	DHAP	1004	µM	Conant & Wolfe, 2007
	DPG	0.74	µM	Conant & Wolfe, 2007
	3PG	886	µM	Conant & Wolfe, 2007
	2PG	128	µM	Conant & Wolfe, 2007
	PEP	63.2	µM	Conant & Wolfe, 2007
	PYR	1815	µM	Conant & Wolfe, 2007
Enzyme Concentrations Used to Fit Model	KIN	90.0	µM	-----
	PGI	31.8	µM	-----
	6PFK	0.69	µM	-----
	FBA	415.9	µM	-----
	TPI	0.161	µM	-----
	GAD	159.0	µM	-----
	PGK	58.0	µM	-----
	PGM	0.2298	µM	-----
	ENO	50.01	µM	-----
	PYK	1.12	µM	-----
Reaction Rates Used to Fit Model	R0	0.0005	µM/s	-----
	R27	0.0264	µM/s	-----
	R28	0.00521	µM/s	-----

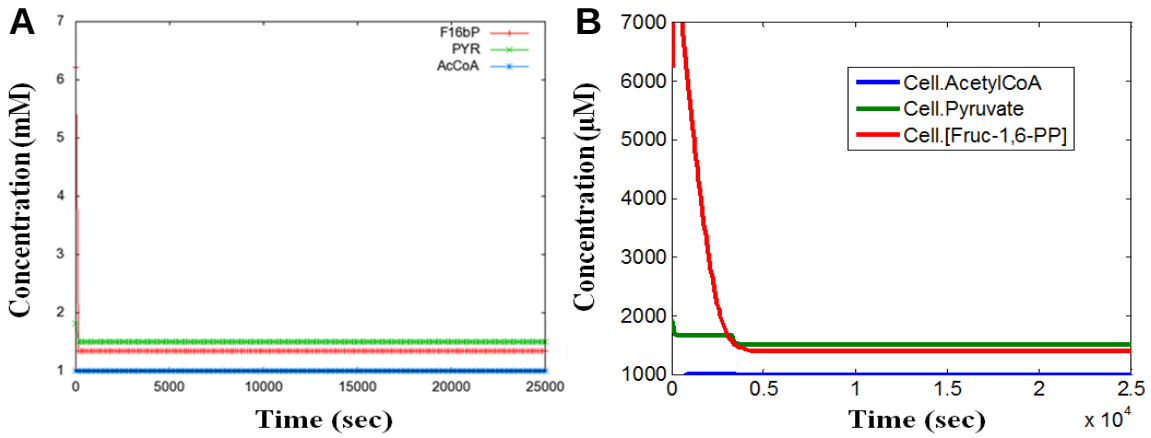

Figure 107. Simulations from (A) BioModel 177 and (B) SimBiology model for the species fructose-1,6-bisphosphate, pyruvate, and acetyl-CoA.

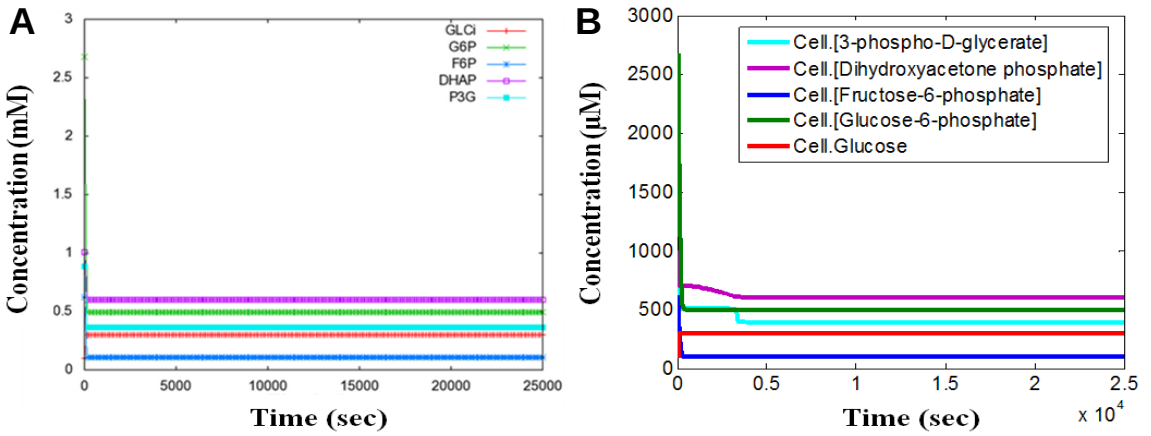

Figure 108. Simulations from (A) BioModel 177 and (B) SimBiology model for the species intracellular glucose, glucose-6-phosphate, fructose-6-phosphate, dihydroxyacetone phosphate, and 3-phosphoglycerate.

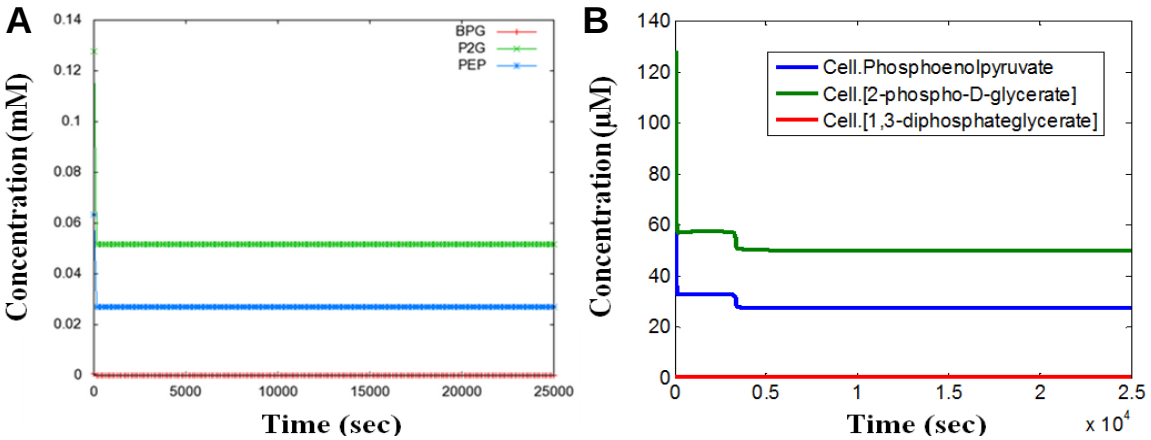

Figure 109. Simulations from (A) BioModel 177 and (B) SimBiology model for the species 1,3-diphosphoglycerate, 2-phosphoglycerate, and phosphoenolpyruvate.

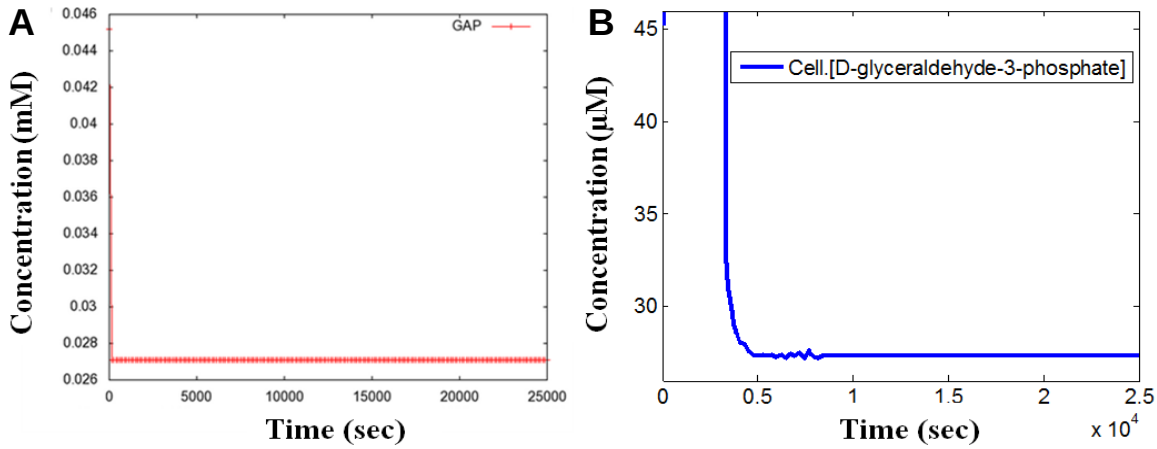

Figure 110. Simulations from (A) BioModel 177 and (B) SimBiology model for the species glyceraldehyde-3-phosphate.

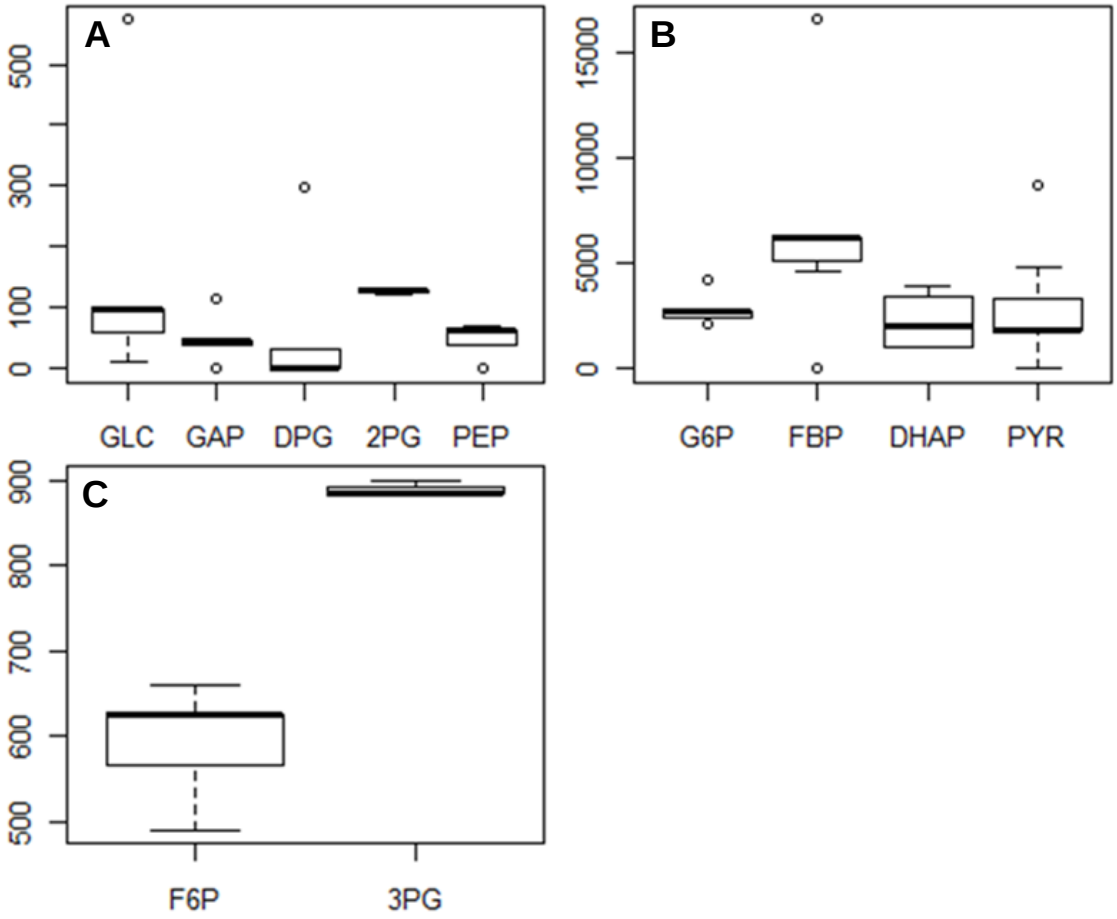

Figure 111. Box plots showing the distribution of initial values for (A) glucose, glyceraldehyde-3-phosphate, 1,3-diphosphateglycerate, 2-phosphoglycerate, phosphoenolpyruvate, (B) glucose-6-phosphate, fructose-1,6-bisphophate, dihydroxyacetone phosphate, pyruvate, (C) fructose 6-phosphate, and 3-phosphoglycerate used in the glycolysis BioModels. Ten outliers out of 84 values were identified.

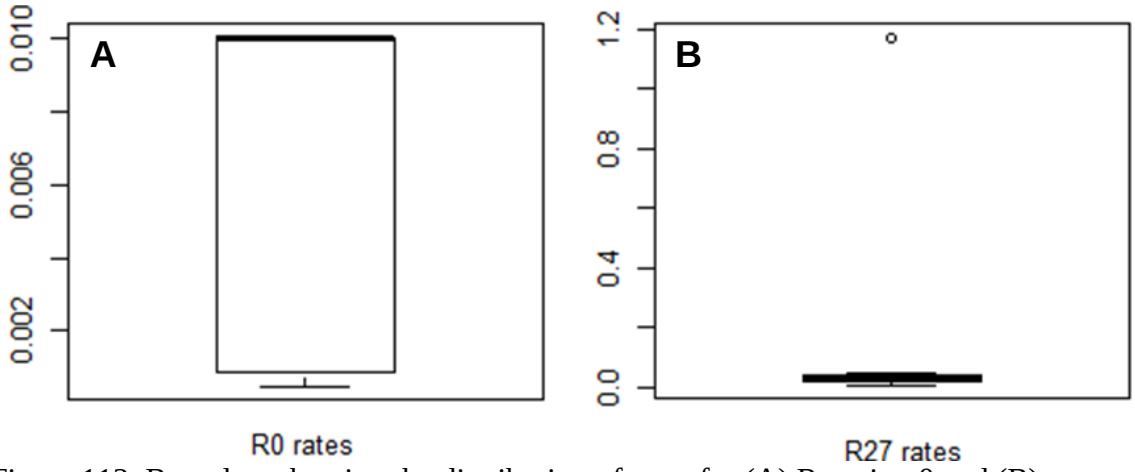

Figure 112. Box plots showing the distribution of rates for (A) Reaction 0 and (B) Reaction 27 used to fit the seven glycolysis BioModels. One outlier out of 14 values was identified from these box plots.

Table XXXVI. Initial substrate concentrations, target enzyme concentrations, and reaction rates used for the final model based on the seven glycolysis BioModels. Values are averages of the seven BioModels once outliers have been removed.

	Species	Value	Unit
Initial Concentrations of Glycolysis Substrates	GLC	70.9	µM
	G6P	2619	µM
	F6P	594	µM
	FBP	5763	µM
	GAP	43.9	µM
	DHAP	2214	µM
	DPG	7.0	µM
	3PG	890	µM
	2PG	126	µM
	PEP	59.9	µM
	PYR	2012	µM
Target Enzyme Concentrations for Final Model	KIN	288	µM
	PGI	46	µM
	6PFK	0.72	µM
	FBA	538	µM
	TPI	0.26	µM
	GAD	252	µM
	PGK	32	µM
	PGM	0.82	µM
	ENO	169	µM
	PYK	1.47	µM
Reaction Rates in Final Model	R0	0.006	µM
	R27	0.0248	µM
	R28	0.00521	µM

Distributions of the glycolysis enzyme values are shown in the box plots in Figure 113. Seven outliers out of 70 values were identified in the box plots. The outliers were removed, and then average enzyme values were calculated. The average enzyme values are shown in Table XXXVI and were used as target values in the model.

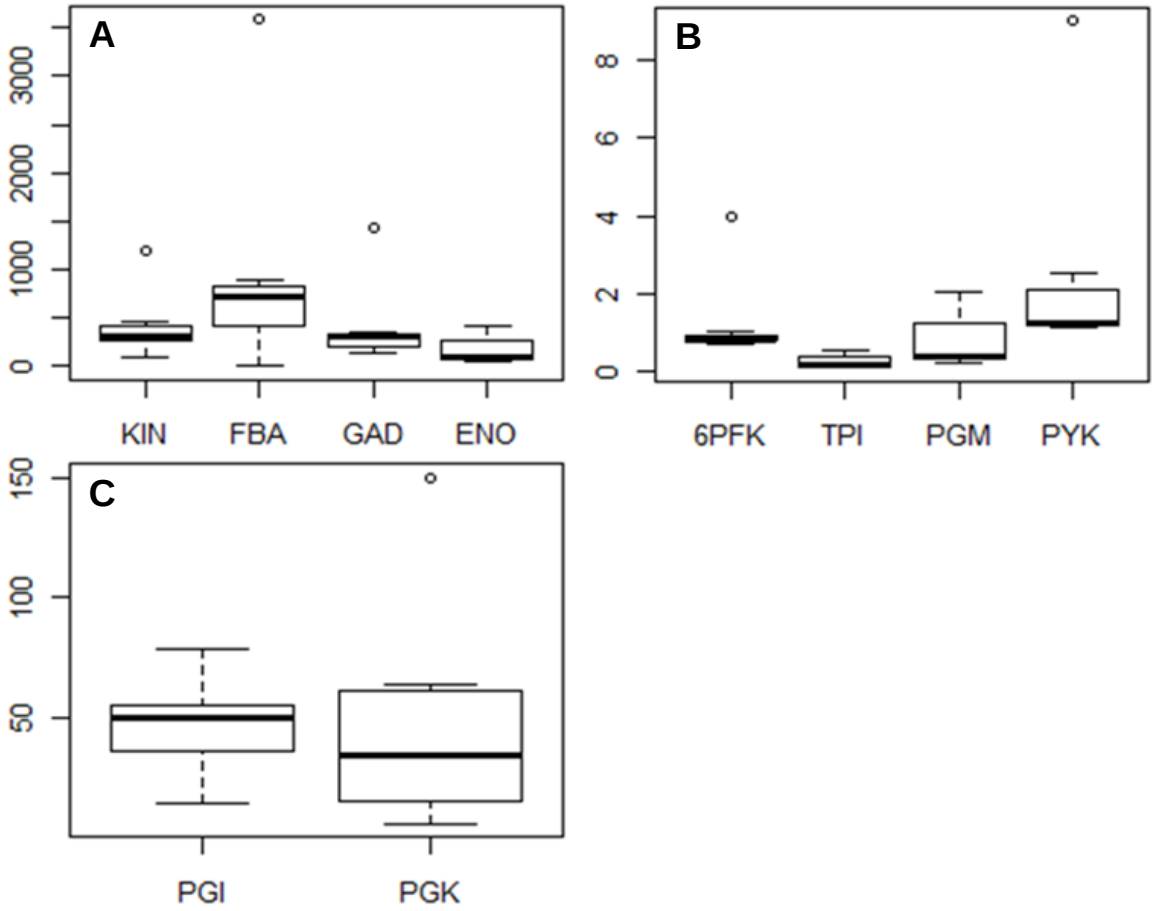

Figure 113. Box plots showing the distribution of values for the enzymes (A) kinase, fructose-bisphosphate aldolase, glyceraldehyde-3-phosphate dehydrogenase, enolase (B) 6-phosphofructokinase, triose phosphate isomerase, phosphoglycerate mutase, pyruvate kinase (C) phosphoglucose isomerase, and phosphoglycerate kinase used to fit the seven glycolysis BioModels. Seven outliers out of 70 values were identified in these box plots.

Due to the presence of the transcriptional network, enzyme concentrations were not held constant in the final model. Initial enzyme concentrations in the final model were set equal to the values in Table XXXVI. Enzyme concentrations during the

simulation are combination of the synthesis and degradation of the enzymes. Each enzyme was monitored during simulations, and then promoter activity and enzyme degradation rates were adjusted in order to achieve enzyme concentrations close to the target values shown in Table XXXVI.

TCA Cycle BioModels:

The BioModels 222 and 232 were used to validate the TCA cycle in the predictive model. The online simulator in the BioModels database was used to create simulations of the substrates in the TCA cycle. Values in the SimBiology model were adjusted to mimic the simulations of each BioModel.

The BioModels 222 and 232 do not account for glycolysis, acetyl-CoA synthesis, or PHB synthesis. In the SimBiology model, these four pathways were shut off by inactivating the forward and reverse directions of Reaction 1, Reaction 13, Reaction 14, and Reaction 26. The concentration of each enzyme was held constant in order to inactivate the transcriptional network portion of the model. The concentration of acetyl-CoA was held constant in both BioModels and in the SimBiology model. The concentrations of CoA, ATP, ADP, NAD^+, and NADH were also held constant during simulation. Initial concentrations of substrates in the TCA cycle were changed to match the initial values used in each BioModel. The values for TCA cycle enzyme concentrations were adjusted until the SimBiology simulations matched the simulations from the BioModel.

BioModel 222 - Singh 2006 TCA Cycle:

BioModel 222 is the only BioModel that simulates the TCA cycle in *E. coli* (Singh & Ghosh, 2006). BioModel 222 includes the glyoxylate bypass in the TCA cycle and has simulations available for ten species in the TCA cycle. BioModel 222 held acetyl-CoA constant during simulations, so acetyl-CoA was also held constant in the SimBiology model. Initial species concentrations in the SimBiology model were set equal to the values used in BioModel 222 that are shown in Table XXXVII. A best fit was determined by adjusting the TCA cycle enzyme concentrations and comparing simulations.

Table XXXVII. Initial substrate concentrations and enzyme concentrations used to compare the SimBiology model to BioModel 222.

	Species	Value	Unit	Reference
Initial Concentrations of TCA Substrates	Ac-CoA	500	µM	Singh & Ghosh, 2006
	OAA	4	µM	Singh & Ghosh, 2006
	CIT	3000	µM	Singh & Ghosh, 2006
	ISO	18	µM	Singh & Ghosh, 2006
	2-OXO	200	µM	Singh & Ghosh, 2006
	SCA	40	µM	Singh & Ghosh, 2006
	SUC	600	µM	Singh & Ghosh, 2006
	FUMA	300	µM	Singh & Ghosh, 2006
	MAL	1800	µM	Singh & Ghosh, 2006
	GLY	4000	µM	Singh & Ghosh, 2006
Enzyme Concentrations Used to Fit Model	CS	28.0	µM	-----
	CHL	1800	µM	-----
	ICHL	10.0	µM	-----
	ICDH	0.3	µM	-----
	OGDH	25770	µM	-----
	SCS	7.0E-6	µM	-----
	SDH	6.5	µM	-----
	FUM	0.1165	µM	-----
	MDH	3.7	µM	-----
	IL	0.1	µM	-----
	MS	10	µM	-----

Simulations for each TCA cycle species closely matched the simulations from BioModel 222 when the enzyme concentrations in Table XXXVII were used. Figure 114 visually compares the values for acetyl-CoA, malate, fumarate, succinyl-CoA, and succinate between BioModel 222 and the SimBiology model. Figure 115 illustrates the closely matched values for oxaloacetate, 2-oxoglutarate, and isocitrate between the two models. Figure 116 shows the comparison between the last two species: citrate and glyoxylate.

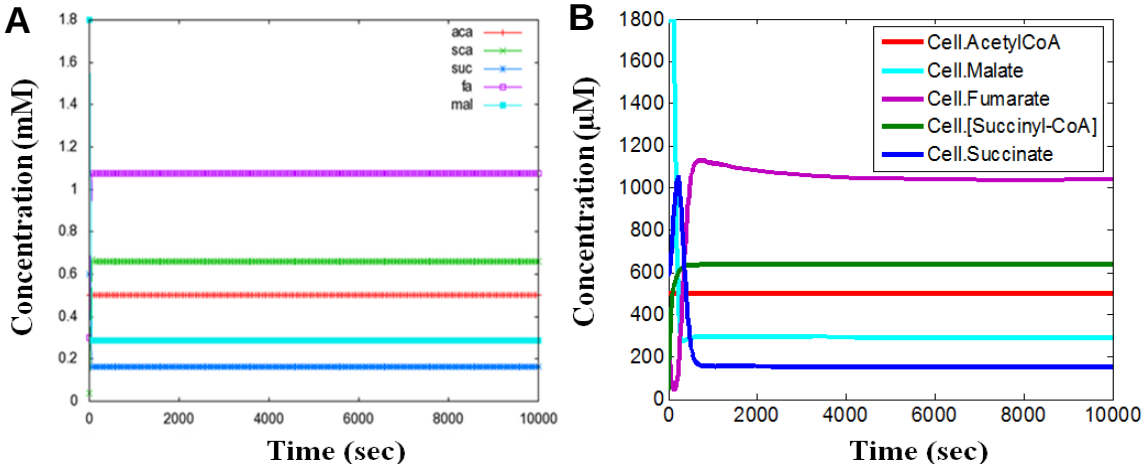

Figure 114. Simulations from (A) BioModel 222 and (B) SimBiology model for the species acetyl-CoA, succinyl-CoA, succinate, fumarate, and malate.

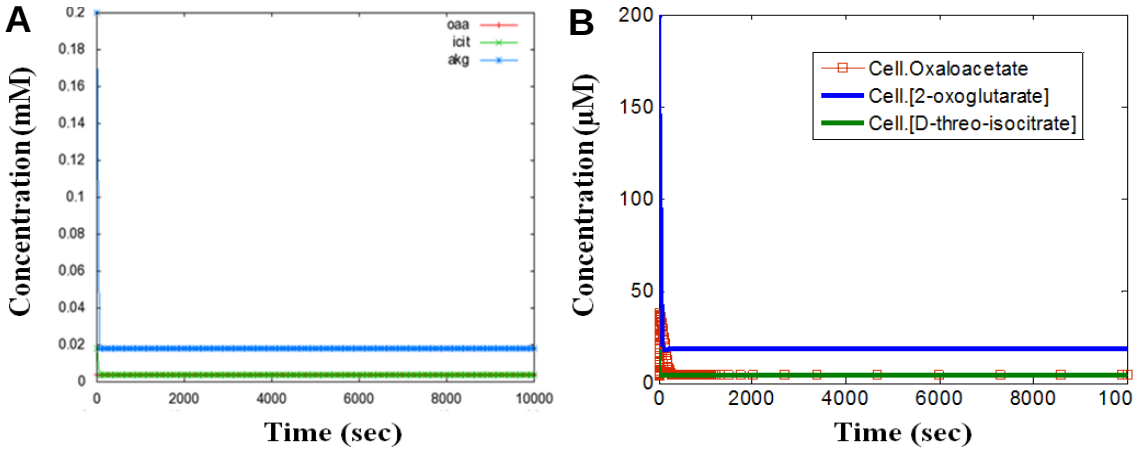

Figure 115. Simulations from (A) BioModel 222 and (B) SimBiology model for the species oxaloacetate, isocitrate, and 2-oxoglutarate.

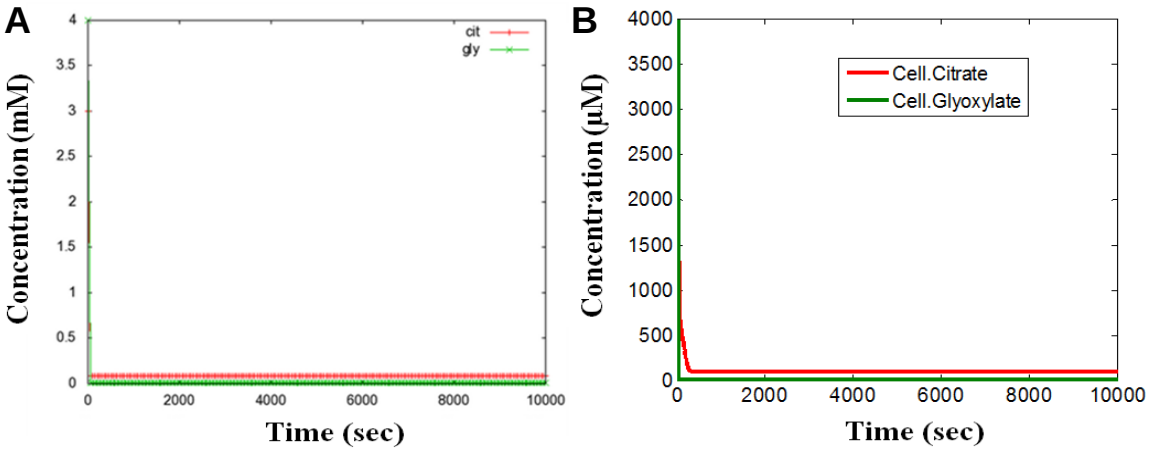

Figure 116. Simulations from (A) BioModel 222 and (B) SimBiology model for the species citrate and glyoxylate.

BioModel 232 - Nazaret 2009 TCA Cycle:

BioModel 232 was the only other BioModel found for the TCA cycle. The model simulates the TCA cycle in *Homo sapiens* (Nazaret *et al*, 2009). This BioModel was not the most desirable to use because it does not model the TCA cycle in a microorganism and it only simulates four of the TCA cycle species. BioModel 232 also does not include the glyoxylate bypass. However, since only two BioModels simulate the TCA cycle, it was decided to try and fit the SimBiology model to BioModel 232. Table XXXVIII shows the initial species concentrations used in BioModel 232 that were also used in the SimBiology model. BioModel 232 did not have initial values for five of the TCA cycle species, so initial values from BioModel 222 were used.

The TCA cycle enzyme concentrations were varied in the SimBiology model in order to find the best fit to BioModel 232. The values of isocitrate lyase and malate synthase were automatically set to zero since BioModel 232 did not include the glyoxylate bypass. However, only three of the enzymes could be confidently adjusted and fit to BioModel 232 since the model only had simulations available for acetyl-CoA,

oxaloacetate, citrate, and 2-oxoglutarate. Table XXXVIII shows the values used to fit the SimBiology model to BioModel 232. The values for citrate synthase, citrate hydro-lyase, and 2-oxoglutarate dehydrogenase were the key to matching the simulations of the four TCA cycle species between models. Figure 117 illustrates the fit between the SimBiology model and BioModel 232 based on four of the TCA cycle species.

Table XXXVIII. Initial substrate concentrations and enzyme concentrations used to compare the SimBiology model to BioModel 232.

	Species	Value	Unit	Reference
Initial Concentrations of TCA Substrates	Ac-CoA	63	µM	Nazaret *et al*, 2009
	OAA	5	µM	Nazaret *et al*, 2009
	CIT	440	µM	Nazaret *et al*, 2009
	ISO	18	µM	Singh & Ghosh, 2006
	2-OXO	225	µM	Nazaret *et al*, 2009
	SCA	40	µM	Singh & Ghosh, 2006
	SUC	600	µM	Singh & Ghosh, 2006
	FUMA	300	µM	Singh & Ghosh, 2006
	MAL	1800	µM	Singh & Ghosh, 2006
Enzyme Concentrations Used to Fit Model	CS	18.0	µM	-----
	CHL	44.5	µM	-----
	ICHL	1.0	µM	-----
	ICDH	1.0	µM	-----
	OGDH	1770.4	µM	-----
	SCS	50.0	µM	-----
	SDH	50.0	µM	-----
	FUM	50.0	µM	-----
	MDH	50.0	µM	-----
	IL	0	µM	-----
	MS	0	µM	-----

Target Values in the TCA Cycle for the SimBiology Model:

For the final SimBiology model, it was decided to use the initial species concentrations in Table XXXVII that were used in BioModel 222. These values were chosen because BioModel 222 was specifically for *E. coli* and had values for each TCA cycle species. Initial enzyme concentrations were set to the values in Table XXXVII. In

the final model, promoter activity and enzyme degradation rates were adjusted to simulate enzyme concentrations consistent with the target values in Table XXXVII.

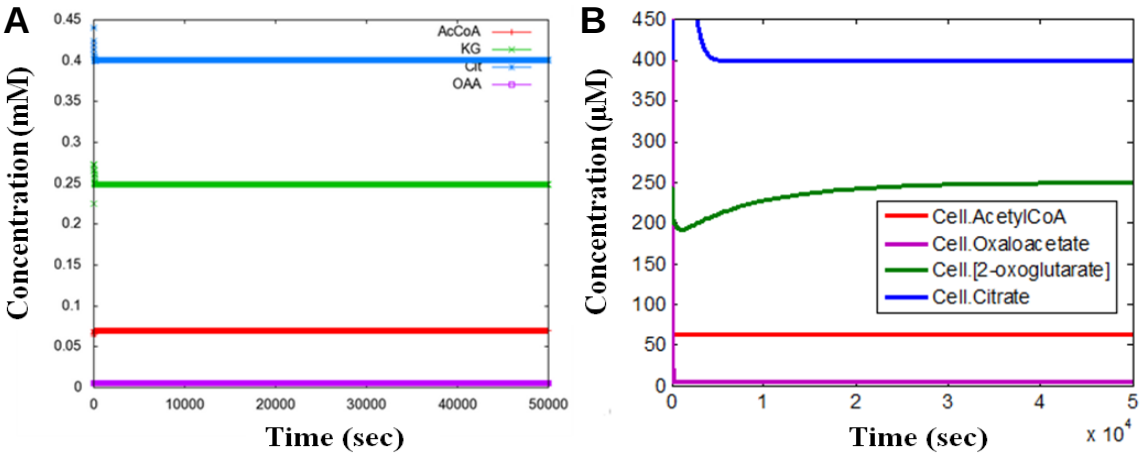

Figure 117. Simulations from (A) BioModel 232 and (B) SimBiology model for the species acetyl-CoA, 2-oxoglutarate, citrate, and oxaloacetate.

Comparing Model with Experimental Data

No BioModels were available for the synthesis of PHB. The PHB synthesis pathway in the model was validated using experimental data for PHB production. Table XXXIX contains preliminary experimental PHB production data for two strains of *E. coli*. Each strain contains the genes for the PHB synthesis pathway, but they are carried in different plasmids. The SimBiology model was built specifically for *E. coli* carrying the pBHR68 plasmid. The data for the 4MHT plasmid was included to demonstrate that the predictive model is capable of being fitted to a specific strain of bacteria.

The enzymes in the PHB synthesis pathway (PhaA, PhaB, and PhaC) were held constant in order to fit the model to the data. Different enzyme concentrations were tried until the simulated PHB closely matched the PHB production data. Figure 118 shows the

simulations that best fit the PHB production data for the two strains. Table XL shows the enzyme concentrations used to achieve these two fits.

Table XXXIX. Experimental data for PHB production in *E. coli* strains containing 4MHT or pBHR68 plasmids.

Strain	Time (hrs)	PHB (g/L)
4MHT*	8	0.0066
	12	0.0262
	24	0.4406
	48	0.4609
pBHR68	8	Not detected
	12	0.0348
	24	0.0604
	48	0.1120

*Plasmid 4MHT consists of the pBHR68 genes, the phasin gene *phaP1*, and the membrane protein gene *hlyA*.

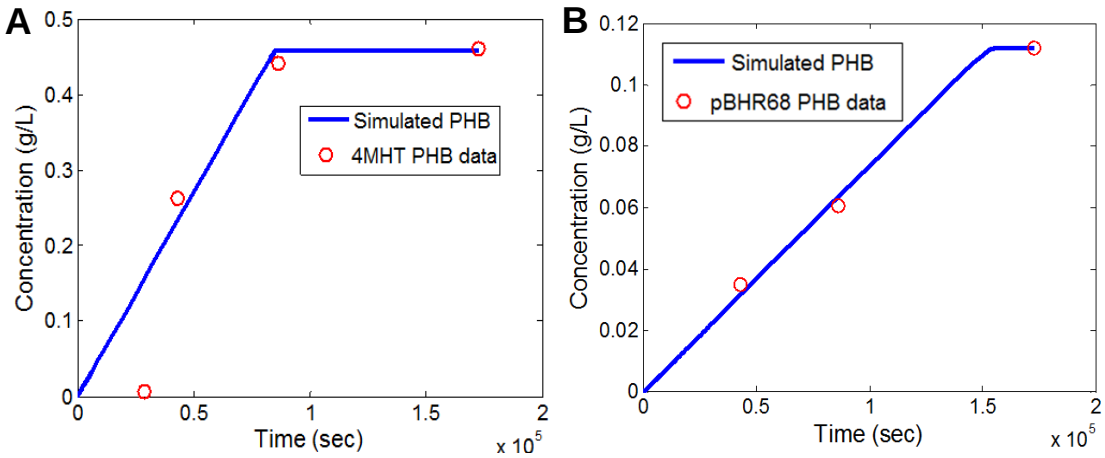

Figure 118. Simulated PHB fit to the PHB production data from the *E. coli* strains with (A) the 4MHT plasmid and (B) the pBHR68 plasmid.

In the final SimBiology model, the enzyme values were not held constant. Promoter activity and enzyme degradation rates were adjusted to generate the desired enzyme concentrations. The concentrations in Table XL for the pBHR68 data were the target values used since the model was created for the pBHR68 strain. Experimental data from metabolic profiling can be used in the same way as the PHB production data. A

better predictive model for a specific microorganism can be created by fitting the model to more experimental data from that specific strain. A tutorial on how to download and use the final model is available in Appendix D.

Table XL. Enzyme concentrations used to fit the model to experimental PHB production data.

Strain	Enzyme	Concentration (µM)
4MHT	PhaA	110
	PhaB	3
	PhaC	5
pBHR68	PhaA	1.3
	PhaB	0.41
	PhaC	0.5

*Plasmid 4MHT consists of the pBHR68 genes, the phasin gene *phaP1*, and the membrane protein gene *hlyA.*

Model Optimization and Results

The final SimBiology model was used to identify target genes and promoters for genetic engineering. In the model, the value K_m is a quantitative measure of the binding affinity an enzyme has with its substrate. Lower values of K_m represent higher substrate affinity while higher values of K_m represent lower substrate affinity. An enzyme's substrate affinity is dependent upon the amino acids that interact with the substrate in the enzyme's active site. These amino acids can be identified in the gene and then site-directed mutagenesis can be used to change one or more of these amino acids. Changing the amino acids of the active site can increase or decrease the enzyme's substrate affinity depending upon the new amino acids used. However, it is easier to make an enzyme less effective at binding a substrate than trying to make it more effective.

In the final SimBiology model, K_m values for each enzyme were adjusted and simulations were conducted to determine if the changes resulted in an increase in PHB production. Adjusting the K_m values resulted in no visible increase in PHB production for 16 enzymes, a slight increase in PHB production for 5 enzymes, and a large increase in PHB production for 9 enzymes.

The transcriptional network portion of the model was also adjusted to optimize the model for increased PHB production. Most promoters, transcription factors, and ligands were not adjusted for optimization because of their wide use in metabolic pathways not included in the model. Adjustments were conducted on the transcriptional network directly associated with the pBHR68 plasmid that encodes the genes of the PHB synthesis pathway.

Adjusting Enzyme Substrate Affinity:

The K_m values for each of the 30 enzymes in this model were increased up to five times or decreased down to a fifth of the original value. These values were used to standardize comparisons of increased PHB production between enzymes. This is roughly the same as making the enzyme active site five times less effective at binding the substrate or five times more effective at binding the substrate. The direction of adjustment that resulted in an increase in PHB production was the simulation kept for comparison. Simulations were compared between enzymes to determine which adjustments resulted in the greatest increase in PHB production.

PHB Synthesis Enzymes:

Decreasing the K_m value for β-ketothiolase (PhaA) increased the PHB production as shown in Figure 119. Decreasing the K_m by one-fifth resulted in a 35.3% increase in

PHB production. If β-ketothiolase has a better binding affinity then it results in higher synthesis of PHB.

The enzyme acetoacetyl-CoA reductase (PhaB) has a K_m value for the substrate acetoacetyl-CoA and the substrate NADPH. A five-fold decrease in the K_m value for acetoacetyl-CoA resulted in a 1.0% increase in the rate of PHB production, and decreasing the K_m for NADPH by a fifth resulted in a 7.6% increase in the rate of PHB production as seen Figure 120. By decreasing both K_m values, an 8.6% increase in the rate of production was observed as seen in Figure 121.

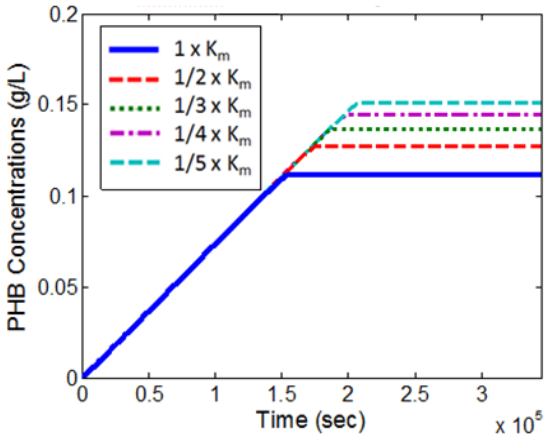

Figure 119. PHB production levels from adjusting PhaA's K_m for acetyl-CoA.

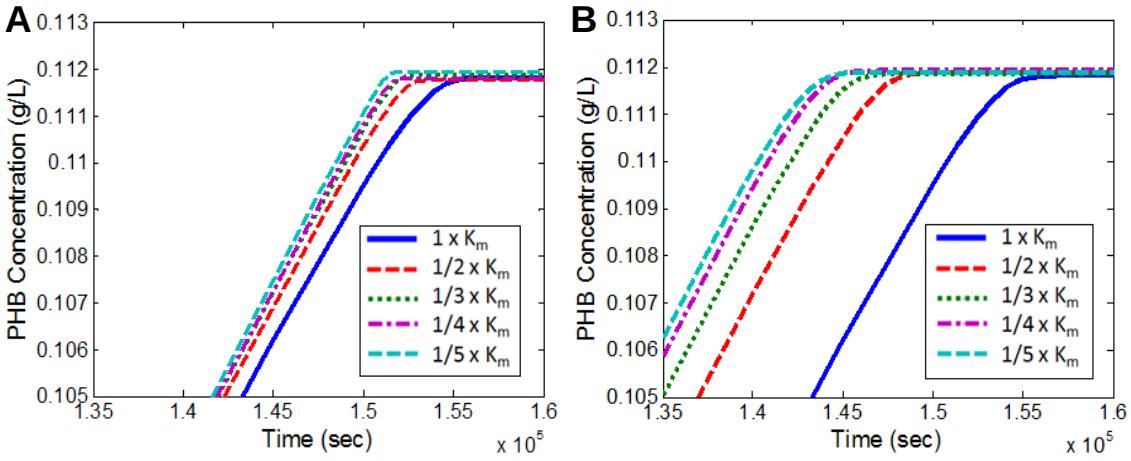

Figure 120. PHB production levels from adjusting PhaB's K_m for (A) acetoacetyl-CoA and (B) NADPH.

The enzyme PHB synthase (PhaC) has a K_m value for the substrate 3-hydroxybutyryl-CoA. Adjusting the K_m value resulted in no visible change in the production of PHB. Figure 122 shows the lack of change in PHB production when compared to the original simulation. Out of the three PHB synthesis enzymes, adjusting β-ketothiolase resulted in the largest increase in total PHB production.

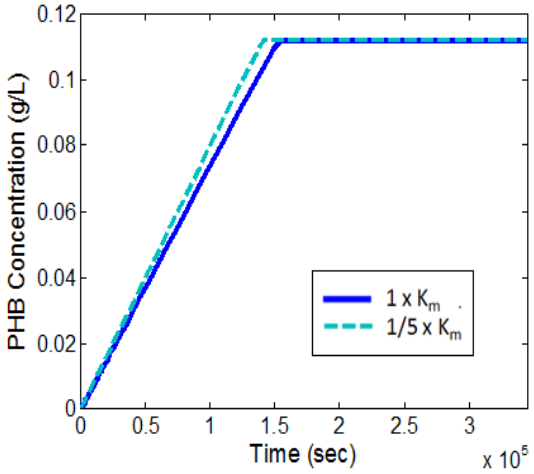

Figure 121. PHB production levels from adjusting PhaB's K_m for acetoacetyl-CoA and NADPH.

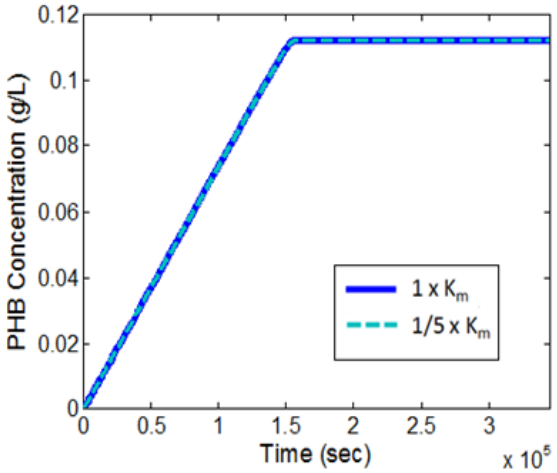

Figure 122. PHB production levels from adjusting PhaC's K_m for 3-hydroxybutyryl-CoA.

TCA Cycle Enzymes:

Citrate synthase has a K_m value for oxaloacetate and acetyl-CoA. Increasing the K_m for oxaloacetate by five fold resulted in 30.3% increase in PHB production as seen in Figure 123. Multiplying the K_m for acetyl-CoA by five resulted in an 87.7% increase in PHB production as seen in Figure 123. A large 113.7% increase in PHB production was observed by increasing both K_m values by five times their original values as seen in Figure 124.

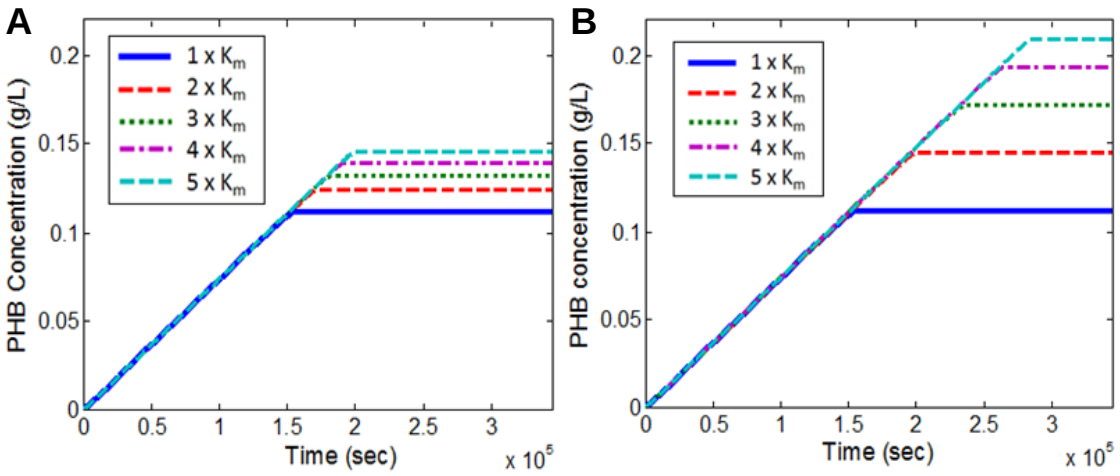

Figure 123. PHB production levels from adjusting citrate synthase's K_m for (A) oxaloacetate and (B) acetyl-CoA.

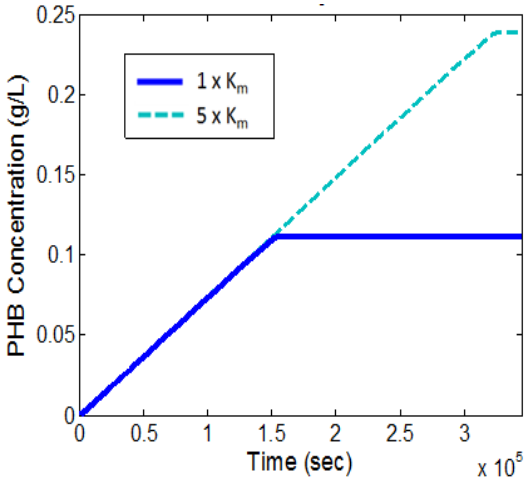

Figure 124. PHB production levels from adjusting citrate synthase's K_m for oxaloacetate and acetyl-CoA.

Adjusting the K_m value for citrate hydro-lyase resulted in no visible increase in the production of PHB. Increasing the K_m value for the enzyme isocitrate hydro-lyase resulted in a very slight increase in PHB production. The simulations for these two enzymes can be found in Appendix C.

Adjusting the substrate affinity for isocitrate dehydrogenase yielded a visible change in the amount of PHB synthesized. Decreasing the enzyme's K_m for isocitrate by one fifth resulted in a 7.8% increase in PHB production as shown in Figure 125. Altering the K_m for the enzyme 2-oxoglutarate dehydrogenase had no visible effect upon the synthesis of PHB. The simulation from adjusting the K_m of 2-oxoglutarate dehydrogenase is found in Appendix C.

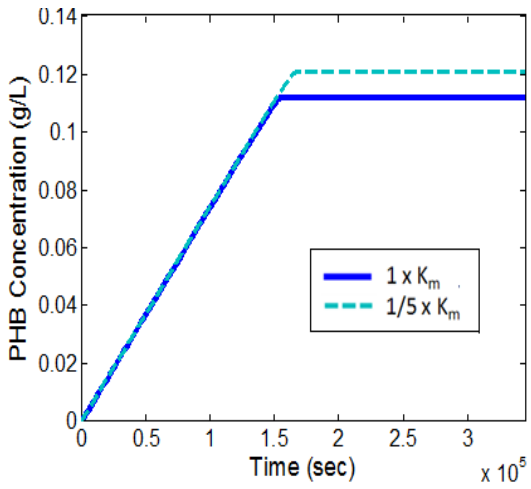

Figure 125. PHB production levels from adjusting isocitrate dehydrogenase's K_m for isocitrate.

The enzyme succinyl-CoA synthetase catalyzed the only reaction not modeled using a kinetic mechanism. The reaction rate was adjusted in place of a K_m value. Increasing the rate of reaction for succinyl-CoA synthetase resulted in a barely noticeable increase in PHB production. This simulation is included in Appendix C.

Adjusting the K_m values for the enzymes succinate dehydrogenase, fumarase, and malate dehydrogenase resulted in no visible increase in PHB production. The simulations for these enzymes are included in Appendix C.

Glyoxylate Bypass Enzymes:

Increasing the K_m for the enzyme isocitrate lyase resulted in an 8.6% increase in the synthesis of PHB as shown in Figure 126. For the enzyme malate synthase, no change in PHB production was observed from adjusting the K_m for glyoxylate and a very slight increase in PHB production was observed from increasing the K_m for acetyl-CoA. The two simulations for malate synthase are included in Appendix C.

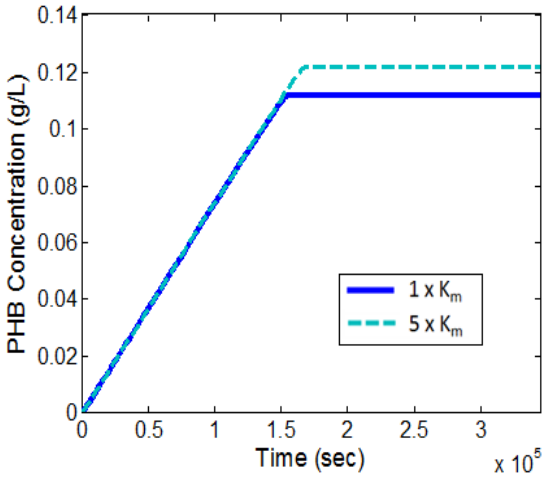

Figure 126. PHB production levels from adjusting isocitrate lyase's K_m for isocitrate.

Glycolysis Enzymes:

Altering the K_m values for the enzymes kinase, phosphoglucose isomerase, and 6-phosphofructokinase resulted in no visible increase in the production of PHB. The simulations for these enzymes are found in Appendix C. Increasing the K_m by five fold for the enzyme fructose-bisphosphate aldolase resulted in a 22.5% increase in PHB

production as seen in Figure 127. For the enzyme triose phosphate isomerase, multiplying the K_m value by five resulted in a 7.1% increase in PHB synthesis as seen in Figure 128.

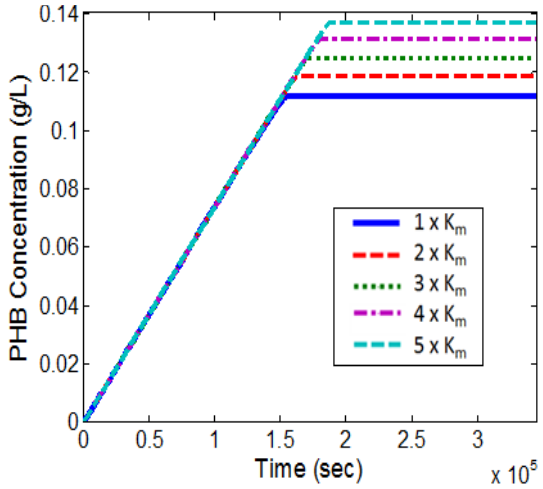

Figure 127. PHB production levels from adjusting fructose-bisphosphate aldolase's K_m for fructose-1,6-bisphosphate.

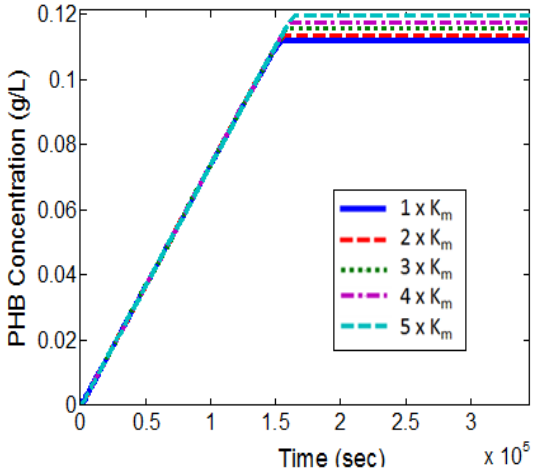

Figure 128. PHB production levels from adjusting triose phosphate isomerase's K_m for dihydroxyacetone phosphate.

The enzyme glyceraldehyde-3-phosphate dehydrogenase binds three substrates so it has K_m values for glyceraldehyde-3-phosphate, NAD^+, and inorganic phosphate. Adjusting the K_m for glyceraldehyde-3-phosphate resulted in no visible increase in PHB production and the simulation is included in Appendix C. An 8.6% increase in PHB

synthesis was observed from increasing K_m by five-fold for inorganic phosphate as shown in Figure 129. Increasing the K_m for NAD^+ by five-fold resulted in a 37.6% increase in the synthesis of PHB as seen in Figure 129. A total increase of 72.8% in PHB production was observed by increasing all three K_m values by five fold as shown in Figure 130.

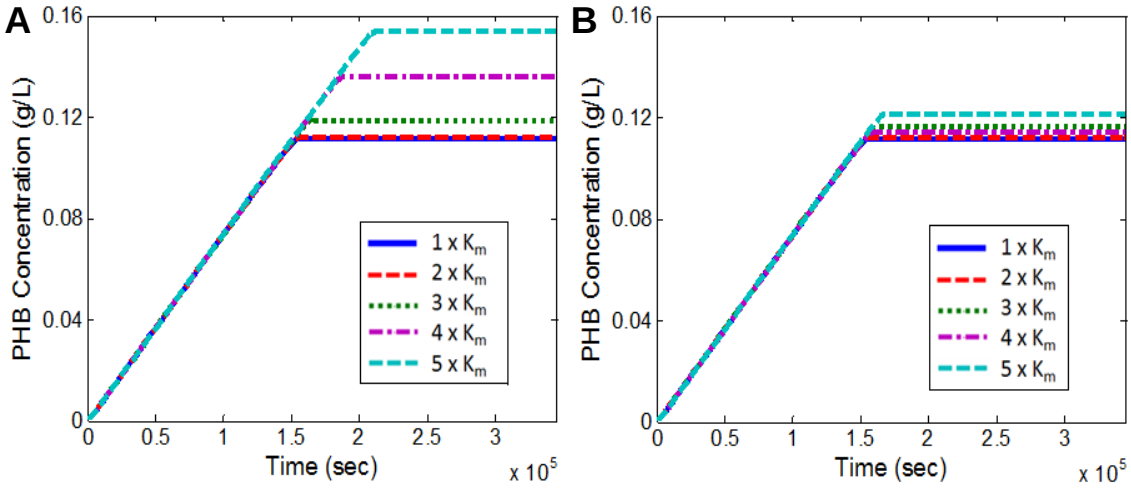

Figure 129. PHB production levels from adjusting glyceraldehyde-3-phosphate dehydrogenase's K_m for (A) NAD^+ and (B) inorganic phosphate.

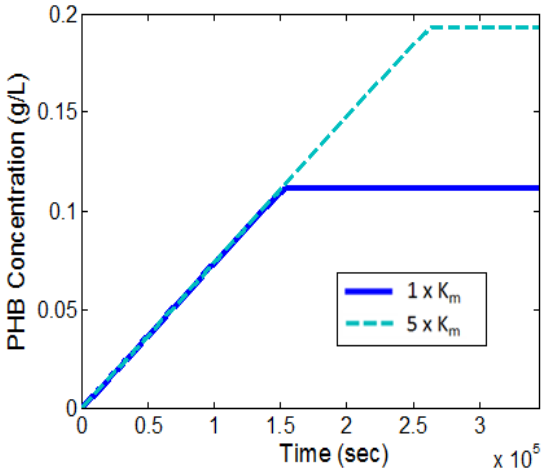

Figure 130. PHB production levels from adjusting glyceraldehyde-3-phosphate dehydrogenase's K_m for NAD^+, glyceraldehyde-3-phosphate, and inorganic phosphate.

No visible increase in PHB production was observed by altering the K_m values for the enzymes phosphoglycerate kinase, phosphoglycerate mutase, and enolase. The enzyme pyruvate kinase has a K_m for phosphoenolpyruvate and ADP. Increasing or decreasing the K_m for phosphoenolpyruvate resulted in no visible change in the production of PHB. A very slight increase in PHB production was observed by increasing the K_m for ADP. The simulations for these four enzymes are available in Appendix C.

Acetyl-CoA Synthesis Enzymes:

The only enzyme in the acetyl-CoA synthesis pathway is the multienzyme complex pyruvate dehydrogenase. Figure 131 shows that an increase in PHB production is the result of decreasing the K_m value for the substrate pyruvate. Decreasing K_m by one-fifth resulted in a 26.0% increase in the synthesis of PHB.

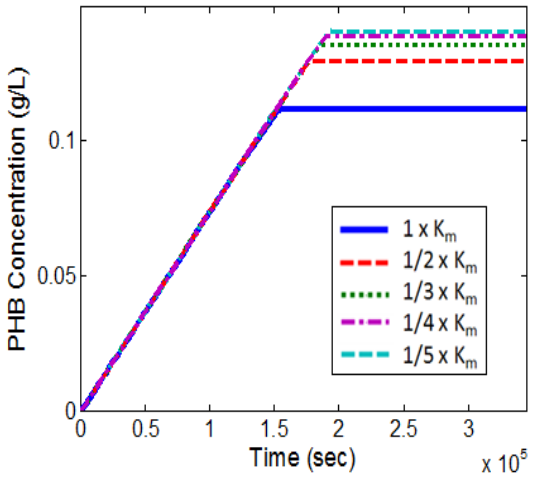

Figure 131. PHB production levels from adjusting pyruvate dehydrogenase's K_m for pyruvate.

Enzyme Summary:

Large increases in PHB production were observed by adjusting the K_m values for β-ketothiolase, acetoacetyl-CoA reductase, citrate synthase, isocitrate dehydrogenase,

isocitrate lyase, fructose-bisphosphate aldolase, triose phosphate isomerase, glyceraldehyde-3-phosphate dehydrogenase, and pyruvate dehydrogenase. The enzyme acetoacetyl-CoA reductase was the only enzyme where changes in K_m increased the rate of PHB production. The largest percent increase (113.7%) came from adjusting the K_m values for citrate synthase, and the second largest increase (72.8%) came from changing the K_m values for glyceraldehyde-3-phosphate dehydrogenase as seen in Table XLI.

Altering K_m values resulted in a slight increase in PHB production for the enzymes isocitrate hydro-lyase, succinyl-CoA synthetase, malate synthase, phosphoglycerate mutase, and pyruvate kinase. The adjustment of K_m values caused no increase in PHB production for the enzymes PHB synthase, citrate hydro-lyase, 2-oxoglutarate dehydrogenase, succinate dehydrogenase, fumarate, malate dehydrogenase, kinase, phosphoglucose isomerase, 6-phosphofructokinase, phosphoglycerate kinase, enolase, glucose-1-phosphatase, fructose-1,6-bisphosphatase, phosphoenolpyruvate carboxykinase, and phosphoenolpyruvate synthetase.

Table XLI. K_m adjustments leading to increased PHB production. Percent increase is from increasing or decreasing K_m by five-fold.

Enzyme	$K_{m, A}$	$K_{m, B}$	$K_{m, C}$	% Increase
β-ketothiolase	↓	NA	NA	35.3
Acetoacetyl-CoA reductase	↓	↓	NA	8.6*
Citrate synthase	↑	↑	NA	113.7
Isocitrate dehydrogenase	↓	NA	NA	7.8
Isocitrate lyase	↑	NA	NA	8.6
Fructose-bisphosphate aldolase	↑	NA	NA	22.5
Triose phosphate isomerase	↑	NA	NA	7.1
Glyceraldehyde-3-phosphate dehydrogenase	↑	↑	↑	72.8
Pyruvate dehydrogenase	↓	NA	NA	26.0

*Increase in rate

Adjusting Ligand Concentration:

The only ligand adjusted for optimization of PHB production was IPTG. The ligand IPTG binds to the LacI repressor and prevents it from repressing transcription of the PHB synthesis genes. Concentrations of other ligands and transcription factors were not tested for optimization because they are widely used in metabolic pathways so the model cannot account for all of the effects that such changes would have on the cell. No significant increase in PHB production was observed from increasing or decreasing the concentration of IPTG as shown in Figure 132.

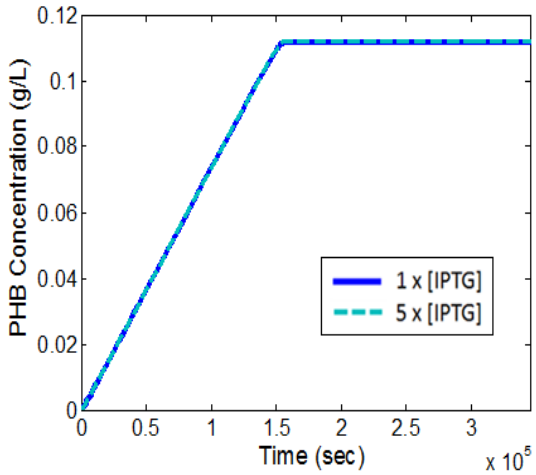

Figure 132. PHB production levels from adjusting concentrations of IPTG.

Adjusting Promoter Activity:

The only promoter tested for model optimization was the *lac* promoter in the pBHR68 plasmid that regulates transcription of the PHB synthesis genes. It is easier to genetically engineer the plasmid than to genetically engineer promoters in the genome. Also, promoters in the genome often regulate the transcription of multiple genes. This model only accounts for a small number of genes, so it cannot accurately predict the effect of altering a promoter in the genome.

The *lac* promoter that regulates the PHB genes was adjusted to increase PHB production because all the genes in the pBHR68 plasmid are accounted for in the model. Multiplying the *lac* promoter activity (β) by a factor of five resulted in an 8.5% increase in PHB production as seen in Figure 133. Also, maximum PHB production was reached by 12 hours compared to the 43 hours observed at normal promoter activity. A factor of five was used to standardize comparison with the increases observed from adjusting K_m values for the enzymes.

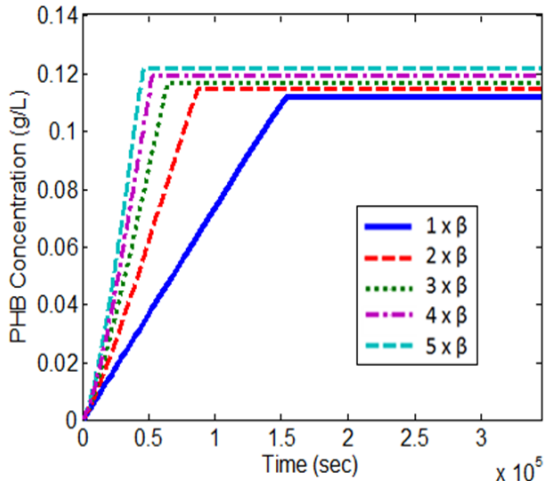

Figure 133. PHB production levels from adjusting activity (β) of the *lac* promoter in the pBHR68 plasmid.

Optimized Model:

An optimized model for PHB production was created by increasing promoter activity by five fold for the *lac* promoter and by increasing all K_m values by five fold for citrate synthase and glyceraldehyde-3-phosphate dehydrogenase. This optimized model resulted in a 226.8% increase in PHB production achieved by 29 hours compared to 43 hours. Figure 134 shows the comparison between the optimized model and the normal model. Altering the enzymes contributed mostly to the increase in total PHB production,

while altering the promoter activity contributed mostly to the increase in the rate of PHB production as illustrated by Figure 134.

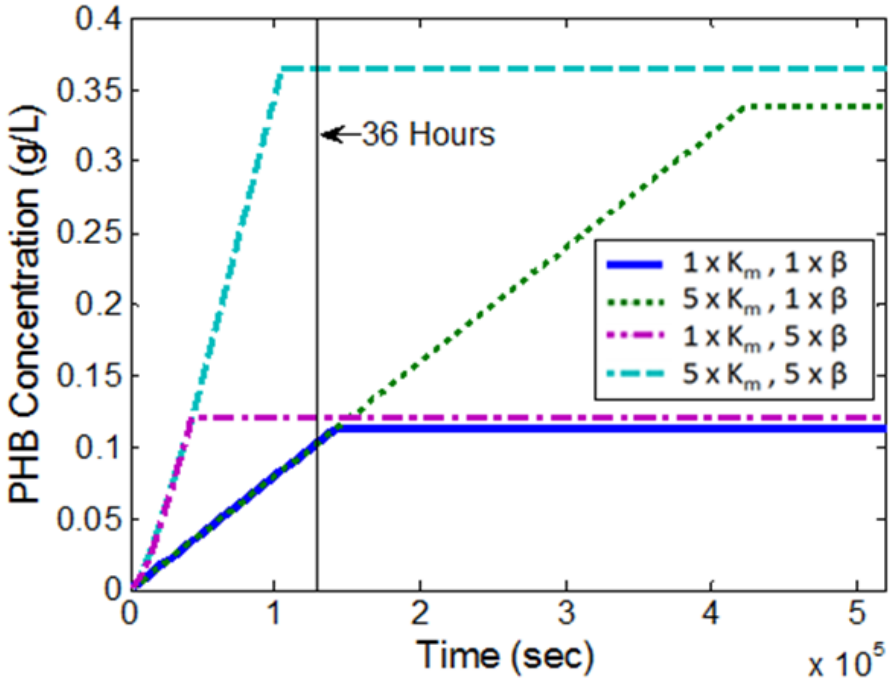

Figure 134. Simulations showing the comparisons between PHB production levels from the unaltered model; PHB production levels from increasing K_m values for citrate synthase and glyceraldehyde-3-phosphate dehydrogenase; PHB production levels from increasing the pBHR68 *lac* promoter activity (β); and PHB production levels from increasing the K_m values of the two enzymes and increasing the pBHR68 *lac* promoter activity (β).

DISCUSSION AND FUTURE WORK

Discussion

The predictive model identified nine enzymes as potential targets for genetic engineering in order to optimize the production of PHB. Four of the enzymes required decreasing K_m in order to increase PHB production. Lowering K_m values is equivalent to increasing an enzyme's substrate affinity. Engineering an enzyme to have a higher substrate affinity is a difficult task because enzymes have evolved to be efficient at binding their substrates. It is easier to make an enzyme less effective at binding its substrate. Increasing the K_m values of five enzymes led to an increase in PHB production. The active sites of these five enzymes could be engineered to be less effective at binding their substrates. Therefore, the nine potential targets for genetic engineering was narrowed down to five enzymes.

Out of the five enzymes, altering the K_m for citrate synthase resulted in the largest increase in PHB production. Due to the 113.7% increase observed by increasing K_m by five fold, citrate synthase is the first target gene for engineering. The two active sites in citrate synthase could be genetically engineered to be less effective at binding the substrates oxaloacetate and acetyl-CoA, and the result should enhance PHB production.

Out of the five enzymes identified as potential targets, increasing the K_m of glyceraldehyde-3-phosphate dehydrogenase caused the second largest increase observed in PHB production. Glyceraldehyde-3-phosphate dehydrogenase is the second target gene for engineering because of the 72.8% increase in PHB synthesis that resulted from increasing the K_m values by five fold. The three active sites for glyceraldehyde-3-

phosphate, NAD^+, and inorganic phosphate could be genetically engineered to be less effective at binding the substrates, and the result should increase PHB production.

The *lac* promoter in the pBHR68 plasmid was the third target identified for genetic engineering. Increasing the *lac* promoter activity by five times resulted in an 8.5% increase in total PHB production and a 275% increase in the rate of PHB production. Genetically engineering the *lac* promoter in the pBHR68 plasmid to have greater activity should result in a significant increase in the rate of PHB production. The only other adjustment that resulted in an increase in the rate of PHB production was decreasing the K_m by a fifth for the enzyme acetoacetyl-CoA reductase. However, this adjustment only resulted in an 8.6% increase in the rate of PHB production. Therefore, the *lac* promoter in the pBHR68 plasmid was chosen as the third target for genetic engineering.

The simulation that made adjustments for all three targets resulted in a 226.8% increase in maximum PHB production and a 275% increase in the rate of PHB production. Genetically engineering a strain of *E. coli* that can produce more PHB in a shorter amount of time will help make commercial PHB production more cost effective. An optimized strain should be achieved by altering the genes for citrate synthase (*gltA*) and glyceraldehyde-3-phosphate dehydrogenase (*gapA*), and by modifying the *lac* promoter in the pBHR68 plasmid.

Instead of genetically engineering citrate synthase and glyceraldehyde-3-phosphate dehydrogenase to be less effective, substrate analogs could be used as competitive inhibitors for the enzymes. For citrate synthase, the compound carboxymethyl-CoA acts as an inhibitor of the transition state with a high binding

affinity. Theoretically, carboxymethyl-CoA could be added to the bioreactor to inhibit citrate synthase. For glyceraldehyde-3-phosphate dehydrogenase, adenosine analogs can be used as tight-binding inhibitors of the NAD^+ active site. Adding an adenosine analog to the bioreactor should slow down the enzyme glyceraldehyde-3-phosphate dehydrogenase.

One major disadvantage of adding a compound to the bioreactor is that the compound could affect more than just the target enzyme. Carboxymethyl-CoA could inhibit other reactions that use acetyl-CoA. Adenosine analogs could inhibit other reactions that use NAD^+. Adding compounds to the bioreactor also increases production cost. Due to the cost and potential side effects of adding substrate analogs to the reactor, it was decided to focus first on genetically engineering the enzymes to be less effective.

Flux balance analysis (FBA) has widely been used in genome-scale metabolic models. However, a model based on FBA would not have been able to predict that lowering the substrate affinity of citrate synthase or glyceraldehyde-3-phosphate dehydrogenase would increase PHB production. FBA is limited to predicting how the addition or deletion of gene affects a product's flux. Deletion of citrate synthase or glyceraldehyde-3-phosphate dehydrogenase would be undesirable because they are both part of key energy pathways in the cell. Also, FBA would not have been able to quantitatively predict how adjusting promoter activity would impact PHB production because FBA does not account for a dynamic transcriptional network.

Certain strains of PHB producing bacteria have been genetically engineered to secrete the produced PHB. Secreting PHB into the growth media can significantly reduce the cost of downstream processing. The secretion pathway could be added to the model to

predict how to optimize a PHB secreting strain of bacteria for greater PHB production. Another way to reduce cost of PHB production is to use a waste material as the initial substrate. Whey is a waste product from cheese production that contains lactose. Lactose could be used instead of glucose in the growth medium. The model could be adjusted to account for the catabolism of lactose instead of glucose.

The design process used to make a predictive model for PHB production can be used to develop predictive models for other bioproducts. Useful bioproducts such as biofuels, biomaterials, and biopharmaceuticals are continually being developed, but often many years of research are required before commercial production becomes cost-effective. Predictive models can be used to develop optimized strains of bacteria for production of specific bioproducts. Predictive models should help reduce time and cost needed to get useful bioproducts out on the market.

Future Work

Metabolic profiling can be used to more precisely fit a predictive model to a specific strain of *E. coli*. Due to the lack of a functioning mass spectrometer, this predictive model was not fitted to metabolic profiling data. This model is not as accurate as it could be if it was fitted to real time data from the specific strain of *E. coli*. Further work should be done to obtain metabolic profiling data to use in the model.

After the model has been fitted to metabolic profiling data, the model should be optimized to verify that altering the effectiveness of citrate synthase, glyceraldehyde-3-phosphate dehydrogenase, and the *lac* promoter in the pBHR68 plasmid will optimize PHB production.

After the target genes have been verified, they should be genetically engineered to mimic the optimized model. The amino acids in the active sites of citrate synthase and glyceraldehyde-3-phosphate dehydrogenase should be identified. One or more of the amino acids should be exchanged with a less effective amino acid through site-directed mutagenesis. This genetic engineering should result in enzymes that are less effective at binding their substrates. The *lac* promoter in the pBHR68 plasmid should be altered to more closely match the consensus sequence that binds RNA polymerase. This genetic engineering should stabilize the RNA binding and increase the activity of the *lac* promoter in the pBHR68 plasmid.

Once the strain of *E. coli* has been genetically engineered for optimized PHB production, metabolic profiling should be conducted again. The predictive model should then be fit to the new metabolic profiling data. By comparing the old model with the new data, the accuracy of the first predictive model can be determined. The new predictive model can then be optimized to identify new targets for genetic engineering. This iterative process should be repeated until a fully optimized strain of *E. coli* for PHB production has been genetically engineered.

The PHB predictive model designed in this project is limited to five metabolic pathways and accounts for only a portion of the transcriptional network. These limitations only allow the PHB predictive model to predict outcomes from modifying 30 genes, one promoter, and one ligand. However, in the future the data needed to build a genome-scale kinetic model will become available (Jamshidi & Palsson, 2008). A genome-scale kinetic model would account for all the metabolic pathways and would include a full, dynamic transcriptional network. Such a model would be able to predict

the outcomes of modifying any gene, promoter, transcription factor, or ligand. A genome-scale kinetic model would be a valuable tool in genetically engineering optimized organisms for the production of bioproducts.

The PHB predictive model developed in this project is a step towards one day realizing a genome-scale kinetic model as shown in Table XLII. Although the data needed to build a genome-scale kinetic model is not yet available, progress comes from implementing ideas with the tools that exist today. Engineers need to build working models with the data and technology currently available, and then the models can be improved as new data and technologies are discovered.

Table XLII. Comparisons between the current PHB predictive model and a future genome-scale kinetic model.

	PHB Predictive Model	Genome-Scale Model
Metabolic Pathways:	5	All
Transcriptional Network:	Partial, dynamic	Full, dynamic
Predict Outcomes from Modifying:	30 genes 1 promoter 1 ligand 0 transcription factors	Any gene Any promoter Any ligand Any transcription factor

REFERENCES

Abo-Amer AE, Munn J, Jackson K, Aktas M, Golby P, Kelly DJ, Andrews SC (2004) DNA interaction and phosphotransfer of the C_4-dicarboxylate responsive DcuS-DcuR two-component regulatory system from *Escherichia coli*. *J Bacteriol* **186**: 1879-1889

Alber BE, Spanheimer R, Ebenau-Jehle C, Fuchs G (2006) Study of an alternate glyoxylate cycle for acetate assimilation by *Rhodobacter sphaeroides*. *Mol Microbiol* **61**(2): 297-309

Allison N, Williams CH, Guest JR (1988) Overexpression and mutagenesis of the lipoamide dehydrogenase of *Escherichia coli*. *Biochem J* **256**: 741-749

Anderson DH, Duckworth HW (1988) *In vitro* mutagenesis of *Escherichia coli* citrate synthase to clarify the locations of ligand binding sites. *Biol Chem* **263**: 2163-2169

Anstrom DM, Kallio K, Remington SJ (2003) Structure of the *Escherichia coli* malate synthase G: pyruvate: acetyl-coenzyme A abortive ternary complex at 1.95 Å resolution. *Protein Sci* **12**: 1822-1832

Azam TA, Iwata A, Nishimura A, Uedo S, Ishihama A (1999) Growth phase-dependent variation in protein composition of the *Escherichia coli* nucleoid. *J Bacteriol* **181**: 6361-6370

Bajad SU, Lu W, Kimbal EH, Yuan J, Peterson C, Rabinowitz JD (2006) Separation and quantification of water soluble cellular metabolites by hydrophilic interaction chromatography-tandem mass spectrometry. *J Chromatogr A* **1125**: 76-88

Belova LL, Sokolov AP, Sidorov IA, Trotsenko YA (2006) Purification and characterization of NADPH-dependent acetoacetyl-CoA reductase from *Methylobacterium extorquens. FEMS Microbiol Lett* **2**: 275-279

Berg IA, Kockelkorn D, Buckel W, Fuchs G (2007) A 3-hydroxypropionate/4-hydroxybutyrate autotrophic carbon dioxide assimilation pathway in Archaea. *Science* **318**(5857): 1782-1786

Birney M, Um H, Klein C (1996) Novel mechanisms of *Escherichia coli* succinyl-coenzyme A synthetase regulation. *J Bacteriol* **178**: 2883-2889

Brown G, Singer A, Lunin VV, Proudfoot M, Skarina T, Flick R, Kochinyan S, Sanishvili R, Joachimiak A, Edwards AM, Savchenko A, Yakunin AF (2009) Structural and biochemical characterization of the type II fructose-1,6-bisphosphatase GlpX from *Escherichia coli*. *J Biol Chem* **284**: 3784-3792

Buchholz A, Takors R, Wandrey C (2001) Quantification of intracellular metabolites in *Escherichia coli* K12 using liquid chromatographic-electrospray ionization tandem mass spectrometric techniques. *Anal Biochem* **295**: 129-137

Butterworth PJ, Tsai CS, Eley MH, Roche TE, Reed LJ (1975) A kinetic study of dihydrolipoyl transacetylase from bovine kidney. *J Biol Chem* **250**: 1921-1925

Byrom D (1987) Polymer synthesis by microorganisms - technology and economics. *Trends Biotechnol* **5**: 246-250

Campos G, Guixe V, Babul J (1984) Kinetic mechanism of phosphofructokinase-2 from *Escherichia coli:* a mutant with a different mechanism. *J Biol Chem* **259**: 6147-6152

Cecchini G, Schröder I, Gunsalus RP, Maklashina E (2002) Succinate dehydrogenase and fumarate reductase from *Escherichia coli*. *Biochim Biophys Acta* **1553**: 140-157

Cho BK, Knight EM, Barrett CL, Palsson BO (2008) Genome-wide analysis of Fis binding in *Escherichia coli* indicates a causative role for A-/AT-tracts. *Genome Res* **18**: 900-910

Choi JI, Lee SY (1997) Process analysis and economic evaluation for poly(3-hydroxybutyrate) production by fermentation. *Bioprocess Eng* **17**: 335-342

Choi JI, Lee SY (1999) Factors affecting the economics of polyhydroxyalkanoate production by bacterial fermentation. *Appl Microbiol Biot* **51**: 13-21

Conant GC, Wolfe KH (2007) Increased glycolytic flux as an outcome of whole-genome duplication in yeast. *Mol Syst Biol* **3**: 129

Crow VL, Wittenberger CL (1979) Separation and properties of NAD+-NADP+-dependent glyceraldehyde-3-phosphate dehydrogenases from *Streptococcus mutans. J Biol Chem* **254**: 1134-1142

Darwin AJ, Tyson KL, Busby SJW, Stewart V (1997) Differential regulation by the homologous response regulators NarL and NarP of *Escherichia coli* K-12 depends on DNA binding site arrangement. *Mol Microbiol* **25**: 583-595

Dettmer K, Aronov PA, Hammock BD (2006) Mass spectrometry-based metabolomics. *Mass Spectrom Rev* **26**: 51-78

Doi Y (1990) *Microbial polyesters*. Wiley-VCH, New York City, NY, USA

Duckworth HW, Anderson DH, Bell AW, Donald LJ, Chu AL, Brayer GD (1987) Structural basis for regulation in gram-negative bacterial citrate synthases. *Biochem Soc Symp* **54**: 83-92

Durchschlag H, Biedermann G, Eggerer H (1981) Large-scale purification and some properties of malate synthase from baker's yeast. *Eur J Biochem* **114**: 255-262

Dworniczak K, Ginalska G, Patkowska M (2008) Isolation and characterization of phosphoglucomutase (PGM) from *Escherichia coli* bacterial cells. *Ann Univ Mariae Curie Sklodowska* **11**: 99-107

Feist AM, Herrgard MJ, Thiele I, Reed JL, Palsson BO (2009) Reconstruction of biochemical networks in microorganisms. *Nat Rev Microbiol* **7**: 129-143

Finkel SE, Johnson RC (1992) The Fis protein: it's not just for DNA inversion anymore. *Mol Microbiol* **6**: 3257-3265

Fraser HI, Kvaratskhelia M, White MF (1999) The two analogous phosphoglycerate mutases of *Escherichia coli*. *FEBS Lett* **455**: 344-348

Gaudu P, Weiss B (1996) SoxR, a [2Fe-2S] transcription factor, is active only in its oxidized form. *Proc Natl Acad Sci USA* **93**: 10094-10098

Giles IG, Poat PC, Munday KA (1976) The kinetics of rabbit muscle pyruvate kinase: initial-velocity, substrate and product inhibition and isotopic-exchange studies of the reverse reaction. *Biochem J* **157**: 577-589

Golby P, Davies S, Kelly DJ, Guest JR, Andrews SC (1999) Identification and characterization of a two-component sensor-kinase and response-regulator system (DcuS-DcuR) controlling gene expression in response to C4-dicarboxylates in *Escherichia coli*. *J Bacteriol* **181**: 1238-1248

Griffith KL, Shah IM, Wolf RE Jr (2004) Proteolytic degradation of *Escherichia coli* transcription activators SoxS and MarA as the mechanism for reversing the induction of the superoxide (SoxRS) and multiple antibiotic resistance (Mar) regulons. *Mol Microbiol* **51**: 1801-1816

Gunsalus RP, Park SJ (1994) Aerobic-anaerobic gene regulation in *Escherichia coli:* control by the ArcAB and Fnr regulons. *Res Microbiol* **145**: 437-450

Gurieff N, Lant P (2007) Comparative life cycle assessment and financial analysis of mixed culture polyhydroxyalkanoate production. *Bioresource Technol* **98**: 3393-3403

Haywood GW, Anderson AJ, Chu L, Dawes EA (1988) Characterization of two 3-ketothiolases possessing differing substrate specificities in the polyhydroxyalkanoate synthesizing organism *Alcaligenes eutrophus. FEMS Microbiol Lett* **52**: 91-96

Haywood GW, Anderson AJ, Dawes EA (1989) The importance of PHB-synthase substrate specificity in polyhydroxyalkanoate synthesis by *Alcaligenes eutrophus*. *FEMS Microbiol Lett* **57**: 1-6

Helfert S, Estevez AM, Bakker B, Michels P, Clayton C (2001) Roles of triose phosphate isomerase and aerobic metabolism in *Trypanosoma brucei. Biochem J* **357**: 117-125

Heyde E, Ainsworth S (1968) Kinetic studies on the mechanism of the malate dehydrogenase reaction. *J Biol Chem* **243**: 2413-2425

Hidalgo E, Demple B (1994) An iron-sulfur center essential for transcriptional activation by the redox-sensing SoxR protein. *EMBO J* **13**: 138-146

Hynne F, Dano S, Sorensen PG (2001) Full-scale model of glycolysis in *Saccharomyces cerevisiae. Biophys Chem* **94**: 121-163

Isabella VM, Lapek JD, Kennedy EM, Clark VL (2009) Functional analysis of NsrR, a nitric oxide-sensing Rrf2 repressor in *Neisseria gonorrhoeae. Mol Microbiol* **71**: 227-239

Ishii N, Suga Y, Hagiya A, Watanabe H, Mori H, Yoshino M, Tomita M (2007) Dynamic simulation of an in vitro multi-enzyme system. *FEMS Microbiol Lett* **581**: 413-420

Ishizuka H, Hanamura A, Kunimura T, Aiba H (1993) A lowered concentration of cAMP receptor protein caused by glucose is an important determinant for catabolite repression in *Escherichia coli*. *Mol Microbiol* **10**: 341-350

Ishizuka H, Hanamura A, Inada T, Aiba H (1994) Mechanism of the down-regulation of cAMP receptor protein by glucose in *Escherichia coli*: role of autoregulation of the *crp* gene. *EMBO J* **13**: 3077-3082

Jamshidi N, Palsson BO (2008) Formulating genome-scale kinetic models in the post-genome era. *Mol Syst Biol* **4**: 171

Jeon Y, Lee YS, Han JS, Kim JB, Hwang DS (2001) Multimerization of phosphorylated and non-phosphorylated ArcA is necessary for the response regulator function of the Arc two-component signal transduction system. *J Biol Chem* **276**: 40873-40879

Jordan PA, Tang Y, Bradbury AJ, Thomson AJ, Guest JR (1999) Biochemical and spectroscopic characterization of *Escherichia coli* aconitases (AcnA and AcnB). *Biochem J* **344**(3): 739-46

Josh JG, Handler P (1964) Phosphoglucomutase. I. Purification and properties of phosphoglucomutase from *Escherichia coli*. *J Biol Chem* **239**: 2741-2751

Joyce MA, Frase ME, Brownie ER, James MNG, Bridger WA, Wolodko WT (1999) Probing the nucleotide-binding site of *Escherichia coli* succinyl-CoA synthetase. *Biochemistry* **38**: 7273-7283

Jurasek L, Marchessault RH (2004) Polyhydroxyalkanoate (PHA) granule formation in *Ralstonia eutropha* cells: a computer simulation. *Appl Microbiol Biot* **64**: 611-617

Kashiwaya Y, Sato K, Tsuchiya N, Thomas S, Fell DA, Veech RL, Passonneau JV (1994) Control of glucose utilization in working perfused rat heart. *J Biol Chem* **269**: 25502-25514

Khanna S, Srivastava AK (2005) Statistical media optimization studies for growth and PHB production by *Ralstonia eutropha. Process Biochem* **40**: 2173-2182

Kolb A, Busby S, Buc H, Garges S, Adhya S (1993) Transcriptional regulation by cAMP and its receptor protein. *Annu Rev Biochem* **62**: 749-495

Krebs A, Bridger WA (1980) The kinetic properties of phosphoenolpyruvate carboxykinase of *Escherichia coli*. *Can J Biochem* **58**: 309-318

Krishna S, Orosz L, Sneppen K, Adhya S, Semsey S (2009) Relation of intracellular signal levels and promoter activities in the *gal* regulons of *Escherichia coli*. *J Mol Biol* **391**: 671-678

Kuznetsova E, Proudfoot M, Gonzalez CF, Omelchenko MV, Borozan I, Carmel L, Wolf YI, Mori H, Savchenko AV, Arrowsmith CH, Koonin EV, Edwards AM, Yakunin AF (2006) Genome-wide analysis of substrate specificities of the *Escherichia coli* haloacid dehalogenase-like phosphatase family. *J Biol Chem* **281**: 36149-36161

Lambeth MJ, Kushmerick MJ (2002) A computational model for glycogenolysis in skeletal muscle. *Ann Biomed Eng* **30**: 808-827

Lavoinne A, Marchand J, Chedeville A, Matray F (1983) Kinetic studies of the reaction mechanism of rat liver phosphoglycerate kinase in the direction of ADP utilization. *Biochimie* **65**: 211-220

Leaf T, Srienc F (1998) Metabolic modeling of polyhydroxybutyrate biosynthesis. *Biotechnol Bioeng* **57**: 557-570

Lee ME, Dyer DH, Klein OD, Bolduc JM, Stoddard BL, Koshland DE Jr (1995) Mutational analysis of the catalytic residues lysine 230 and tyrosine 160 in the (NADP(+)) dependent isocitrate dehydrogenase from *Escherichia coli. Biochemistry* **34**: 378-382

Lee SY (1996) Bacterial polyhydroxyalkanoates. *Biotechnol Bioeng* **49**: 1-14

Lehninger AL, Nelson DL, Cox MM (2008) *Lehninger Principles of Biochemistry.* W. H Freeman and Company, New York, NY, USA

Lewis M (2005) The *lac* repressor. *C R Biol* **328**: 521-548

Li Z, Demple B (1994) SoxS, an activator of superoxide stress genes in *Escherichia coli*. Purification and interaction with DNA. *J Biol Chem* **269**: 18731-18377

Lin EC (1976) Glycerol dissimilation and its regulation in bacteria. *Annu Rev Microbiol* **30**: 535-578

Linton E (2010) A synthetic biological engineering approach to secretion-based recovery of polyhydroxyalkanoates and other cellular products. *MS Thesis USU*

Liu M, Garges S, Adhya S (2004) lacP1 promoter with an extended -10 motif. Pleiotropic effects of cyclic AMP protein at different steps of transcription initiation. *J Biol Chem* **279**: 54552-54557

Liu X, Bisswanger H (2003) Solvent isotope effect on the reaction catalysed by the pyruvate dehydrogenase complex from *Escherichia coli*. *J Biol Chem* **384**: 673-679

Lorca GL, Ezersky A, Lunin VV, Walker JR, Altamentova S, Evdokimova E, Vedadi M, Bochkarev A, Savchenko A (2007) Glyoxylate and pyruvate are antagonistic effectors of the *Escherichia coli* IclR transcriptional regulator. *J Biol Chem* **282**: 16476-16491

Lu W, Bennett BD, Rabinowitz JD (2008) Analytical strategies for LC-MS-based targeted metabolomics. *J Chromatogr B* **871**: 236-242

Lunin VV, Li Y, Schrag JD, Iannuzzi P, Cygler M, Matter A (2004) Crystal structures of *Escherichia coli* ATP-dependent glucokinase and its complex with glucose. *J Bacteriol* **186**: 6915-6927

Luo GX, Nishimura JS (1991) Site-directed mutagenesis of *Escherichia coli* succinyl-CoA synthetase: histidine 142α is a facilitative catalytic residue. *J Biol Chem* **266**: 20781-20785

Mackintosh C, Nimmo HG (1988) Purification and regulatory properties of isocitrate lyase from *Escherichia coli* ML308. *Biochem J* **250**: 25-31

Madison LL, Huisman GW (1999) Metabolic engineering of poly(2-hydroxyalkanoates): from DNA to plastic. *Microbiol Mol Biol R* **63**: 21-53

Maklashina E, Iverson TM, Sher Y, Kotlyar V, Andrell J, Mirza O, Hudson JM, Armstrong FA, Rothery RA, Weiner JH, Cecchini G (2006) Fumarate reductase and succinate oxidase activity of *Escherichia coli* complex II homologs are perturbed differently by mutations of the flavin binding domain. *J Biol Chem* **281**: 11357-11365

Makman RS, Sutherland EW (1965) Adenosine 3', 5'-Phosphate in *Escherichia coli. J Biol Chem* **240**: 1309-1314

Man WJ, Li T, O'Conner CD, Wilton DC (1995) The binding of propionyl-CoA and carboxymethyl-CoA to *Escherichia coli* citrate synthase. *Biochim Biophys Acta* **1250**: 69-75

Mantzaris NV, Kelley AS, Daoutidis P, Srienc F (2002) A population balance model describing the dynamics of molecular weight distributions and the structure of PHA copolymer chains. *Chem Eng Sci* **57**: 4643-4663

Martin RG, Jair KW, Wolf RE, Rosner JL (1996) Autoactivation of the *marRAB* multiple antibiotic resistance operon by the MarA transcriptional activator in *Escherichia coli*. *J Bacteriol* **178**: 2216-2223

Martin RG, Bartlett ES, Rosner JL, Wall ME (2008) Activation of the *Escherichia coli* marA/soxS/rob regulon in response to transcriptional activator concentration. *J Mol Biol* **380**: 278-284

Mashego MR, Rumbol K, Mey MD, Vandamme E, Soetaert W, Heijnen JJ (2007) Microbial metabolomics: past, present and future methodologies. *Biotechnol Lett* **29**: 1-16

Matsuoka Y, Srere PA (1973) Kinetic studies of citrate synthase from rat kidney and rat brain. *J Biol Chem* **248**: 8022-8030

McCormack JG, Denton RM (1981) A comparative study of the regulation by Ca^{2+} of the activities of the 2-oxoglutarate dehydrogenase complex and NAD^{+}-isocitrate dehydrogenase from a variety of sources. *Biochem J* **196**: 619-624

Meyer D, Schneider-Fresenius C, Horlacher R, Peist R, Boos W (1997) Molecular characterization of glucokinase from *Escherichia coli* K-12. *J Bacteriol* **179**: 1298-1306

Mills SA, Marletta MA (2005) Metal binding characteristics and role of iron oxidation in the ferric uptake regulator from *Escherichia coli. Biochemistry* **44**: 13553-13559

Moffet FJ, Bridger WA (1970) The kinetics of succinyl coenzyme A synthetase from *Escherichia coli.* A reaction with a covalent enzyme-substrate intermediate not exhibiting "ping-pong" kinetics. *J Biol Chem* **245**: 2758-2762

Molina I, Pellicer MT, Badia J, Aguilar J, Baldoma L (1994) Molecular characterization of *Escherichia coli* malate synthase G: differentiation with the malate synthase A isoenzyme. *Eur J Biochem* **224**: 541-548

Mothes G, Babel W (1994) *Methylbacterium rhodesianum* MB 126 possesses two acetoacetyl-CoA reductases. *Arch Microbiol* **161**: 277-280

Mothes G, Rivera IS, Babel W (1997) Competition between β-hydroxybutyrate synthesis in *Methylobacterium rhodesianum*. *Arch Microbiol* **166**: 405-410

Mukherjee A, Smitherman TC, Robinson JB, Butsch RW, Richards EG, Srere PA (1980) Studies on human heart citrate synthase. *Adv Myocardiol* **1**: 329-337

Muslin EH, Li D, Stevens FJ, Donnelly M, Schiffer M, Anderson LE (1995) Engineering a domain-locking disulfide into a bacterial malate dehydrogenase produces a redox-sensitive enzyme. *Biophys J* **68**: 2218-2223

Nazaret C, Heiske M, Thurley K, Mazat JP (2009) Mitochondrial energetic metabolism: a simplified model of TCA cycle with ATP production. *J Theor Biol* **258**: 455-464

Nemeria N, Yan Y, Zhang Z, Brown AM, Arjunan P, Furey W, Guest JR, Jordan R (2001) Inhibition of the *Escherichia coli* pyruvate dehydrogenase complex E1 subunit and its tyrosine 177 variants by thiamin 2-thiazolone and thiamin 2-thiothiazolone dephosphates. *J Biol Chem* **276**: 45969-45978

Nickbarg EB, Knowles JR (1988) Triose phosphate isomerase: energetics of the reaction catalyzed by the yeast enzyme expressed in *Escherichia coli. Biochemistry* **27**: 5939-5947

Nielsen K, Sørensen PG, Hynne F, Busse HG (1998) Sustained oscillations in glycolysis: an experimental and theoretical study of chaotic and complex periodic behavior and of quenching of simple oscillations. *Biophys Chem* **72**(1-2): 49-62

Oberhardt MA, Palsson BO, Papin JA (2009) Applications of genome-scale metabolic reconstructions. *Mol Syst Biol* **5**: 320

Oberto J, Nabti S, Jooste V, Mignot H, Rouviere-Yaniv J (2009) The HU region is composed of genes responding to anaerobisis, acid stress, high osmolarity and SOS induction. *PLoS One* **4**: e4367

Oeding V, Schlegel HG (1973) Beta-ketothiolase from *Hydrogenomonas eutropha* H16 and its significance in the regulation of poly-beta-hydroxybutyrate metabolism. *Biochem J* **134**: 239-48

Ohashi Y, Hirayama A, Ishikawa T, Nakamura S, Shimizu K, Ueno Y, Tomita M, Shoga T (2007) Depiction of metabolome changes in histidine-starved *Escherichia coli* by CE-TOFMS. *Mol Biosyst* **4**: 135-147

Orth JD, Thiele I, Palsson BO (2010) What is flux balance analysis? *Nature Biotechnology* **28**: 245-248

Oshima T, Ishikawa S, Kurokawa K, Aiba H, Ogasawara N (2006) *Escherichia coli* histone-like protein H-NS preferentially binds to horizontally acquired DNA in association with RNA polymerase. *DNA Res* **13**: 141-153

Pellicer MT, Fernandez C, Badia J, Aquilar J, Lin EC, Baldom L (1999) Cross-induction of *glc* and *ace* operons of *Escherichia coli* attributable to pathway intersection. Characterization of the *glc* promoter. *Journal Biol Chem* **274**: 1745-1752

Perdiguero E, Arriaga D, Busot F, Soler J (1995) Isocitrate lyase from *Cephalosporium acremonium*. Role of Mg^{2+} ions, kinetics, and evidence for a histidine residue in the active site of the enzyme. *Biochemistry* **34**: 6059-6068

Pereira DS, Donald LJ, Hosfield DJ, Duckworth HW (1994) Active site mutants of *Escherichia coli* citrate synthase. Effects of mutations on catalytic and allosteric properties. *Biochemistry* **269**: 412-417

Plater AR, Zgiby SM, Thomson GJ, Qamar S, Wharton CW, Berry A (1999) Conserved residues in the mechanism of the *E. coli* Class II FBP-aldolase. *J Mol Biol* **285**: 843-855

Ploux O, Masamune S, Walsh CT (1988) The NADPH-linked acetoacetyl-CoA reductase from *Zoogloea ramigera. Eur J Biochem* **174**: 177-182

Pomposiello PJ, Demple B (2001) Redox-operated genetic switches: the SoxR and OxyR transcription factors. *Trends Biotechnol* **19**: 109-114

Price ND, Papin JA, Schilling CH, Palsson BO (2003) Genome-scale microbial *in silico* models: the constraints-based approach. *Trends Biotechnol* **21**: 162-169

Pritchard L, Kell DB (2002) Schemes of flux control in a model of *Saccharomyces cerevisiae* glycolysis. *Eur J Biochem* **269**(16): 3894-904

Purich DL, Allison RD (2000) *Handbook of Biochemical Kinetics.* Academic Press, San Diego, CA, USA

Quail MA, Guest JR (1995) Purification, characterization and mode of action of PdhR, the transcriptional regulator of the pdhR-aceEF-lpd operon of *Escherichia coli. Mol Microbiol* **15**: 519-529

Raman K, Chandra N (2009) Flux balance analysis of biological systems: applications and challenges. *Brief Bioinform* **10**: 435-449

Ramseier TM, Bledig S, Michotey V, Feghali R, Saier MH (1995) The global regulatory protein FruR modulates the direction of carbon flow in *Escherichia coli*. *Mol Microbiol* **16**: 1157-1169

Ray WJ, Roscelli GA (1964) A kinetic study of the phosphoglucomutase pathway. *J Biol Chem* **239**: 1228-1236

Reddy CSK, Ghai R, Rashmi, Kalia VC (2003) Polyhydroxyalkanoates: an overview. *Bioresource Technol* **87**: 137-146

Ritchie GAF, Senior PJ, Dawes EA (1971) The purification and characterization of acetoacetyl-coenzyme A reductase from *Azotobacter beijerinckii. Biochem J* **121**: 309-316

Robertson AGS, Nimmo HG (1995) Site-directed mutagenesis of cysteine-195 in isocitrate lyase from *Escherichia coli* ML308. *Biochem J* **305**: 239-244

Ronen M, Rosenberg R, Shraiman BI, Alon U (2002) Assigning numbers to arrows: Parameterizing a gene regulation network by using accurate expression kinetics. *Proc Natl Acad Sci USA* **99**: 10555-10560

Rose IA, Weaver TM (2004) The role of the allosteric B site in the fumarase reaction. *Proc Natl Acad Sci USA* **101**: 3393-3397

Saito T, Suzuki K, Yamaoto J, Tetsuya F, Miwa K, Tomita K, Nakanishi S, Odani S, Suzuki J, Ishikawa K (1989) Cloning, nucleotide sequence, and expression in *Escherichia coli* of the gene for poly(3-hydroxybutyrate) depolymerase from *Alcaligenes faecalis. J Bacteriol* **171**: 184-189

Sawers G, Suppmann B (1992) Anaerobic induction of pyruvate formate-lyase gene expression is mediated by the ArcA and FNR proteins. *J Bacteriol* **174**: 3474-3478

Schellenberger J, Que R, Fleming RMT, Thiele I, Orth JD, Feist AM, Zielinski DC, Bordbar A, Lewis NE, Rahmanian S, Kang J, Hyduke DR, Palsson BO (2011) Quantitative prediction of cellular metabolism with constraint-based models: the COBRA Toolbox v2.0. *Nat Protoc* **6**: 1290-1307

Schröder I, Wolin CD, Cavicchioli R, Gunsalus RP (1994) Phosphorylation and dephosphorylation of the NarQ, NarX, and NarL proteins of the nitrate-dependent two-component regulatory system of *Escherichia coli. J Bacteriol* **176**: 4985-4992

Senior PJ, Dawes EA (1973) The regulation of poly-β-hydroxybutyrate metabolism in *Azotobacter beijerincki*. *Biochem J* **134**: 225-238

Shang L, Fan DD, Kim MI, Choi J, Chang HN (2007) Modeling of poly(3-hydroxybutyrate) production by high cell density fed-batch culture of *Ralstonia eutropha*. *Biotechnol Bioprocess Eng* **12**: 417-423

Shen J, Gunsalus RP (1997) Role of multiple ArcA recognition sties in anaerobic regulation of succinate dehydrogenase (sdhCDAB) gene expression in *Escherichia coli*. *Mol Microbiol* **26**: 223-236

Sigman DS (1990) *The Enzymes: Mechanisms of Catalysis.* Academic Press, San Diego, CA, USA

Singh VK, Ghosh I (2006) Kinetic modeling of tricarboxylic acid cycle and glyoxylate bypass in *Mycobacterium tuberculosis*, and its application to assessment of drug targets. *Theor Biol Med Model* **3**: 27

Slater S, Houmiel KL, Tran M, Mitsky TA, Taylor NB, Padgette SR, Gruys KJ (1998) Multiple β-ketothiolases mediate poly(β-hydroxyalkanoate) copolymer synthesis in *Ralstonia eutropha*. *J Bacteriol* **180**: 1979-1987

Sliwkowski MX, Hartmanis MG (1984) Simultaneous single-step purification of thiolase and NADP-dependent 3-hydroxybutyryl-CoA dehydrogenase from *Clostridium kluyveri*. *Anal Biochem* **141**(2): 344-7

Snoep JL, Westphal AH, Benen JA, Teixeira de Mattos MJ, Neijssel OM, Kok A (1992) Isolation and characterisation of the pyruvate dehydrogenase complex of anaerobically grown *Enterococcus faecalis* NCTC 775. *Eur J Biochem* **203**: 245-250

Spiekermann P, Rehm BHA, Kalscheuer R, Baumeister D, Steinbüchel A (1999) A sensitive, viable-colony staining method using Nile red for direct screening of bacteria that accumulate polyhydroxyalkanoic acids and other lipid storage compounds. *Arch Microbiol* **171**: 73-80

Spring TG, Wold F (1971) The purification and characterization of *Escherichia coli* enolase. *J Biol Chem* **246**: 6797-6802

Stafford GP, Ogi T, Hughes C (2005) Binding and transcriptional activation of non-flagellar genes by the *Escherichia coli* flagellar master regulator FlhD2C2. *Microbiology* **151**: 1779-1788

Steinbüchel A, Schlegel HG (1991) Physiology and molecular genetics of poly(β-hydroxybutyric acid) synthesis in *Alcaligenes eutrophus*. *Mol Microbiol* **5**: 523-542

Sutton VR, Mettert EL, Beinert H, Kiley PJ (2004) Kinetic analysis of the oxidative conversion of the $[4Fe\text{-}4S]^{2+}$ cluster of FNR to a $[2Fe\text{-}2S]^{2+}$ cluster. *J Bacteriol* **186**: 8018-8025

Teusink B, Passarge J, Reijenga CA, Esgalhado E, Van der Weijden CC, Schepper M, Walsh MC, Bakker BM, Van Dam K, Westerhoff HV, Snoep JL (2000) Can yeast glycolysis be understood in terms of in vitro kinetics of the constituent enzymes? Testing biochemistry. *Eur J Biochem* **267**(17): 5313-29

Tsuchiya D, Shimizu N, Tomita M (2009) Cooperativity of two active sites in bacterial homodimeric aconitases. *Biochem Biophys Res Commun* **379**(2): 485-8

Tucker NP, Hicks MG, Clarke TA, Crack JC, Chandra G, Le Brun NE, Dixon R, Hutchings MI (2008) The transcriptional repressor protein NsrR senses nitric oxide directly via a [2Fe-2S] cluster. *PLoS One* **3**: e3623

Um H, Klein C (1993) Evidence for allosteric regulation of succinyl-CoA synthetase. *Biochem J* **295**: 821-826

Valentini G, Chiarelli L, Fortin R, Speranza ML, Galizzi A, Mattevi A (2000) The allosteric regulation of pyruvate kinases. A site-directed mutagenesis study. *J Biol Chem* **275**: 18145-18152

Van Wegen RJ, Ling Y, Middelberg APJ (1998) Industrial production of polyhydroxyalkanoates using *Escherichia coli*: an economic analysis. *Chem Eng Res Des* **76**: 417-426

Van Wegen RJ, Lee SY, Middelberg APJ (2001) Metabolic and kinetic analysis of poly(3-hydroxybutyrate) production by recombinant *Escherichia coli*. *Biotechnol Bioeng* **74**: 70-80

Varshavsky A (1997) The N-end rule pathway of protein degradation. *Genes Cells* **2**: 13-28

Walsh K, Koshland DE (1985) Branch point control by the phosphorylation state of isocitrate dehydrogenase. A quantitative examination of fluxes during a regulatory transition. *J Biol Chem* **260**: 8430-8437

Wang C, Alaupovic P (1980) Glyceraldehyde-3-phosphate dehydrogenase from human erythrocyte membranes. Kinetic mechanism and competitive substrate inhibition by glyceraldehydes 3-phosphate. *Arch Biochem Biophys* **205**: 136-145

Wang X, Kemp RG (1999) Identification of residues of *Escherichia coli* phosphofructokinase that contribute to nucleotide binding and specificity. *Biochemistry* **38**: 4313-4318

Waygood EB, Mort JS, Sanwal BD (1976) The control of pyruvate kinase of *Escherichia coli*. Binding of substrate and allosteric effectors to the enzyme activated by fructose 1,6-bisphosphate. *Biochemistry* **15**: 277-282

Willms CR, Oliver RM, Henney HR, Mukherjee BB, Reed LJ (1967) Alpha-keto acid dehydrogenase complexes. V1. Dissociation and reconstitution of the dihydrolipoyl transacetylase of *Escherichia coli*. *J Biol Chem* **242**: 889-897

Woods SA, Schwartzbach SD, Guest JR (1988) Two biochemically distinct classes of fumarase in *Escherichia coli*. *Biochim Biophys Acta* **954**: 14-26

Yamamoto K, Matsumoto F, Oshima T, Fujita N, Ogasawara N, Ishihama A (2008) Anaerobic regulation of citrate fermentation by CitAB in *Escherichia coli*. *Biosci Biotechnol Biochem* **72**: 3011-3014

Yoshizaki F, Oshima T, Imahori K (1971) Studies on phosphoglucomutase from an extreme thermophile, *Flavobacterium thermophilum* HB8. I. Thermostability and other enzymatic properties. *J Biochem* **69**: 1083-1089

Zaslaver A, Mayo AE, Rosenberg R, Bashkin P, Sberro H, Tsalyuk M, Surette MG, Alon U (2004) Just-in-time transcription program in metabolic pathways. *Nat Genet* **36**: 486-491

Zheng M, Doan B, Schneider TD, Storz G (1999) OxyR and SoxRS regulation of *fur*. *J Bacteriol* **181**: 4639-4643

APPENDICES

Appendix A. Transcription Factor Chart

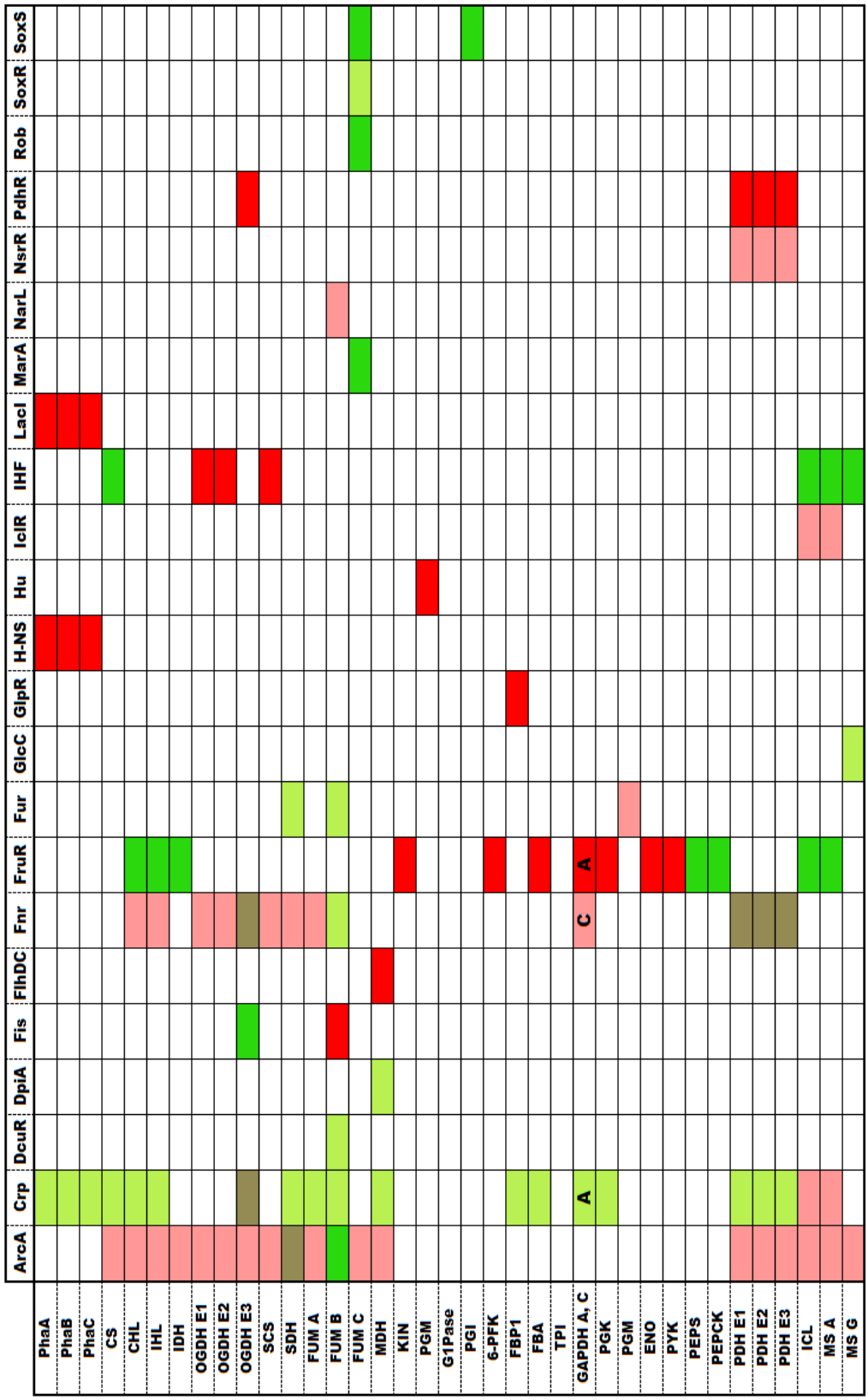
ArcA
Crp
DcuR
DpiA
Fis
FlhDC
Fnr
FruR
Fur
GlcC
GlpR
H-NS
Hu
IclR
IHF
LacI
MarA
NarL
NsrR
PdhR
Rob
SoxR
SoxS
PhaA
PhaB
PhaC
CS
CHL
IHL
IDH
OGDH E1
OGDH E2
OGDH E3
SCS
SDH
FUM A
FUM B
FUM C
MDH
KIN
PGM
G1Pase
PGI
6-PFK
FBP1
FBA
TPI
GAPDH A, C
PGK
PGM
ENO
PYK
PEPS
PEPCK
PDH E1
PDH E2
PDH E3
ICL
MS A
MS G
A
C
A
Activator when unmodified
Activator when modified
Repressor when unmodified
Repressor when modified
Dual Regulator

Appendix B. HPLC-MS Analytical Methods

HPLC-MS Analytical Methods

Metabolic profiling samples can be analyzed for concentration of metabolites using high performance liquid chromatography coupled with mass spectrometry (HPLC-MS). Standards should be used to identify and analyze concentrations of glucose, pyruvate, citrate, 2-oxoglutarate, succinate, fumarate, malate, oxaloacetate, and beta-hydroxybutyrate. Dilutions of the standards should be used to create a standard curve for each compound.

Mass spectrometric analysis can be conducted on an Agilient 6130 single quadropole mass spectrometer. High performance liquid chromatography can be performed on an Agilent 1200 Series HPLC. Solvent A should be an aqueous buffer, and Solvent B should be acetonitrile. Two methods could be used to separate desired metabolites. Method 1 is a reversed-phase liquid chromatography utilizing a C18 column. Method 2 is a hydrophilic interaction liquid chromatography utilizing an aminopropyl column (Bajad *et al*, 2006).

Concentrations of the metabolites can be analyzed for each time sample utilizing HPLC-MS. An independent two-sample student's t-statistic test could then be used to compare the differences in concentrations of the above-mentioned metabolites between the strain containing the PHB producing plasmid and the control to determine if the addition of the PHB synthesis pathway significantly alters the kinetics of glycolysis and the TCA cycle.

Appendix C. Simulations

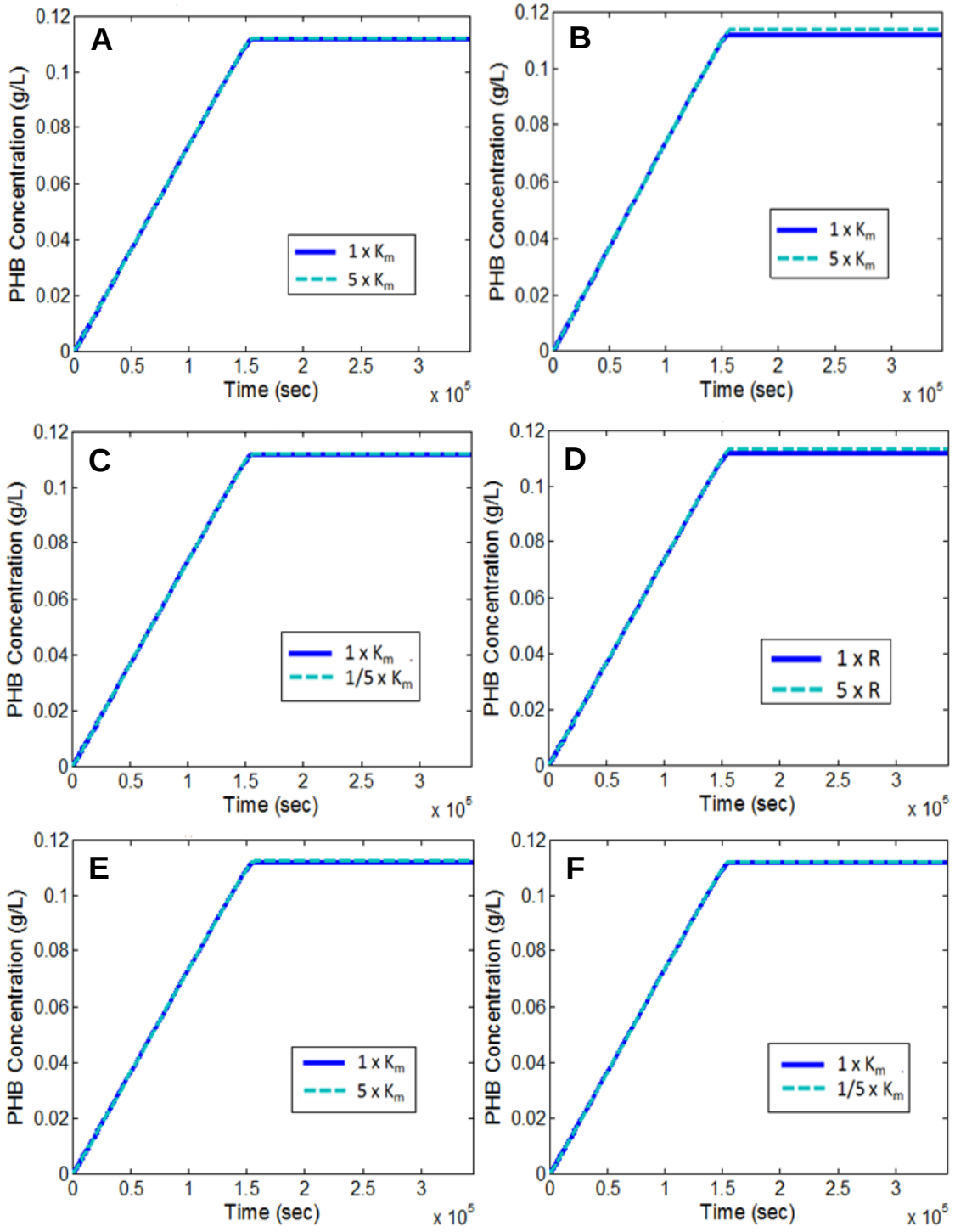

Figure 135. PHB production levels from adjusting (A) citrate hydro-lyase's K_m for citrate, (B) isocitrate hydro-lyase's K_m for aconitate, (C) oxoglutarate dehydrogenase's K_m for 2-oxoglutarate, (D) succinyl-CoA synthetase's reaction rate, (E) succinate dehydrogenase's K_m for succinate, and (F) fumarase's K_m for fumarate.

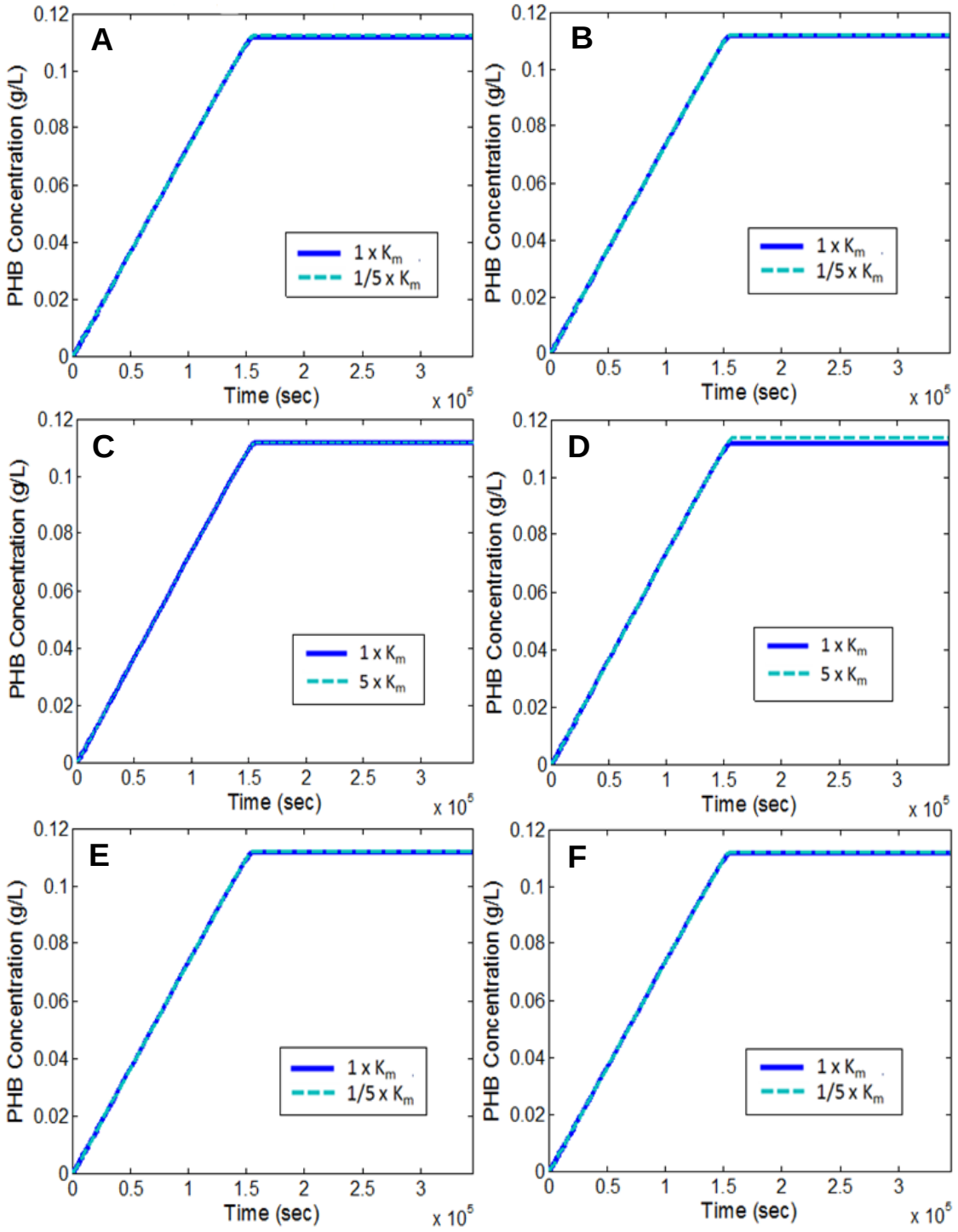

Figure 136. PHB production levels from adjusting (A) malate dehydrogenase's K_m for malate, (B) malate dehydrogenase's K_m for NAD^+, (C) malate synthase's K_m for glyoxylate, (D) malate synthase's K_m for acetyl-CoA, (E) kinase's K_m for glucose, and (F) kinase's K_m for ATP.

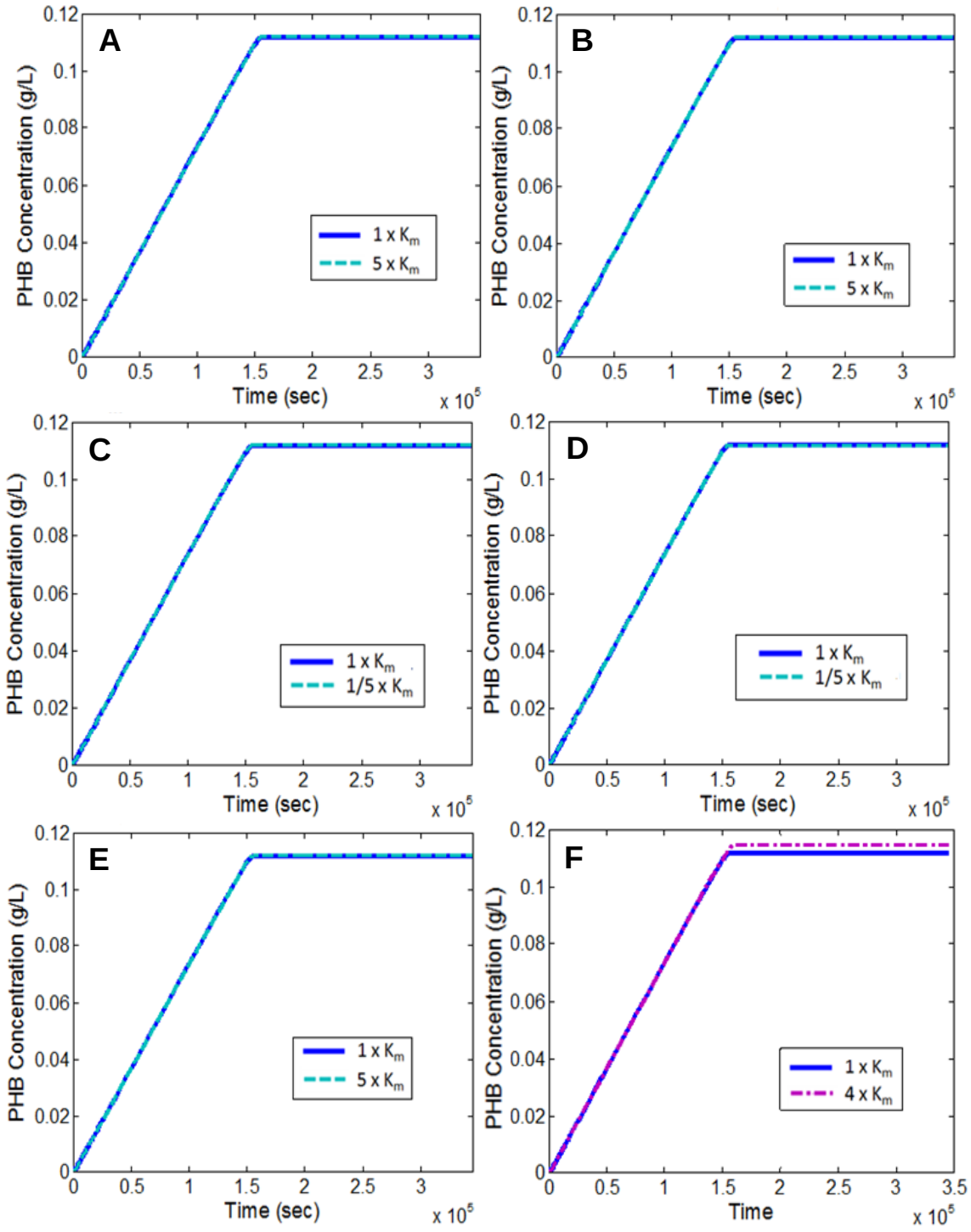

Figure 137. PHB production levels from adjusting (A) phosphoglucose isomerase's K_m for glucose-6-phosphate, (B) phosphoglucose isomerase's K_m for fructose-6-phosphate, (C) 6-phosphofructokinase's K_m for fructose-6-phosphate, (D) 6-phosphofructokinase's K_m for ATP, (E) glyceraldehyde-3-phosphate dehydrogenase's K_m for glyceraldehyde-3-phosphate, and (F) phosphoglycerate mutase's K_m for 3-phosphoglycerate.

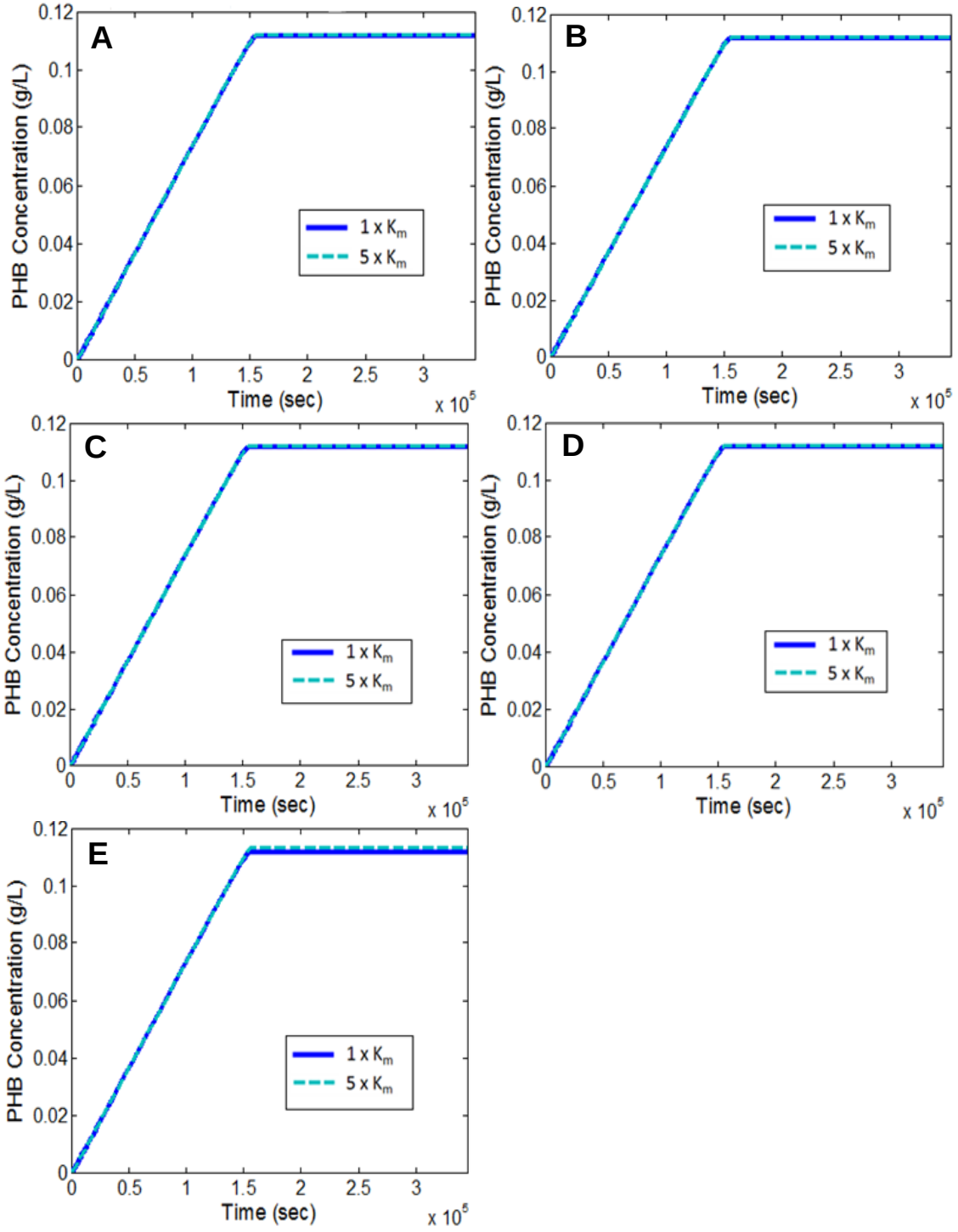

Figure 138. PHB production levels from adjusting (A) phosphoglycerate kinase's K_m for 1, 3-diphosphateglycerate, (B) phosphoglycerate kinase's K_m for ADP, (C) enolase's K_m for 2-phosphoglycerate, (D) pyruvate kinase's K_m for phosphoenolpyruvate, and (E) pyruvate kinase's K_m for ADP.

Appendix D. SimBiology Model Tutorial

Instructions are for SimBiology Version 3.2 (R2010a)

Download File

Predictive Model: http://digitalcommons.usu.edu/engineering_datasets/1/

Open SimBiology Project

Open MATLAB

Type **"sbiodesktop"** to open SimBiology

Go to **File**, then select **Open Project**, then select the Predictive Model

How to Open Diagram View:

In the **Project Explorer** window pane, expand **Model Session**, then expand **SimBiology Model** and select **Diagram View**

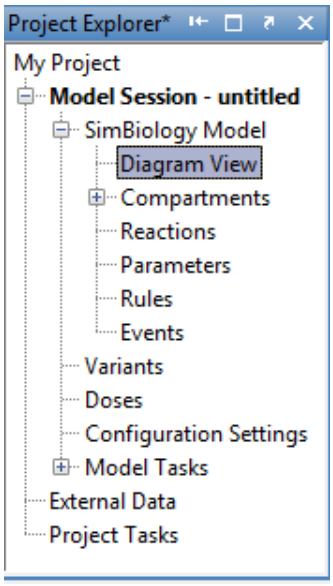

Editing Properties of Species

Double-click on the **Species** block

Settings Tab

- Here changes can be made to the initial amount of the species
- Select whether the species is held constant, or if the amount is determined by a boundary condition

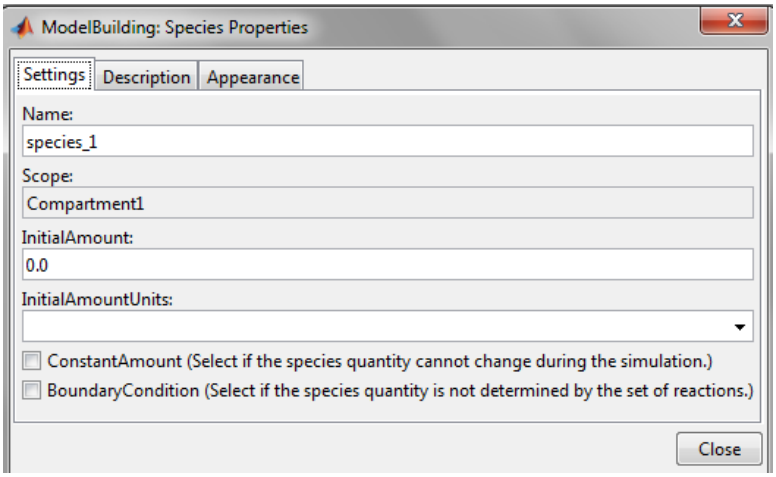

Editing Properties of Reactions

Double-click on the **Reaction** block

Settings

- Here changes can be made to the kinetic law and parameters
- Reaction rate expression can be edited by clicking on the pencil icon
- K_m values can be changed by double-clicking the **Value** cell for K_m and entering a new value
- Make a reaction unactive during the simulation by unchecking the **Active** checkbox

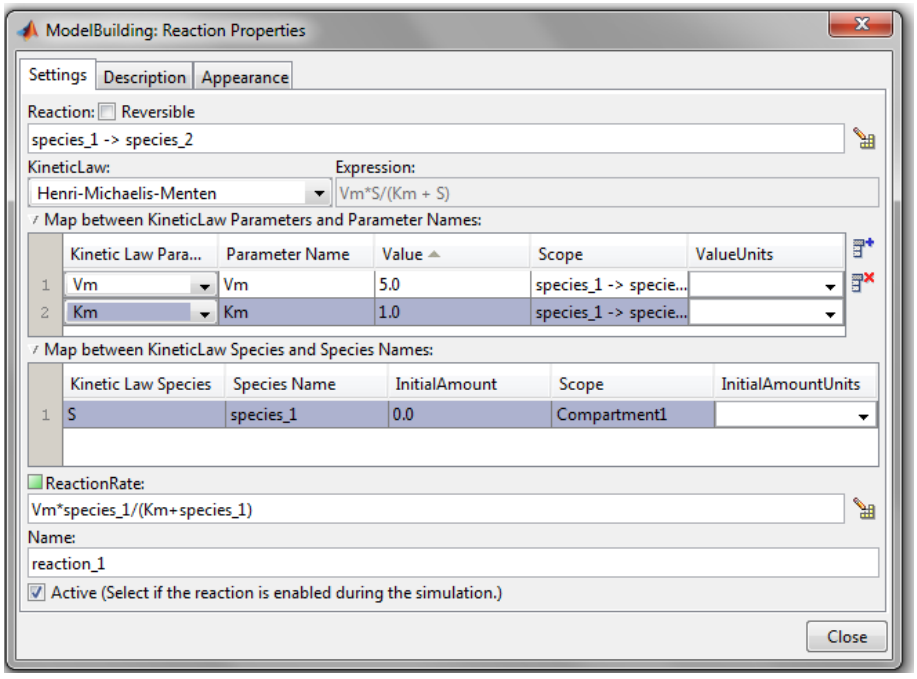

Cloned/Split Species

- A block is cloned or split to separate a species that participates in multiple reactions.
- Although there could be multiple split/clone blocks, there is only one species. Changes made to any settings in the **Species Properties** dialog box will be propagated to each of the split/clone blocks.

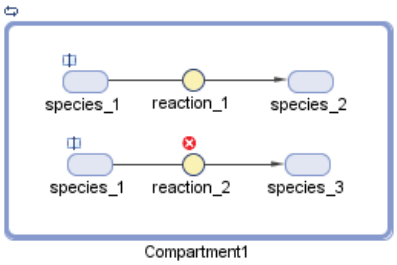

Parameter Properties

Changing a Parameter's Scope:

- In the **Project Explorer** window pane select **Parameters**
- **Right-click** on the desired parameter in the **Scope** column. Select **"Change Parameter Scope."** This toggles the scope between the reaction and the overall model. A parameter must have a global scope if it is used in an **Event** or a **Rule**.

Constant:

- The default setting for all parameters is for them to be held constant throughout the entire simulation. To change the parameters value partway through the simulation (through use of an **Event**), then uncheck the **ConstantValue** box in the parameter settings.

Rules

In the **Project Explorer** window pane select **Rules**

4 Types of Rules:

1. Algebraic — Evaluated continuously during a simulation
2. Initial Assignment — Evaluated once at the beginning of the simulation
3. Repeated Assignment — Evaluated at every time-step of the simulation

4. Rate — Evaluated continuously during the simulation

Tip: To use a parameter in a rule, remember to set the **Scope** of the parameter to "**model**." To use an algebraic or rate rule to vary the value of a parameter during the simulation, clear the **ConstantValue** checkbox for the parameter in the **Parameters** pane. Also, if using a rule to define a species concentration, clear the **ConstantAmount** checkbox and check the **BoundaryCondition** checkbox.

Events

In the **Project Explorer** window pane select **Events**

Events are used to describe sudden changes in model behavior. An event can specify discrete transitions in model component values that occur when a user-specified condition become true.

Uses:

To activate or deactivate certain species (activator or inhibitor species), change parameter values, change reaction rates in response to addition or removal of species

Trigger:

The trigger can be time-dependent or time-independent

Event Functions:

Event functions are the results when the event is turned on by the trigger

Active:

The Active check box must be marked for the event to work. To simulate the model without the event, then clear the Active check box.

Tip:

To use a parameter in an event, remember to set the Scope of the parameter to model and to clear the ConstantValue check box for the parameter in the Parameters pane. Also, the solver must be set to sundial in order to simulate events.

Configuration Settings

In the **Project Explorer** window pane expand **Model Session** and select **Configuration Settings**

Before running a simulation, use the **Configuration Settings** to set the simulation time, solver, etc.

Custom Configuration Settings:

To store simulation settings for later use, type a name for the settings in the **Enter Name** edit box, and click **Add** to create your custom configuration settings. Any changes made in the **Settings and Data Logging** tabs will be saved with the project.

Custom Configuration Settings Available in Predictive Model

- **CoFactor**: Simulates cofactors in model
- **PHB synthesis**: Simulates species in PHB synthesis pathway
- **TCA cycle**: Simulates species in TCA and Glyoxylate pathways
- **Glycolysis**: Simulates species in the Glycolysis pathway
- **Glucose_PHB**: Simulates key species of the entire model

Settings:

- Set simulation time
- Choose solver (Use **sundial** if using **Events**)
- Select the species to be logged

Simulation

In the **Project Explorer** window pane expand **Model Session**, then expand **Model Tasks** and select **Simulation**

- In the **Settings** tab, select the **Configuration Settings** to use for the simulation
- Next, select the **Plots** tab
  - Double click the "**y**" argument box to select which species to plot
  - Under Plot Behavior, select if the simulation should be a new figure or if it should be added to the current axes
- Click the **Run** icon in the main Toolbar
- A graph of your simulation will appear in the **Figures** window pane

Importing Data

In the main task bar, select **File**, and then select **Add Data**, and choose **From File**

- Select a file to download
- Select if the first row contains header information
- Look at the **Data Preview**, and if it looks good, then click **Okay**

Plotting Multiple Simulations in a Single Figure

In the **Project Explorer** window pane expand **Model Session**, then expand **Model Tasks** and select **Simulation**

- In the **Plots** tab, select whether the plot should be put in a new Figure or if the plot should be added to the current axes. If "**Add to current axes**" is selected then the simulation will be plotted on the Figure last selected. This is the best way to overlay different simulations.

Plotting a Dataset with a Simulation in a Single Figure

In the **Project Explorer** window pane expand **Model Session**, then expand **Model Tasks** and select **Simulation**

- In the **Plots** tab, select an **XY Plot Type** and click **"Add Plot Type"**
- For the first plot (**Time Plot Type**), choose the Plot Behavior "**New Figure**"
    - Double-click on the "**y**" argument to select which species to plot from the simulation.
- For the second plot (**XY Plot Type**), choose the Plot Behavior "**Add to current axes**"
    - Double-click on the "**x**" argument to select the x-variable from the imported dataset. Double-click on the "**y**" argument to select the y-variable from the imported dataset.
- As long as both **Create Plot** checkboxes are checked, a Figure will be created containing the simulation and the dataset